OPTICAL DETERMINATION OF THE HIGH PRESSURE REFRACTIVE INDEX AND VISCOSITY OF LIQUIDS ENTRAPPED IN POINT CONTACTS

by Graham Rene Paul

A thesis submitted for the degree of

DOCTOR OF PHILOSOPHY

of the University of London

and also for the

DIPLOMA OF IMPERIAL COLLEGE

November 1971

Lubrication Laboratory,
Department of Mechanical Engineering,
Imperial College of Science and Technology,
London S.W.7.

ABSTRACT

Elastohydrodynamic oil film measurements for normally approaching point contact are obtained using optical interferometry. A novel optical technique is developed to determine the refractive index of the oil film simultaneously with this measurement and hence the absolute film thickness is found.

Oil entrapments were formed by dropping a ball onto a flat surface. These are small pockets of fluid trapped inside the contact region. They were measured at discrete intervals of time using the new optical technique.

A computer programme was written to calculate the pressure inside the contact due to the elastic distortion of the surfaces. From this and the measurement of the refactive index, the change of density with pressure was found using the theoretical Lorentz-Lorenz relationship. Reynold's equation was then solved at discrete values of the radius of the contact and hence the variation of the viscosity with pressure was found. This was done for four fluids.

One of the fluids tested appeared to go into a 'glassy state' at a high enough pressure and its viscosity then became independent of the pressure. This fluid showed very little flow inside the entrapment and a qualitative explanation was found for this based on the independence of the viscosity with pressure.

Measurements were made of the approach velocity of the two surfaces and the values were compared with those predicted by existing theory. Due to the assumptions made by this theory there was not a good correlation between the two. However, the large increase in the central pressure above the equivalent Hertzian maximum, predicted by the theory, was confirmed.

Some high speed photography demonstrated that under certain conditions the ball will bounce away from the surface and

return producing a much smaller entrapment. The conditions that produced this bouncing effect were investigated and it was found that both load and the fluid temperature were critical in determining whether or not the ball would bounce.

ACKNOWLEDGEMENTS

The author gratefully acknowledges the following in support of this work:

Dr. A. Cameron for his willing and enthusiastic supervision and encouragement during the course of this work.

Mr. A. Ranger for assistance in computing the pressure due to the distortion of the surfaces.

Dr. R. Gohar, Dr. F. Westlake, Dr. V. Wedeven and Mr. R. Gentle for their valuable discussions.

Mr. R. Dobson for all his encouragement and help on technical matters.

N.A.S.A. Lewis Research Centre for a grant to carry out this work.

Dr. Welford for his help in developing the new refractive index measuring technique.

Mr. Day for his assistance and discussion.

TABLE OF CONTENTS

TABLE OF CONTENTS (Cont.)

LIST OF FIGURES

LIST OF FIGURES (Cont.)

NOMENCLATURE

V.... non-dimensional approach velocity of the centre of the contact region with respect to the flat surface

H.... non-dimensional film thickness

R.... Reduced radius of the two bodies given by $\frac{1}{R} = (\frac{1}{R_1} + \frac{1}{R_2})^{\frac{1}{2}}$ R_1 and R_2 are the radii of the two bodies

E.... the reduced Young's Modulus given by $\frac{1}{E} = \frac{1}{2}(\frac{1}{E_1} + \frac{1}{E_2})$ where E_1 is the Young's Modulus of the ball and E_2 the modulus of the flat surface

τ.... the Frictional Force per Unit area

$\frac{\partial u}{\partial z}$ .. the rate of shear

η.... the viscosity

$\bar{\eta}$.... the effective viscosity through the contact

η_o... the viscosity at atmospheric pressure

n.... the refractive index of the medium

h.... the physical film thickness

θ.... the angle of incidence of the incident beam in air

λ.... the wavelength of the light used

P.... the Phase change on reflection

N.... the order of the Interference

I.... the intensity of the light forming the interference

δ.... the Path Difference between two rays

R'... the reflectivity from a surface

V'... the fringe visibility

ρ.... the density of the fluid

σ.... Poisson's ratio

p_{max}. the maximum pressure

t.... time from formation of entrapment

T.... the Fluid temperature

w.... the deformation of the two surfaces

p.... the pressure at (r,θ,φ)

φ.... the angle of incidence of the incident beam in the fluid

CHAPTER 1

INTRODUCTION

1.1 Concept of the Project

Most of the methods of measuring film thickness in Elastohydrodynamic lubrication (E.H.L.) require information about some property of the fluid. Capacitance measurements require a knowledge of the dielectric constant, resistance measurements require the resisivity,reluctance measurements the reluctance of the fluid and interferometry the refractive index.

These properties are all functions of the high pressures generated in an E.H.L. contact. It was decided to develop a technique to measure the refractive index of a fluid actually inside an E.H.L. contact. Changes of up to 20% were expected under the extremely high pressures inside these point contacts. These changes can be estimated from the change in pressure, however, to calculate the pressure from the elastic deformation of the contact, the absolute distortion must be known. This is, of course, impossible to do optically until the refractive index is known. It would be possible using a complicated iterative procedure requiring the pressure-refractive index characteristics of the fluid. This iterative procedure would work by assuming the refractive index distribution in the contact, calculating the elastic distortion and hence the pressure distribution and then from the known pressure, refractive index characteristics, calculate the refractive index which would result from the pressure distribution. This would be compared with the initial assumed index distribution, which would then be adjusted and the process repeated until the assumed and calculated refractive indices

became equal. This would be a difficult process and the convergence would probably not be very good. Furthermore, the refractive index-pressure relationship is not known.

The measurement of the refractive index in an E.H.L. contact is therefore the object of this work.

Choice of System

Recent work in E.H.L. has concentrated on steady state conditions, but often E.H.L. film thickness varies with time, and so it was thought important that the normal approach of opposing solids should be investigated. It was decided to study fluid entrapments, which are formed by dropping a ball onto a flat surface - described by both Dowson and Jones (1) and Foord, Hamman and Cameron (2) in 1967. These are small pockets of fluid trapped inside the contact area when the ball is dropped onto the flat surface in the presence of the fluid.

Christensen (3) predicted that the pressure inside the contact would be considerably greater than the equivalent Hertz maximum and that the fluid would leak away until eventually the normal Hertzian shape was reached. It appears that no experimental work on the accuracy of Christensen's theory has been published and so a comparison of his theoretical results with experimental results could prove illuminating.

Viscosity

By studying the behaviour of fluids as they flowed from an entrapment it was hoped to measure their viscosities. Most high pressure viscometers have an upper limit of viscosity of about 10^3 Newton seconds/m^2 (10^4 poise). For fluids which are

viscous at atmospheric pressure this limit is usually reached at very low pressures compared with those developed in E.H.L. contacts. It was thought desirable to measure the viscosity of these fluids up to a much higher viscosity.

1.2 Survey of Research on Entrapments

Very little work has been done either experimentally or theoretically on entrapments. Probably the first person to comment on entrapment formation was Rabinowicz (4) in 1952. He observed that a transfer of metal resulted when a sphere was impacted against a metal plate, both in dry and lubricated conditions. In the lubricated case, however, a small region in the centre of the indentation was free from metal transfer. Rabinowicz concluded that a small amount of oil must have been trapped between the surfaces. Some of the first interferometric pictures of an entrapment were obtained by Dowson and Jones (1). They used a steel ball dropping onto a plain glass surface. A few qualitative remarks were made about the time it took the fluid to escape.

Foord, Hamman and Cameron (2) obtained interferometric pictures of an entrapment using a considerably more sophisticated optical system. They describe a large entrapment formed with 5-phenyl-4-ether. The minimum film thickness, which occurs round the edges of the entrapment was less than 200^{o}A. The entrapment remained unchanged over a period of 5 hours. Westlake and Cameron (5) examined entrapments in rather more detail. Using a highly sophisticated optical system with a semi-reflecting dielectric coating on the glass flat, and a high-speed camera, they took multi-beam interference pictures. With the 5-phenyl-4-ether oil the minimum film thickness was very small. They also found

that during the last part of the descent of the ball there was very little side leakage of the fluid. In other words a column of liquid inside the contact area remained almost stationary and the ball distorted around this column. This effect was less marked for a high viscosity cylinder stock (BP 1065), which was the other fluid they tested. Klemz, Gohar and Cameron (6) did a series of photoelastic measurements using two discs. When the rotating discs were stopped in the presence of a fluid, they found that there was an increase in the maximum pressure in the contact. This gradually decreases until the normal Hertz pressure distribution is obtained. Under dry conditions the pressure returned to the Hertz distribution as soon as the rotation was stopped. From this they deduced that oil had been trapped inside the contact region, creating a higher maximum pressure. This oil flowed out until the normal Hertzian shape returned. Roberts and Tabor (7) used an optically smooth rubber ball dropping onto a glass flat. The general shape of the resulting entrapments were similar to those found by previous workers, however the pressures were very much lower - of the order of 5×10^3 Newtons/m^2, whereas the other workers had used pressures of greater than 10^7 Newtons/m^2. Brenner (10) in 1961 published a paper showing that the pressures between normally approaching bodies in a fluid was greatly increased when the influenc. of the fluid was considered. Christensen (3) in 1965 published a theoretical treatment of the elastohydrodynamics of normal approaching spherical bodies. Several conclusions were reached. The more relevant ones are listed below:

1) For relatively large values of the film thickness, load and relative approach velocity are much more influenced by the increase of viscosity with pressure than by the elastic

deformation.

2) For relatively small values of the film thickness the elastic distortions became increasingly important in their effect on load and approach velocity.

3) Very high pressures, considerably in excess of the Hertz maximum, can be generated by normal approach. The maximum pressure being proportional to the modulus of elasticity of the materials times the viscosity pressure coefficient.

Fig. 1 is reproduced from Christensen's paper and shows that the square root of the relative approach velocity of the centre should be proportional to the central film thickness. The equation is:

$$V^{\frac{1}{2}} = KH \qquad \text{.....(1)}$$

where $K = 2.26$

H the non-dimensional film thickness is given by:

$$H = h\frac{(\pi\alpha E)^2}{32R}$$

V the non-dimensional relative approach velocity given by:

$$V = \frac{6\eta_o(\pi\alpha E)^4\alpha}{2^9 R} v$$

R is the reduced radius of the two bodies given by:

$$\frac{1}{R} = \tfrac{1}{2}\left(\frac{1}{R_1} + \frac{1}{R_2}\right)$$

Therefore:

$$v^{\frac{1}{2}} = h\left(\frac{5.1}{12\eta_o\alpha R}\right)^{\frac{1}{2}} \qquad \text{.....(2)}$$

This theoretical relationship does not appear to have been verified experimentally. J.W. Kannel (8) points out that at large viscosities, the viscosity increases less than exponentially. Such an assumption was basic to Christensen's theory. He goes on to point out that if the viscosity was allowed to increase exponentially up to a given limit and then kept constant, the maximum pressure developed

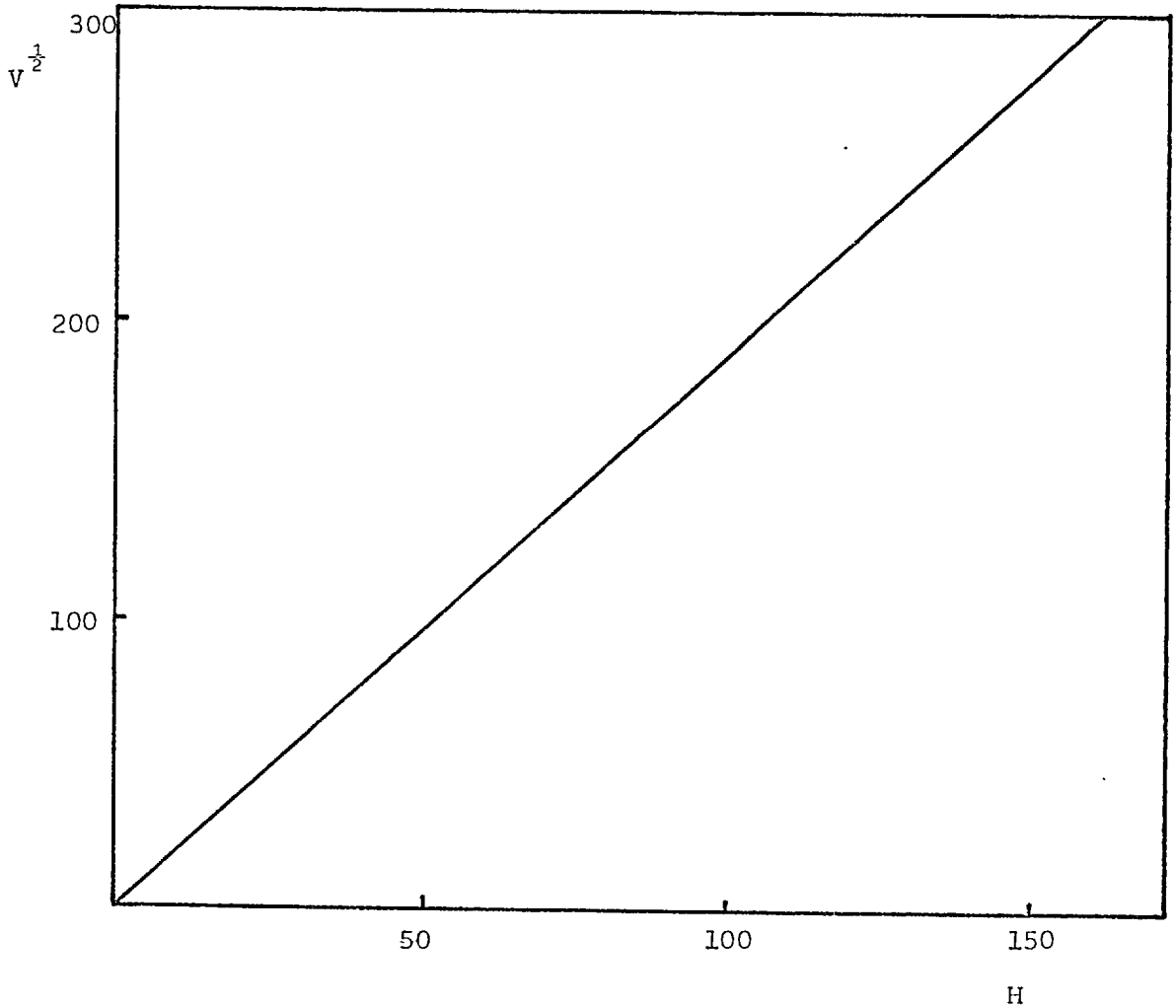

THEORETICAL (RELATIVE APPROACH VELOCITY)$^{\frac{1}{2}}$ AGAINST THICKNESS BY CHRISTENSEN (3)

FOR CENTRE OF CONTACT AND VALID FOR CENTRAL PRESSURES GREATER THAN 5×10^7 N/m^2

FIG. 1

in the contact would reach a critical value and would then only increase slowly with load.

Christensen (9) also did some experimental work with a dropping ball. By measuring the indentation in the flat surface he was able to show qualitatively that the maximum central pressure was a function of the elasticity of the surfaces and of the viscosity pressure coefficient. It is appropriate at this point to give a brief introduction and survey of the measurement of the viscosity of fluids, as a considerable portion of the work done on entrapments was concerned with this measurement.

1.3 Survey of Measurements of Viscosity

The definition of viscosity was first given by Clark Maxwell in the 1866 Bakerian lecture (11). His definition although stated for air, applies for any laminar flow of a fluid. It is reproduced in full:

This coeffecient may be best defined by considering a stratum of air between two parallel horizontal planes of indefinite extent at a distance 'a' from one another. Suppose the upper plane to be set in motion in a horizontal direction with a velocity of 'a' feet per second and to continue in motion until the air in the different stratum has taken up its final velocity, then the velocity of the air will increase uniformly as we pass from the lower plane to the upper. If the air in contact with the planes has the same velocity as the planes themselves then the velocity will increase v/a feet per second for every foot we ascend.

The friction between any two contiguous strata will then be equal to that between either surface and the air in contact with it. Suppose that this friction is equal to a tangential force 'f'

on every square foot, then

$$f = \mu \frac{v}{a}$$

where μ is the coefficient of viscosity, v the velocity of the upper plane and a the distance between them.

If the experiment could be made with the two infinite planes as described we would have μ at once for

$$\mu = f \frac{a}{v} \qquad \text{.....(3)}$$

In a previous paper (12), read at the British Association meeting at Aberdeen in 1859 he gives the relation:

$$F = \mu \frac{du}{dz} \qquad \text{.....(4)}$$

This differential relationship is the one normally employed. For the sake of consistency with current literature η will be used as the symbol for viscosity. The expression for viscous shear:

$$\tau = \eta \frac{\partial u}{\partial z} \qquad \text{.....(5)}$$

where τ = frictional force per unit area

η = viscosity

$\frac{\partial u}{\partial z}$ = rate of shear

follows from Newton's hypothesis made in 'Principia' (13). This suggests that the shear stress is directly proportional to the velocity gradient. Fluids which obey this hypothesis are said to be Newtonian. Those which do not are usually 2 phase systems with a substance such as asphalt. wax or polymer dispersed in them (14).

From equation (5) it is possible to define the units of viscosity. In the cgs system they are dynes cm^{-2} sec. and are called 'poise', in SI units they are Newtons second/$metre^2$. Results will be given in both units, however, references will quote the units used by the various authors. Viscosities at atmospheric pressure are normally measured by the time the fluid takes to flow

from a container through a capillary tube. Most of these are based on a design by Ostwald (15).

At pressures above atmospheric the viscosity is normally measured by 'falling weight'. This method was adapted to high pressure measurement by Bridgemann (16). It consists of a cylindrical weight enclosed in a cylindrical tube of slightly larger internal diameter. The tube is filled with the specimen whose viscosity is to be measured and the weight allowed to fall through the oil for a measured distance between electrical contacts. The time of fall is measured and represents the time required for a certain volume of oil to flow through an annular clearance between the weight or "sinker" and the tube wall. In order to allow for changes in volume of the specimen with varying temperature and pressure, the tube is connected to a flexible reservoir. The whole system is then placed in a pressure chamber filled with a pressure transmitting fluid. The chamber is immersed in a constant temperature bath, and connected to a pressure gauge.

The viscometer has to be calibrated against oils of known viscosity. This must be done at atmospheric pressure, the effect of pressure on the dimensions of the apparatus has to be calculated and allowances made for these changes. The maximum viscosity measurable with this type of instrument is about 10^4 poise or 10^3 N.S/M^2. Above this viscosity the fall time of the sinker becomes excessively large.

The disadvantage of this type of viscometer are as follows:

1) The apparatus is expensive and cumbersome to use.

2) It does not give absolute measurements but must be calibrated at atmospheric pressure with known fluids.

3) The maximum viscosities that can be measured are about 10^4 poise or 10^3 N.S/M^2.

More recently Winer (17) has developed a capillary viscometer to measure viscosity up to 10^3 poise or 10^2N.S/M^2 and pressures of 80,000 PSI (5.5×10^8 N/M^2) and shear rates of up to 10^6 sec.

This again is a very large and expensive piece of apparatus, and is limited to viscosities below about 10^3 poise. The most widely-used pressure viscosity law is the simple exponential law first suggested by Barus (18):

$$\eta = \eta_o e^{\alpha p} \qquad \text{.....(6)}$$

where η is the viscosity at atmospheric pressure
p is the pressure
α is the viscosity pressure coefficient usually termed 'alpha value'

The validity of this law is discussed later.

Measurements of alpha values of various oils have been made by Westlake (5) by measuring film thickness in an elasto-hydrodynamic point contact and comparing the measured film thickness with an emperical formula derived from previously calibrated oils. He assumed that the exponential law held for the fluid, up to pressure in the inlet region. Johnson and Cameron (20) have calculated viscosities from the film thickness using a disc machine. This was done by measuring the traction between the two discs at very low sliding speeds and hence isothermal conditions. The film thickness between the discs was taken as constant and calculated from the formula of Dowson and Higginson (21). The 'effective viscosity' was then found from the relation:

$$\bar{\eta} = \frac{Th}{2a(U_1-U_2)}$$

where $2a$ is the width of the nip
h is the film thickness
U_1, U_2 are the rolling speeds

The 'effective viscosity' is the integral of the viscosity across the contact and was found to increase with increasing rolling speed. To form a basis for comparison the rolling speed was extrapolated back to zero. The apparent viscosity was found by a graphical solution which assumed that the pressure distribution across the contact area was Hertzian. Corrections were made for the tangential elastic compliance of the discs. The calculations assumed that the exponential law held for low pressures. This is necessary for both the estimate of the film thickness and for the graphical solution of the actual viscosity.

The results show that the exponential law held fairly well for the oil tested (Shell Turbo 33), up to a viscosity of about 10^4 poise (10^3 N.S/M^2) after which there was a marked decrease in the rate of change of viscosity with pressure. This decrease in the viscosity pressure coefficient at high viscosities had not been noted before. It is also one of the important findings described later in this work.

Johnson and Cameron's technique allowed viscosities up to 10^6 poises to be determined - 2 decades higher than a conventional high pressure viscometer.

Measurements of viscosity using the principle of an oscillating quartz crystal viscometer were introduced by Mason (50). This technique can measure viscosities up to high pressures and at very high shear rates. It is however limited to rather low viscosities, less than 100 poise (10 NS/m^2).

CHAPTER 2

BASIC INTERFEROMETRY

2.1 Introduction

Interferometry has been used to make significant contributions to lubrication research by many people. In 1919, Hardy (22) measured lubricating films on glass using interference colours. More recently the use of interferometry has been extended to E.H.L. films. Work was done by Kirk (23) in 1962, Archard and Kirk (24) in 1963 and Blok and Koens (25) in 1965. Since then the use of interferometry has mostly been exploited in the lubrication laboratory of Imperial College. The classic work was that of Cameron and Gohar (26) and later Foord, Hamman and Cameron (2).

2.2 Basic Interferometry

If a beam of light is split into two and then recombined the resultant intensity, in general, depends on the path difference between the two distances traversed by the beams. The intensity changes from a maximum to a minimum when the difference in path length changes by half the wavelength of the light.

Consider a beam of parallel light incident on a semi-reflecting glass plate just separated from a reflecting surface (Fig. 2). Some of the beam is reflected at A and the rest by the surface at C, ignoring absorption. As h is very small, of the order of the wavelength of light, the two resultant beams of light will interfere. This means that the resulting intensity depends on the phase difference between the 2 rays. If they are in phase they 'constructively' interfere giving rise to an intensity which is greater than that of the sum of the two rays acting

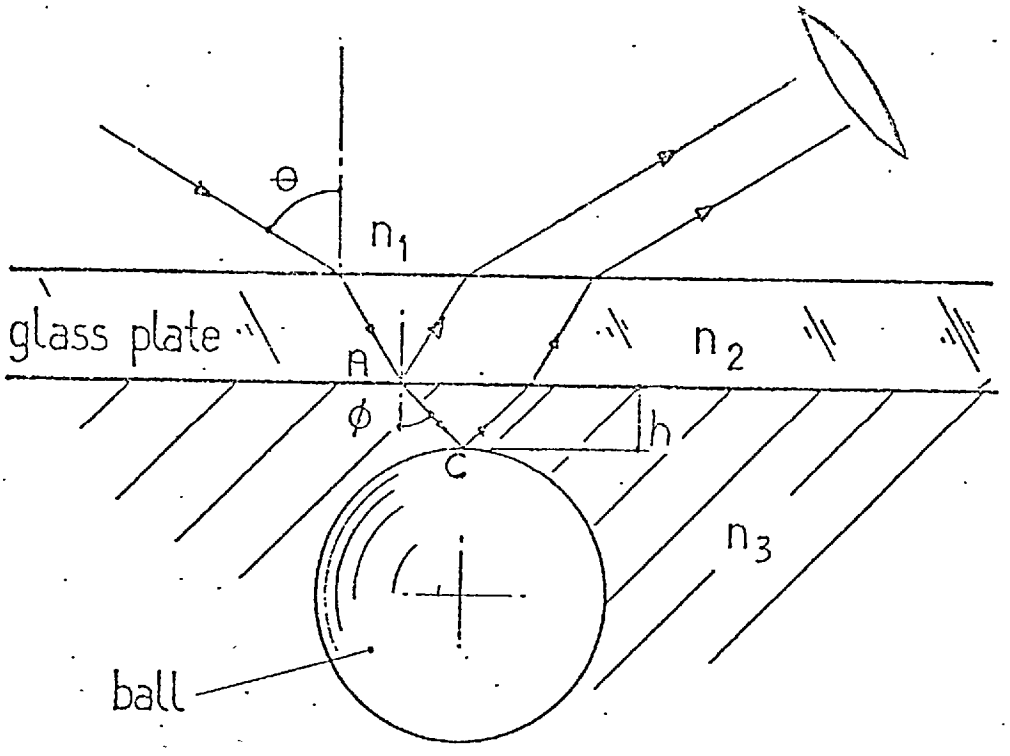

INTERFERENCE FRINGES

THE FILM THICKNESS IS GREATLY EXAGGERATED

FIG. 2

separately. Conversely, if the rays are nearly out of phase, they 'destructively' interfere, giving rise to an intensity which is less than the sum of the two rays acting separately.

The phase difference depends on the 'optical' path difference between the two rays, which is:

$$2nh\cos\varphi \qquad \text{.....(7)}$$

where n is the refractive index of the medium

and h is the physical gap thickness

There is also in general a phase change of the light when it is reflected at either surface. A factor $\frac{\lambda P}{2\pi}$ must then be added to the path difference, because the phase change is usually not the same for the 2 reflections, hence P represents the difference in phase change on reflection between the two surfaces. Constructive interference occurs when the path difference is equal to an integral number of wavelengths, $N\lambda$. Therefore when:

$$N\lambda = 2nh\cos\varphi - P\frac{\lambda}{2\pi} \qquad \text{.....(8)}$$

bright fringes are produced. N is called the 'fringe order' and can take integral values of 0, 1, 2, ... Destructive interference occurs when:

$$(N + \tfrac{1}{2})\lambda = 2nh\cos\varphi - P\frac{\lambda}{2\pi} \qquad \text{.....(9)}$$

dark fringes are produced.

If λ, φ and P are constant the fringe order is proportional to the optical path difference 2nt. These fringes are called 'fringes of equal thickness'. In other words they form a contour map of the surface, each fringe corresponding to a particular optical thickness. By measuring φ and the fringe order N, and knowing λ and P, this optical thickness can be found. N is usually found by counting up from the zero order fringe, which occurs when the two surfaces are in contact after making allowance for the phase change. The angle φ is not usually measured directly,

but is found from θ by using Snells law:

$$\frac{n_1}{n_3} = \frac{\sin\varphi}{\sin\theta} \qquad \ldots\ldots\ldots (10)$$

This is derived in any elementary textbook on optics. Strictly speaking the passage of the light through the glass plate must be taken into consideration, but because the sides are parallel this has no effect on the angle the beam enters the fluid and hence on the above equation.

A more detailed treatment of interference can be found in the standard texts, such as Tolansky (27) or Francon (28).

Some aspects of interferometry of particular interest to this study are now elaborated.

2.3 Fringe Visibility

The clarity, or contrast in the fringes is usually described as their 'visibility'. Michelson (29) defined it as:

$$V' = \frac{Imax - Imin}{Imax + Imin} \qquad \ldots\ldots\ldots (11)$$

where Imax and Imin are respectively the maximum and minimum intensities of the fringes. If I min = 0 the visibility is unity. If I min = I max the visibility is zero and no fringes will be visible. Obviously the greater the visibility, the clearer the fringes will be. To obtain a good visibility certain interferometric criteria must be met. These are given in the following sections.

2.4 Intensity of Interfering Ray

The resulting intensity of two rays which are coherent (i.e. in phase and of the same frequency), is given by Fresnel's classical formula:

$$I = I_1 + I_2 + 2\sqrt{I_1}\sqrt{I_2}\cos\frac{2\pi\delta}{\lambda} \qquad \ldots\ldots\ldots (12)$$

where I_1 and I_2 are the intensities of the two rays and δ is the path difference between the 2 rays.

Maximum intensities occur for $\cos \frac{2\pi\delta}{\lambda} = 1$ and minimum intensity for when $\cos \frac{2\pi\delta}{\lambda} = -1$. Therefore:

$$Imax = I_1 + I_2 + 2\sqrt{I_1}\sqrt{I_2} \qquad \text{.....(13)}$$

$$Imin = I_1 + I_2 - 2\sqrt{I_1}\sqrt{I_2} \qquad \text{.....(14)}$$

The visibility is:

$$V' = \frac{2\sqrt{I_1}\sqrt{I_2}}{I_1 + I_2} \qquad \text{.....(15)}$$

This has a maximum of one when the intensities are equal. When this is true, the intensity follows a $\cos^2$ law given by:

$$I = \cos^2 \frac{2\pi\delta}{\lambda} \qquad \text{.....(16)}$$

2.5 Coherence

For visible interference fringes to be observed the interfering rays must be mutually coherent. This means that the phase difference of the two beams must be constant in the interference zone. Light consists of wavetrains which are of finite length. If the wavetrains are shorter than the path difference over which the interference is to take place there will be no fixed phase relationship between the two rays and no fringes will be visible. Wavetrains emitted by a source vary in length; hence, the interfering rays may be partially coherent.

If Y is the degree of coherence the Fringe Visibility given in equation (17) becomes:

$$V' = \frac{2\sqrt{I_1}\sqrt{I_2}}{I_1 + I_2} Y \qquad \text{.....(18)}$$

All sources have wavetrains of finite length. Good thermal sources have a coherence length of 10^{-3}m. Laser sources however have a coherence length of several metres.

2.6 Light Source

If an extended source of light is used, consideration must be given to the fact that the light beam will not be completely parallel, and to the path difference introduced by light emitted from various parts of the source. If a laser source is used, however, both of these problems can be ignored, as the light from a laser source is parallel to better than 1 milliradian and can be considered as coming from a point source.

2.7 Surface Roughness

If the local changes in surface roughness are equal to $\frac{\lambda}{4n}$ the dark fringes will become light and vice versa. From this it is apparent that for good fringe visibility the surface roughness must be considerably less than this value.

2.8 Reflectivity

As a direct result from Maxwell's equations, it is easy to show that the reflectivity at normal incidence from a dielectric is given by:

$$R' = \left(\frac{n_1 - n_2}{n_1 + n_2}\right)^2 \qquad \text{.....(19)}$$

where n_1 and n_2 are the refractive indices of the 2 media. As can be seen from this, the greater the difference in refractive index, the greater the reflection. However, the reflectance between even the highest index glass (n = 1.93) and oil under pressure (n = 1.55) is only 1.4%.

Higher reflectances can be obtained by coating the transparent material with thin films of metal or dielectric material. The use of coating is discussed later.

The derivation of equation (19) is done in Jenkins and White (30).

2.9 Anti-Reflection Coating

At a normal air/glass interface about 4% of the light is reflected. When a coherent source of light, such as a laser is used in an optical interference system, these reflections can prove quite disastrous. Reflections from the surface of lenses, and other optical components, can cause unwanted interference patterns to appear in the field of view. To prevent this it is necessary to coat the glass surface with an anti-reflection layer. Such a layer is made by depositing a dielectric on the glass surface. They must have a refractive index n_2 given by:

$$n_2 = (n_1 n_3)^{\frac{1}{2}} \qquad \text{.....(20)}$$

where n_1 is the index of the glass

and n_3 is the surrounding medium, usually air.

The film thickness t of the coating must be given by:

$$t = \frac{\lambda}{4n_2} \qquad \text{.....(21)}$$

The theoretical reason for this is explained in (31). Briefly, however, it can be seen from equation (19) that this choice of refractive indices will lead to equal reflections from the two interfaces. By making the film thickness exactly $\frac{1}{4n_2}\lambda$, the two reflections will destructively interfere (assuming normal incidence) and there will be no reflection from the surface. This destructive interference does not destroy any energy, or lose light. The film can be considered to rearrange the electric and magnetic vectors incident upon it, so that all the incident light is transmitted.

In practice it is impossible to get a film precisely $\frac{1}{4}$ wavelength thick, especially on contoured surfaces, or to have exactly the right refractive index. The reflectivity can be greatly reduced by choosing the nearest material available. If several layers are deposited the reflectivity can be lowered to almost zero.

2.10 Lorentz-Lorenz Relationship

In this work the refractive index of the fluid in the contact is measured. For calculation of the viscosity, the density is required. Fortunately, there is an accurate relation combining the two (32). It reads:

$$\frac{n^2 - 1}{n^2 + 2}\rho = \text{const.} \qquad \text{.....(22)}$$

where n is the refractive index at pressure P

ρ is the density index at pressure P

This is derived from classical electromagnetic theory. It has been experimentally verified for paraffinic oil up to a pressure of 100,000 PSI by Pouther, Richey and Berz (33) to an accuracy within 0.6%. As a point of interest the unusual name of the relation was investigated. The two people responsible for it were H.A. Lorentz (1853-1928), for many years Professor of Mathematical Physics at the University of Leyden, Holland, who was awarded the Nobel prize in 1902 for work on the relations between light magnetism and matter, and L. Lorenz of Copenhagen, who by a strange coincidence derived the same from the elastic solid theory a few months before Lorentz obtained it from the electromagnetic theory. The almost simultaneous publication of their independent work led to both their names being associated with it. The derivation of this formula is done by Dekker (32).

2.11 Dispersion

This is the name given to the variation of refractive index with the wavelength of the light. This effect must be considered if the light is not monochromatic. Usually, however, the amount of dispersion is too small to make any significant difference.

2.12 Birefringence

The optical properties of any body can be described by three refractive indices measured along three mutually perpendicular axes. When they are equal, the material is said to be optically isotropic. Birefringence is defined as the difference between any two of them. Normally liquids are isotropic. It was thought possible that very thin films, particularly under stress might show birefringence. If this happens, the optical thickness becomes dependent on the polarisation of the incident light. The light from a laser is plane polarised by the brewster windows at the end of the tubes. By rotating the plane of polarisation it would be possible to detect any birefringence by a change in the fringe positions. This was done by Westlake and Cameron (5) but no birefringence was ever observed.

2.13 Summary of Criteria for Optical Interference

To obtain useful fringes of maximum visibility the following criteria must be satisfied:

1. The two interfering beams should be of equal intensity.
2. The light source must have a coherence length greater than the path difference between the two beams.
3. The light source must give a beam of light sufficiently parallel so that the path length does not vary significantly for different parts of the beam.
4. The phase change on reflection must either be known, or the system calibrated for it.
5. Surface roughness must be considerably less than a quarter of the wavelength of the light source.

CHAPTER 3

MEASURING THE REFRACTIVE INDEX IN A CONTACT

3.1 Refractometry

Refractometry is essentially the measurement of the ratio of 2 velocities; that of light in the media and in vacuo. In practice this is always done indirectly. Two basic methods of measurement exist, and can be described as either goniometric or interferometric. The former refer to methods which determine the change in direction of a beam of light, whilst the latter determine the retardation of a beam of light resulting from the transmission of light through the medium.

Goniodic Methods

One of the most accurate methods is to measure the deviation of light through a prism made of the medium to be tested. This can easily give results accurate to better than 5 places of decimals. If a liquid is to be tested, a prism is hollowed out, leaving thin, parallel walls and the space filled with it. The disadvantage with this system is that a prism has to be accurately constructed. This can be a difficult process. The method will only give a 'bulk' refractive index and will not detect local variations in either a liquid or solid.

Critical angle systems, where the angle of total internal reflection is measured, are very common. An Abbé Refractometer is an example of this. These methods give a very simple and practical way of measuring the refractive index of either a liquid or a solid. With a liquid only a small drop is required to measure the index and for a solid, one optically smooth face is sufficient. Once again, however, this method is only suitable for measurements of the refractive

index over a comparatively large area. The critical angle method measures the refractive index of the surface and it would not be suitable for detecting changes of refractive index over a small area, especially if the index was varying with time. A complete description of these 2 refractometers is given in Applied Optics and Optical Engineering (34).

Interferometric methods

These usually work by splitting a beam of light into two and then recombining them to give interference fringes. If a known thickness of the medium to be measured is placed in one of the beams then by counting the number of fringes the interference pattern is changed, the refractive index can be determined.

Typical examples are the Jamin and the Michelson refractometers (35). The obvious disadvantage of this system is that the thickness of the medium must be known. It again only gives an average, or bulk refractive index.

An ingenious method of measuring both film thickness and refractive index has recently been described by Israelarchrili (36). This method uses transmission fringes of white light and compares the displacement of odd and even fringes as the film thickness is changed. It is only valid unfortunately for film thicknesses of less than 300^{o}A.

Ellipsometry is an extremely elegant method for measuring the refractive index and film thickness of thin films. In its simplest form, it works by measuring the ellipticity of a beam of initially plane polarised light after it has been reflected by the thin film. Again this can only be done over comparatively large areas.

The Schlieren technique uses the diffraction of light to show up changes in the refractive index. It is used mainly in

situations such as Wind Tunnels and would not be suitable to detect changes in very small thicknesses of films as the sensitivity is not great enough.

3.2 A New Technique for Refractive Index Measurement

What is needed is a simple and accurate method of measuring the refractive index and optical thickness of a film of oil from $0 \rightarrow 3 \times 10^{-6}$ m thick over an area of about 10^{-8} m^2. None of the standard methods of measuring the refractive index met these requirements and so a new technique had to be developed.

After careful consideration and consultation with Dr. Welford of the Technical Optics Section of Imperial College, it was decided to attempt this by comparing the interferometric fringes obtained from light incident at two different angles. This has the advantage of giving both the refractive index and the absolute film thickness. The theory of the method is given below.

If the interference pattern is measured at two different values of θ (see Fig. 2) and the fringe order counted at a given position then from equation (8) (ignoring phase change):

$$N_1 \lambda = 2 n_3 h \cos \varphi_1 \qquad \text{.....(23)}$$

$$N_2 \lambda = 2 n_3 h \cos \varphi_2 \qquad \text{.....(24)}$$

and from equation (9):

$$\frac{\sin \varphi_1}{\sin \theta_1} = \frac{1}{n_3} \qquad \text{..... ..(25)}$$

$$\frac{\sin \varphi_2}{\sin \theta_2} \quad \frac{1}{n_3} \qquad \text{.....(26)}$$

Where the suffixes 1 and 2 refer to measurements made at θ_1 and θ_2 respectively.

From (23) and (24) we have:

$$\frac{N_1}{N_2} = \frac{\cos \varphi_1}{\cos \varphi_2} \qquad \text{.....(27)}$$

Using (25) and (26) to eliminate cos φ_1 and cos φ_2 in (27) and rearranging gives:

$$n_3^2 = \frac{N_1^2 \sin^2 \theta_2 - N_2^2 \sin^2 \theta_1}{N_1^2 - N_2^2} \qquad \text{.....(28)}$$

It can be seen that by measuring the angles of incidence of two beams and by counting the resultant fringe orders in each pattern at a given position it is possible to solve for the refractive index. Once this has been done either equation (23) or (24) can be used to obtain the absolute film thickness.

3.3 Test Apparatus Design

It was decided to check the theory described in the previous section by building a test apparatus.

The most important decision to be made in the design of this apparatus was on the optical system to be used.

Optical System

The first choice to be made was whether to use a monochromatic or white light source. For white light fringes, the maximum thickness of film that can be measured is about 10,000°A. Above this thickness the coloured fringes are so narrow and close together that to the eye they give apparent white light fringes. These are called "White of Higher Order". This difficulty can be surmounted by using a spectrometer to detect the bands. This has been done, for instance, by Higginson, G.R. and Read, S. (Ref. 38). This would be a difficult technique to use in a time dependent problem such as a dropping ball. Monochromatic fringes from a coherent source can measure much thicker films. The only limit being on the coherence of the light, which from a laser source can be several metres. The fringes produced by a monochromatic source

are easily measured, and are not dependent on the colour discrimination of the observer, a feature of white light fringes. They have the disadvantage that they only give measurements at discreet intervals, about every 2200^{o}A in a typical case. As the films to be measured were up to 30,000^{o}A thick and the profile would vary smoothly, this was not thought to be a significant disadvantage. A monochromatic light source was therefore chosen. The next decision to be made was on how to obtain reflection from the two surfaces so as to obtain useful fringes (see section 2.13).

In previous work various methods have been described to produce good interferometric fringes. Cameron and Gohar (26) used a polished steel ball and a high refractive index glass (1.91). The fringe visibility with this system was very low as the reflectance of the steel ball in oil was about 50% and of the glass only 1.2%. The two beams were therefore of widely different intensities.

Wedevern and Cameron (39) and Foord and Cameron (2) both used chrome deposited layers on the flat glass surface. This enabled them to choose optimal reflectivities for maximum visibility and so gave much better fringes than Gohar and Cameron. The disadvantages of the chrome layer were that it has quite a high absorption and the phase change on reflection is an unknown function of the angle of incidence.

Westlake and Cameron (5) used dielectric layers. These work in a reverse way to the anti-reflection layers described in section 2.9. Very high reflectivities with very low absorption can be obtained with this method. This results in very sharply defined maxima of fringe intensity, or in other words very narrow fringes.

In all the previous work only one beam of light, which was

at normal incidence, had been used. To test the theory, however, it was necessary to measure the fringes at two different angles. This ruled out dielectric coatings as the reflectivity is only a maximum for one angle and falls off rather rapidly at others. Chrome layers, which gave a 20% reflectance at normal incidence which is the optimum when used in conjunction with a steel ball, would be far too highly reflecting at 45^{o}. The phase change on reflection from the chrome layer is an unknown and would be a function of angle. This would be difficult to calibrate to enable absolute measurements to be made.

Eventually, a novel method of obtaining the required reflectivity was conceived. The reason for having a coating on the glass plate is so that the reflectivity matches that of the highly reflecting ball, but if the ball is made of uncoated glass, which has a much lower reflectivity, this is not necessary. By doing this and leaving the surface of the plate uncoated, the reflectivity from each surface is exactly equal. This follows directly from the symmetry of Maxwell's equations (see section 2.8).

The reflectivity is due to the difference in the refractive index of the oil and glass and so by using either a high or low refractive glass the full range of oils can be covered. The absorption of the glass is very low and so this means that the two beams reflected back are of virtually equal intensities. One of the requirements for fringes of good visibility.

The phase change of light reflected from glass in air has been found to be exactly π, and it has been generally accepted that this is not affected by oil instead of air (39). This was substantiated by the initial calibration experiments. To compensate for the lack of reflectivity from the glass-oil interfaces a

3 mW Helium-Neon Laser light source was used. This gave a beam parallel to better than 1 miliradian. The glass surfaces were polished to be optically smooth. The system then satisfied all the criteria listed in section 2.13. The fringes produced by this optical system are essentially two beam fringes. The intensity of the fringes therefore varies according to the square of the cosine of the phase difference of the two beams. Multiple Beam Interferometry, which requires very high reflectivities produces much sharper fringes. The accuracy with which the centre of the 2 beam fringe or the multiple beam fringes systems could be measured was not found to significantly differ. The greatest error in measuring the refractive index and absolute distortion comes from interpolating between each fringe maxima.

Mechanical System

This apparatus was constructed to test the theory before a rig was made to study oil entrapments. For this reason it was kept as simple as possible. Rather than design a complicated mechanical system to vary the angle of the incident light the whole apparatus was mounted on a spectrometer table, which also made the measurement of θ a very easy process.

3.4 Test Apparatus

The apparatus is shown in Fig. 3.

The spectrometer table could be rotated, to vary the angle of incidence (θ) of the incoming beam. The resultant fringes were viewed with a microscope attached to one of the arms of the spectrometer. Originally the fringes were measured with a filar eyepiece, but later it was found more convenient and accurate to photograph them. To do this a Pentax 35mm camera was attached to

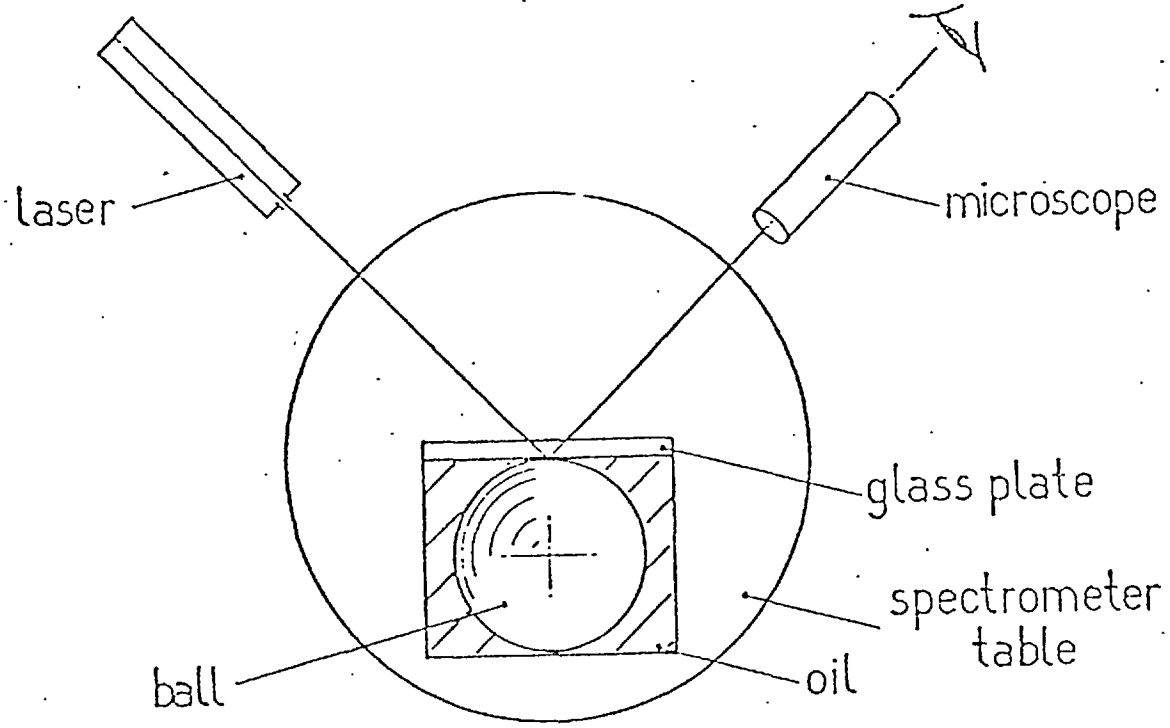

EXPERIMENTAL APPARATUS

TO TEST REFRACTIVE INDEX DETERMINATION

FIG. 3

the end of the microscope tube. The ball was mounted concentrically with the spectrometer table so that the reflection of the laser beam was always in line with the microscope.

3.5 Method

The ball was pressed against the glass plate and the microscope rotated until the interference pattern produced by light reflected from the ball and plate was in view. A photograph of the fringe pattern was then taken. The spectrometer table was then rotated to obtain a different value of θ and the process repeated. The angle θ was found by measuring the angle the spectrometer table had to be rotated through, so that the image of the laser beam was reflected normally by the glass plate.

From the photographs the fractional fringe orders at given radii from the centre were measured by drawing a graph of fringe order against the radius, and extrapolating between the points. The values were then substituted in equation (28) to find the refractive index.

3.6 Results

The oil was at atmospheric pressure, and so the results obtained experimentally could be compared with those measured with an Abbé refractometer. There appeared to be little correlation; for an oil of refractive index of 1.4, results between 1.3 and 2.5 were obtained. Even air showed an index of about 1.4, which varied from day to day.

Months of work followed these continual failures, to determine their cause and eventually the reasons for these anomalous results were run to earth. The cause was as follows:

When the fringes were viewed at different angles the focus of the microscope had to be adjusted to allow for the variation of optical path length due to the light having to travel obliquely through the glass plate. It is impossible to see, just by looking at the fringes, whether or not they are in focus. This is because fringes produced with a laser light source are almost completely non-localised. Putting this in other words, they appear wherever in space the beams from the two surfaces cross - one of the effects caused by the extremely long coherence length of the laser light. The fringes being viewed were formed by an expanding spherical wave from the ball and plane wave from the glass plate. As the spherical wave expands the apparent size of the fringes increases (see Fig. 4). To measure the true image size the microscope must be focussed at the interface between the two surfaces. (The separation of the surfaces being negligibly small).

When this fact was realised, a vertical line was deposited on the glass to focus the microscope on. This helped but the results were still not very accurate. It was then realised that looking through a glass plate introduces astigmatism. This means that the focal distance is different in the horizontal and vertical planes. The microscope was being focussed on a vertical line, but the fringes were being measured in a horizontal plane. This error was cured by depositing a scale with horizontal lines.

When the experiments were repeated with the focussing lines the results were much better. The experimental accuracy was now limited by the accuracy the fringes could be measured, for a given pair of angles.

The accuracy could be improved by increasing the difference between the fringe orders N_1 and N_2. This can be done by increasing

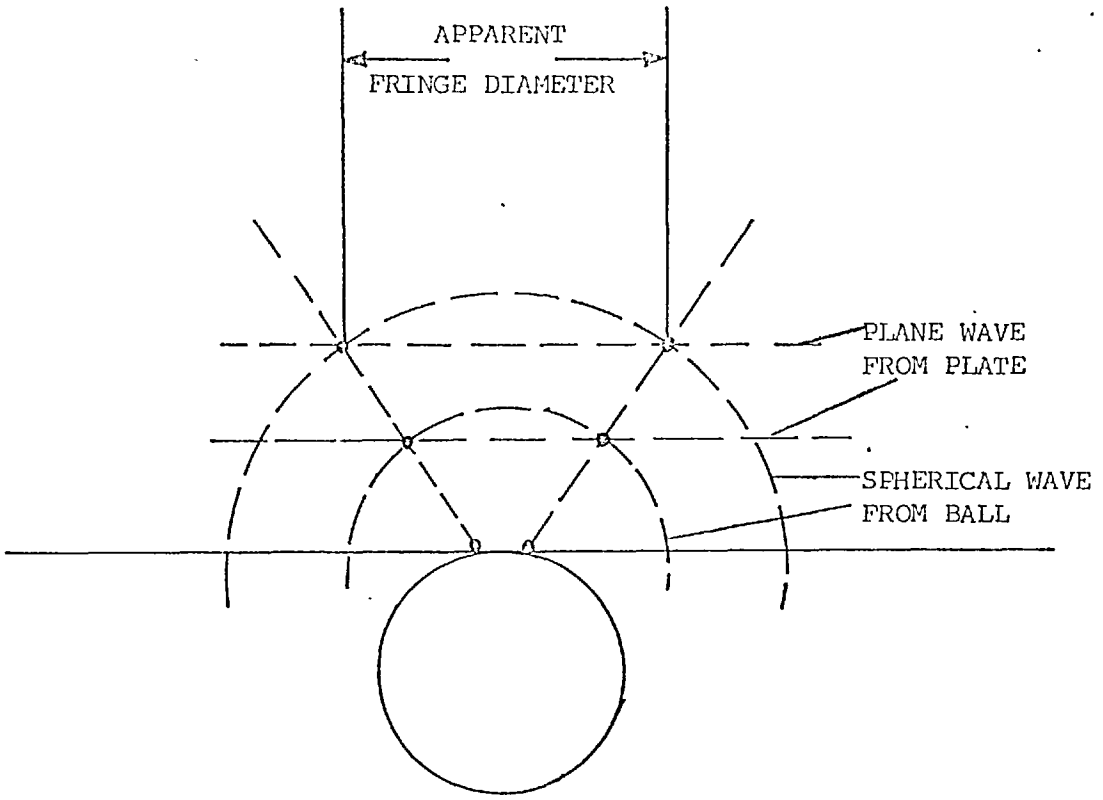

DIAGRAM SHOWING THE IMPORTANCE OF CORRECT FOCUSSING

FIG. 4

the separation between φ_1 and φ_2. However, if φ_2 is increased too much the spacing between each fringe becomes excessive. The optimum angles for φ_1 and φ_2 proved to be $\varphi_1 = 0$ and $\varphi_2 \approx 45^\circ$. Using a flat plate this angle for φ_2 was impossible to reach as it made θ_2 imaginary.

By Snell's Law, $\frac{\sin \theta}{\sin \varphi} = n_3$

If $\varphi = 45^\circ$ and $n_3 = 1.5$,

$$\sin \theta = 1.06.$$

However, if a hemispherical piece of glass was substituted for the front plate an angle of 45° for θ_2 could easily be achieved.

The smallest angle for θ_1 that could be reached without going to a complicated optical system with semi-reflecting mirrors was 8°.

However, as can be seen from equation (23):

$$N_1 \lambda = 2 n_3 h \cos \varphi_1$$

this only changes N_1 by a factor of $\frac{\cos 0^\circ}{\cos 8^\circ} = 1.01$ which makes a negligible effect on the difference between N_1 and N_2.

The hemisphere slightly changes the formula for calculating the refractive index. Using as before Snell's Law, and the standard equation of interference (see Fig. 4):

$$2 n_3 h \cos \varphi_1 = N_1 \lambda \qquad \text{.....(29)}$$

$$2 n_3 h \cos \varphi_2 = N_2 \lambda \qquad \text{.....(30)}$$

$$\frac{n_3}{n_2} = \frac{\sin \theta_1}{\sin \varphi_1} = \frac{\sin \theta_2}{\sin \varphi_2} \qquad \text{.....(31)}$$

where the symbols have their previous meanings.

Substituting for $\cos \varphi_1$ and $\cos \varphi_2$ and rearranging gives:

$$n_3^2 = n_2^2 \left(\frac{N_1^2 \sin^2 \theta_2 - N_2^2 \sin^2 \theta_1}{N_1^2 - N_2^2}\right) \qquad \text{.....(32)}$$

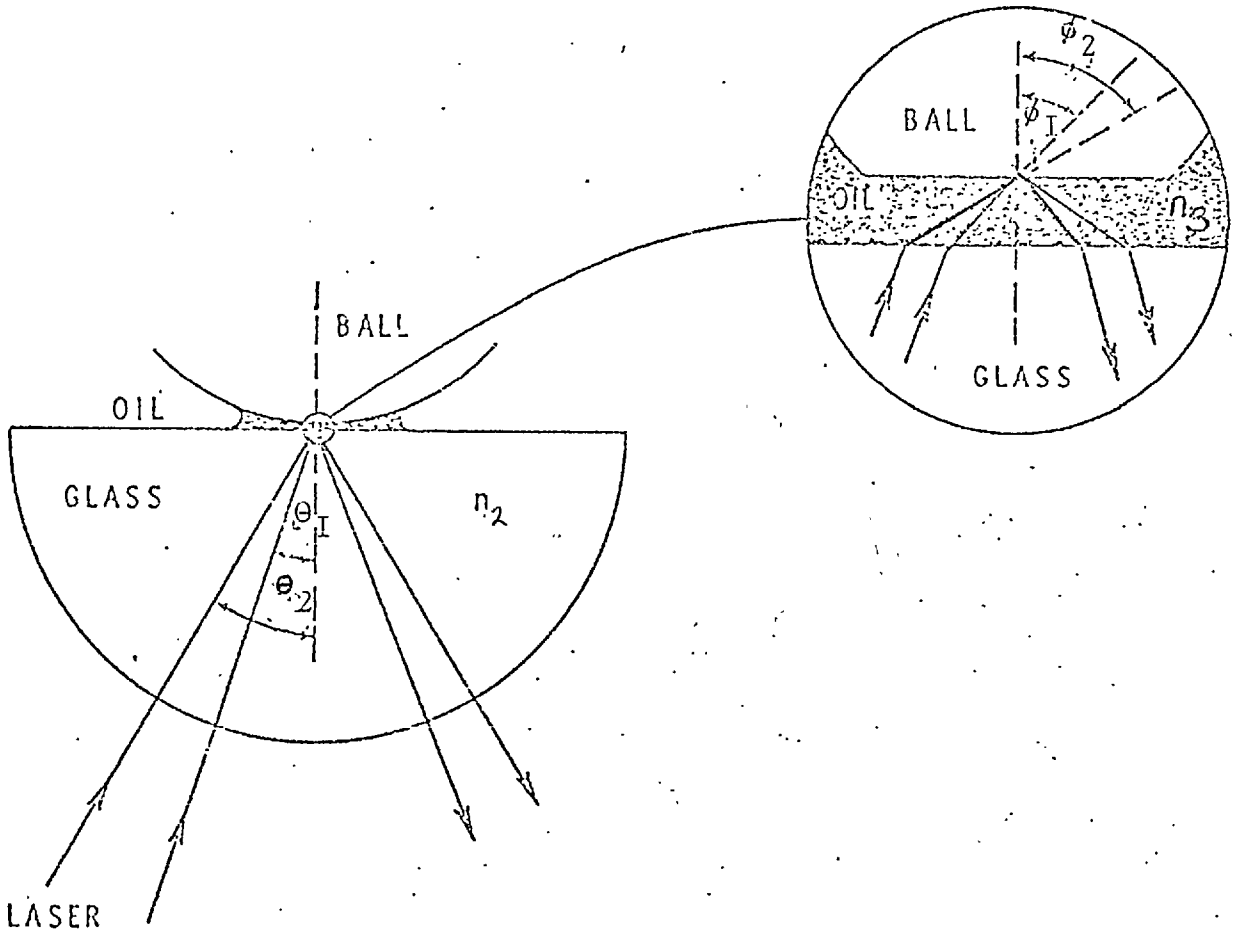

DIAGRAM OF HEMISPHERE TO REPLACE THE FRONT PLATE

FIG. 5

so provided that n_2, the refractive index of the glass is known, the index of the film can be found by measuring N_1, N_2, θ_1 and θ_2. The experiment was repeated using the modified apparatus. The measured values of the refractive index were now very close to the correct values, the accuracy being greatly improved with the hemisphere. This is shown in Fig. 6, where the calculated refractive index is shown at several different values of N_1 and N_2.

3.7 Conclusions on the New Refractive Index Measurements

A completely new technique has been developed to measure simultaneously the refractive index and film thickness to a high degree of accuracy for any thickness greater than 2×10^{-7}m. This is the first time that this has been achieved. The technique is simple and should prove very useful for future optical measurements of thin films under high pressures. Using this it should be possible to examine a rolling contact and obtain sufficient detail to 'see' the pressure spike theoretically predicted but as yet un-observed. The work was not directed to this goal as it was realised that the apparatus could be used as a high pressure viscometer, which will be discussed later.

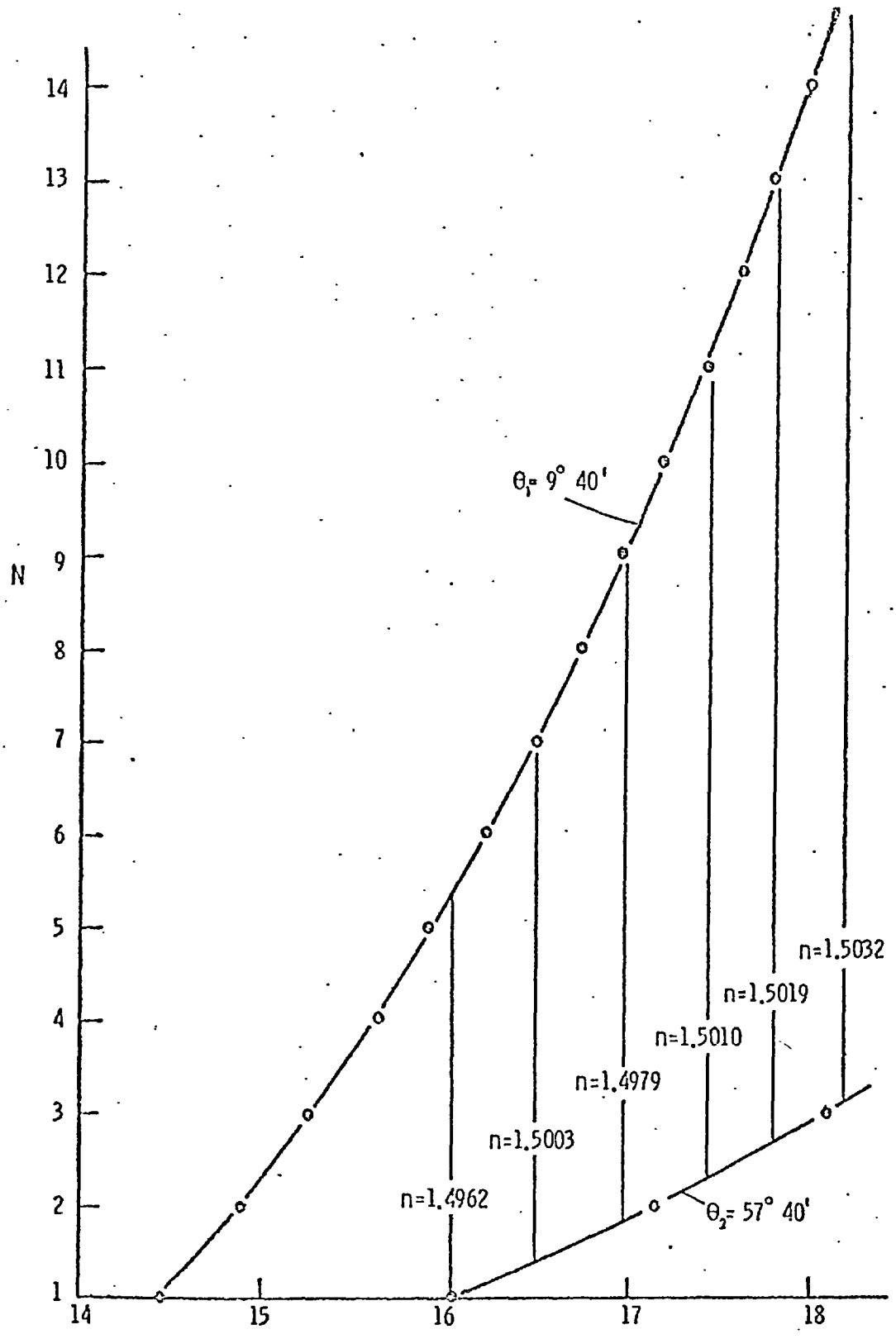

Graph of N (fringe order) Plotted Against D (fringe diameter) in Arbitrary Units

FINAL RESULTS WITH TEST APPARATUS USING OIL OF 1.501 REFRACTIVE INDEX

CHAPTER 4

EXPERIMENTAL APPARATUS AND PROCEDURE

4.1 Introduction

At this stage of the work there existed a reliable and accurate method of measuring the refractive index and the film thickness of a fluid over a small area. A modified apparatus was now designed to measure an oil entrapment. These are pools of oil trapped inside the contact area when a ball is dropped onto a flat surface. A cross-section of an entrapment is shown in Fig. 7. Note that the magnification in the x direction is about 100 times less than in the y direction. Also all the distortion is shown in the ball, in practice both surfaces are distorted, but it is more convenient to show all of it in one surface. Many factors influence the actual size of the entrapment. The most important ones are the load, the approach velocity, elasticity and radii of the surfaces and the pressure viscosity characteristic of oil concerned. A typical size for a glass ball dropping on a glass flat from 3×10^{-3}m with viscous oil would be about 3×10^{-4} m diameter and with a depth of 3×10^{-6}m. As the fluid escapes from the edge of the entrapment, both the shape and the refractive index will change. The system described in the previous chapter had to be modified so that the fringes could be measured simultaneously at the two angles. To allow the ball to fall in a vertical plane, the apparatus had to be turned through 90^{o}. The basic optical system, using uncoated glass surfaces was still retained and after a considerable period of development and testing the following apparatus was built to study entrapments.

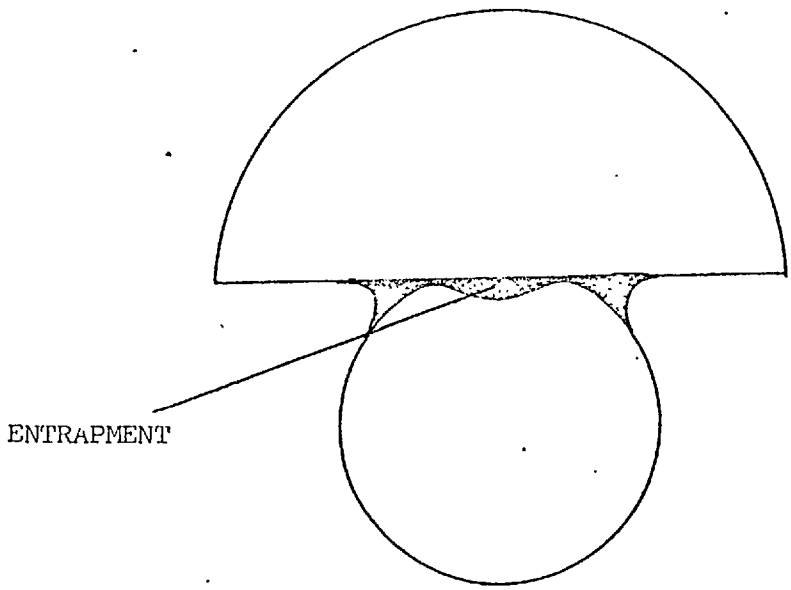

CROSS-SECTION THROUGH A TYPICAL ENTRAPMENT

(THE DEPTH IS GREATLY EXAGGERATED)

FIG. 7

4.2 Apparatus

Photographs and a diagram of the apparatus are shown in Figs. 8, 9 and 10.

The velocity of the ball could be measured by means of the magnetic bar, which as the ball dropped, produced an E.M.F. in the coil. This E.M.F. was proportional to the velocity of the ball, and was recorded on a U.V. recorder.

The ball could be released by withdrawing pin A which was achieved by switching on the magnetic coil.

The load on the ball could be varied by changing the weights at B. The dashpots were added to slow down the ball, to prevent surface damage and bouncing, which is elaborated on later.

The ball and hemisphere were both made of extra dense flint glass, index 1.742. The surfaces were optically smooth. The hemisphere had two photographically deposited scales lines 6.9×10^{-4} m apart, symmetrically about the centre of the flat surface. The outer surface was coated with an anti-reflection layer.

The ball was fixed in an aluminium cylinder. This was mounted symetrically above the hemisphere which was cemented onto a fixing plate. Both ball and the hemisphere were readily removed for ease of cleaning.

The optical system to obtain an image at two angles simultaneous took a great deal of development work. The final system adopted is as shown in Fig. 9. For some of the high speed cine photography a second laser was used instead of the beam splitter, to increase the illumination.

The incident beam was divided by the beam splitter, and about 90% of the beam was directed onto the entrapment at an angle

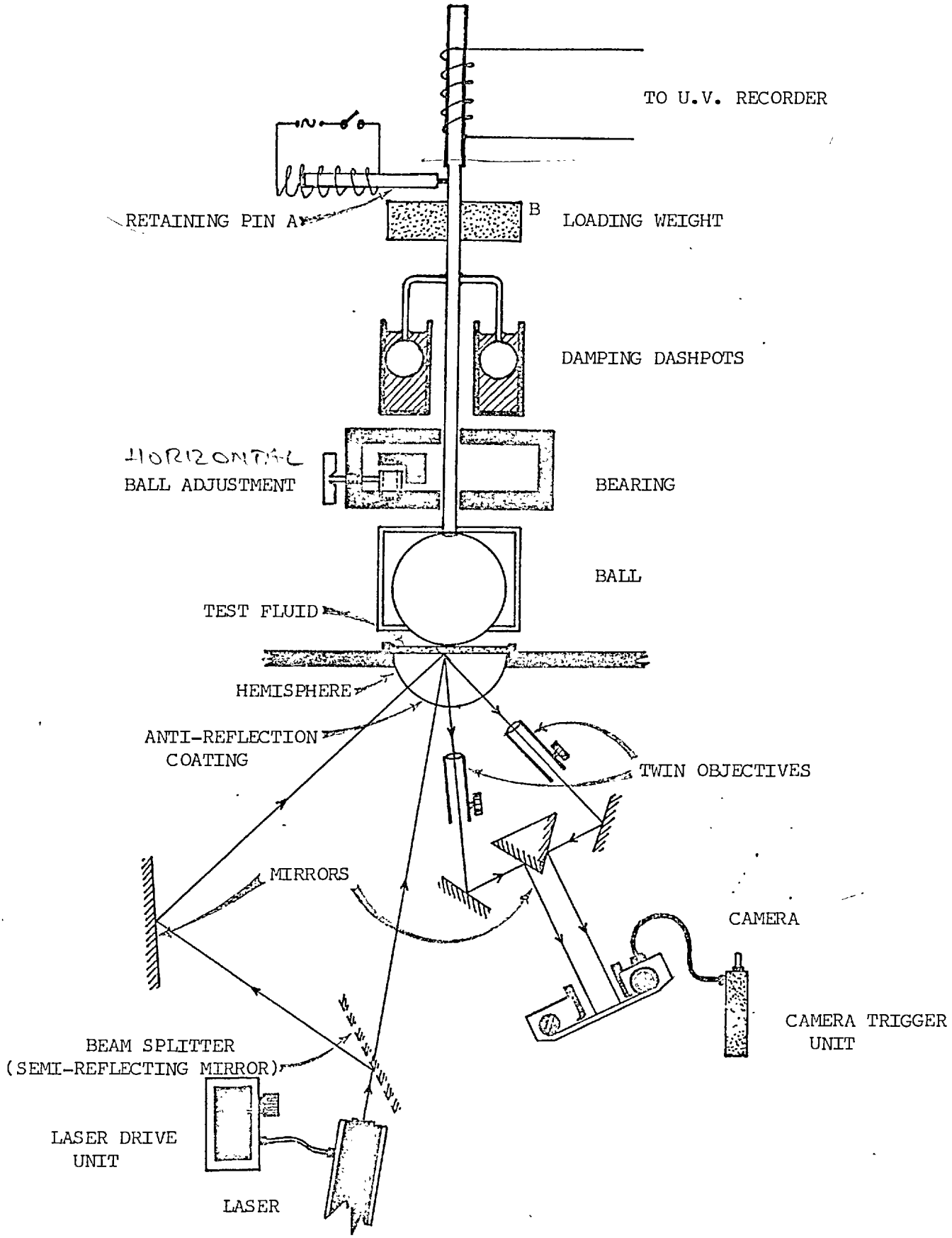

SCHEMATIC DIAGRAM OF THE EXPERIMENTAL APPARATUS
FIG. 8

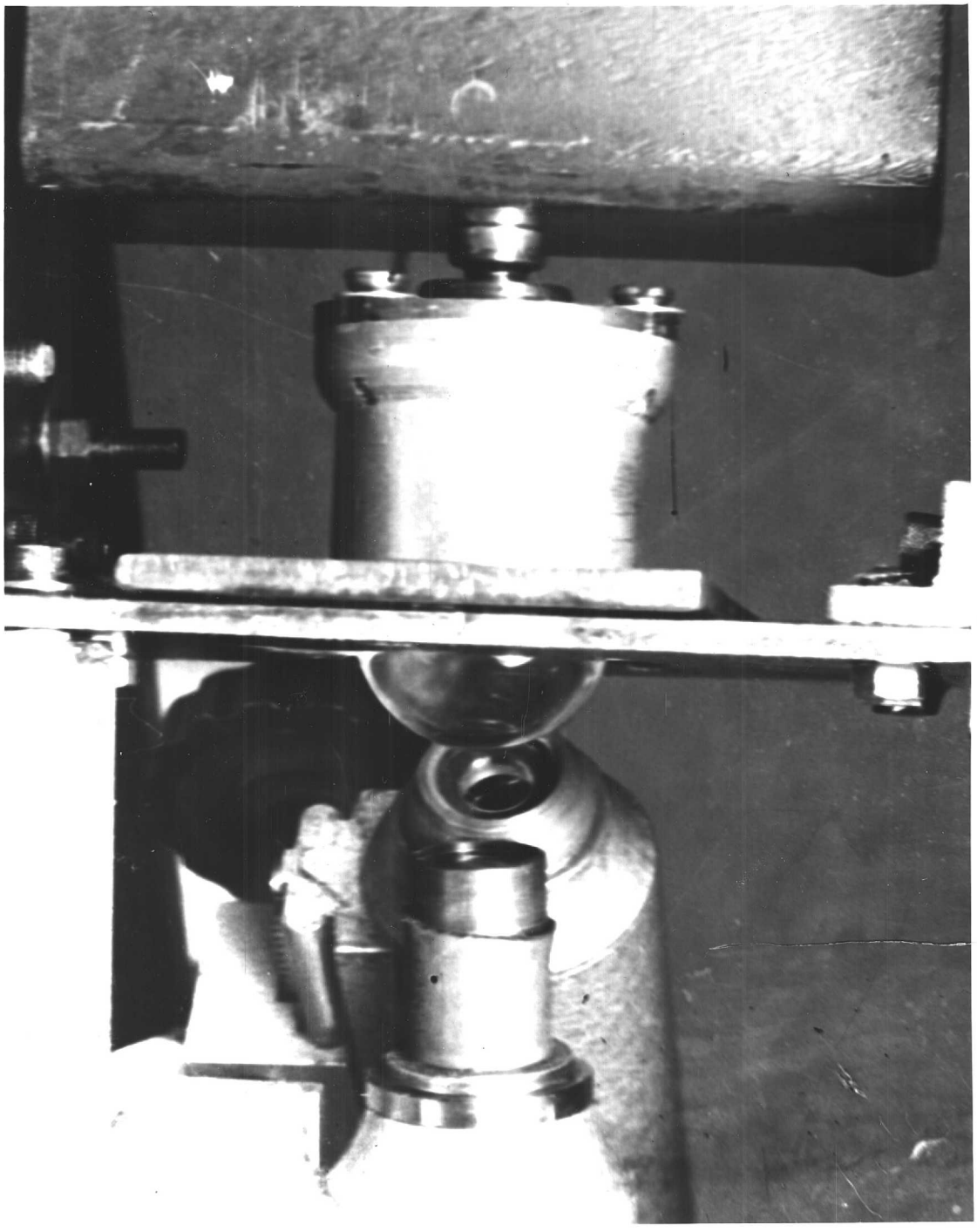

CLOSE UP OF BALL IN HOLDER, RESTING ON HEMISPHERE

FIG. 9

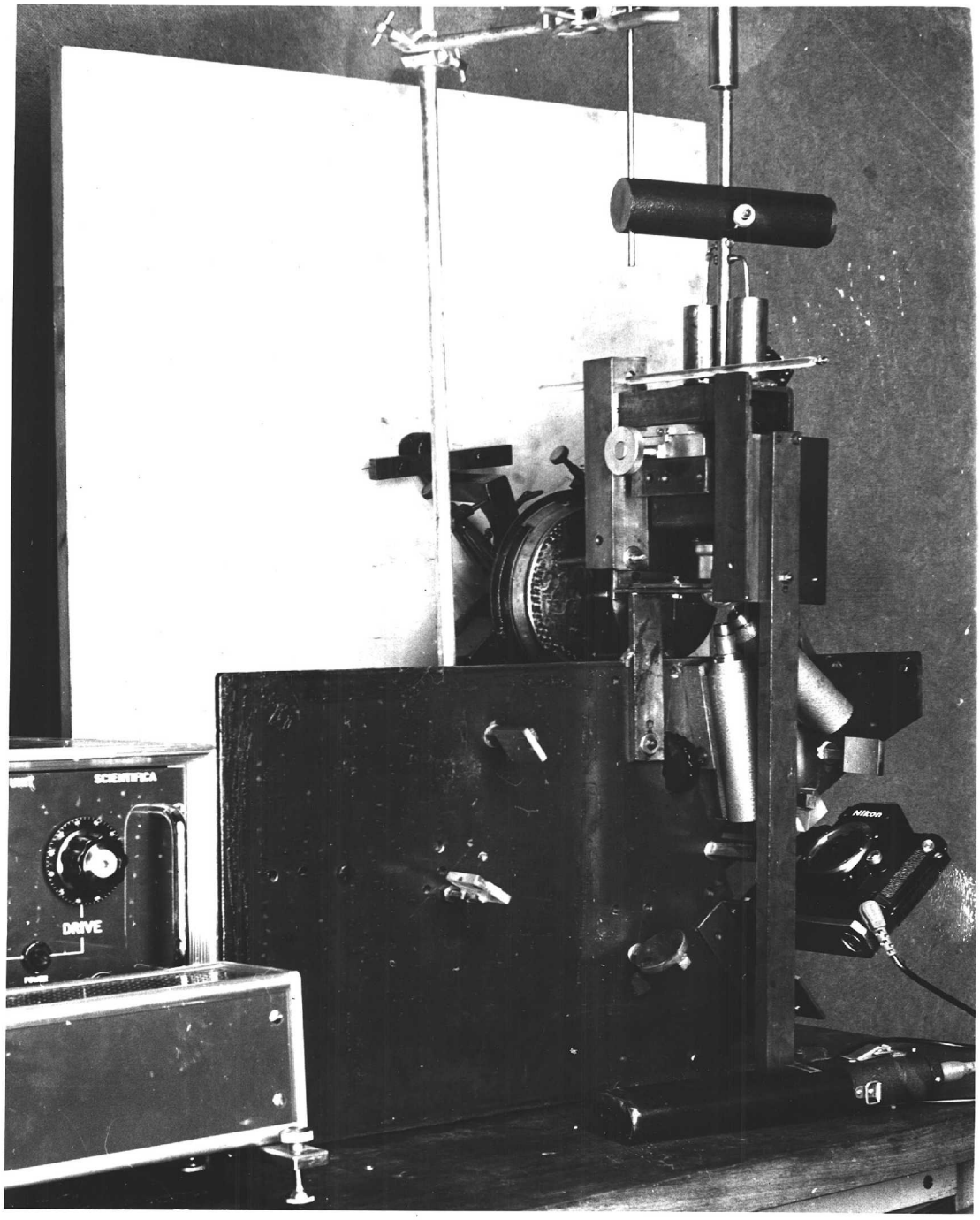

PHOTOGRAPH OF THE EXPERIMENTAL APPARATUS

FIG. 10

of about 8^{o} and the rest was directed in at about 47^{o}. This difference being to correct for the greatly increased reflectivity of glass at 47^{o} compared to 8^{o}. Originally, θ_2 was made to be 45^{o}, but it was found that the part of the beam which went through into the ball was reflected back onto the entrapment and destroyed the interference fringes.

The emerging beams were focussed by the means of two identical x5 objectives. The images were then reflected by the optical system shown, so that the two images were side by side on the viewing screen of the camera. The objectives could be moved independently to focus the images and could be locked into position to ensure that the images remained exactly in focus. The path lengths of the two beams was kept equal, so that the magnification would remain equal. To eliminate any possible distortion by an eyepiece, the images were formed without using one.

The optical system was left without a light-proof cover. This was so as to avoid the complicated bellows arrangement that would have been necessary to allow for focussing of the microscopes. For this reason the experiments were carried out in subdued lighting. Total darkness was not required as the exposure times of the camera were less than $\frac{1}{250}$ sec.

Initially, a motorised Nikon F was used, which took pictures at the rate of 3 per second, but for some of the later work on the formation of entrapments, it became necessary to use a camera with a faster framing speed. The ideal camera was found to be a 16mm Miliken. This had a framing speed of 400f.p.s. This stopped the film at each frame as opposed to faster cameras which use rotating prisms and so do not give such good picture definition. The time interval between each picture was found from the reciprocal

of the framing speed. For the Nikon this speed was checked by measuring the time for 36 frames to be taken. This cameto 12 $\pm$ .1 seconds. With the Miliken the camera had a marker which exposed a dot on the film 100 times a second. It was found with this that the speed of the Miliken was 400 $\pm$ 1 f.p.s. When focussing with the Nikon F, the image on the ground glass screen was enlarged with a low power microscope, to increase the accuracy of focussing. The Miliken had a built-in optical system to magnify the image size. The only disadvantage being that the image could not be viewed after the film was loaded in the camera.

4.3 Experimental Procedure

The hemisphere and ball were thoroughly cleaned in an ultrasonic cleaner and then were put back in position. A few drops of the fluid to be tested were placed on the centre of the hemisphere. Measurements could be made with much smaller quantities of fluid if necessary. The ball was then allowed to rest on the hemisphere, and weights were added to provide the required load. (Usually between 1 and 3 kilograms).

The images of the scale were then very carefully focussed on the screen of the camera. This was extremely critical, as a small error could lead to large errors in the results. When the focussing was achieved the objectives were locked into position. The ball was left resting on the surface, in case any distortion, caused by the loading, affected the focus.

The ball was raised about 0.004m from the surface of the hemisphere and locked into position by the locating pin A. If the approach velocity of the ball was to be measured, the U.V. recorder was switched on. The camera was started and the pin removed to allow the ball to drop. For the Miliken, a couple of seconds had to

be allowed for the camera to build up to its full framing rate.

The length of time the camera was left running depended very much on the fluid under test. For some fluids all trace of an entrapment had disappeared after less than 1 second. Where as for others they were still apparent after 5000 secs. The Miliken camera had to be left running for the whole period of the measurements as it could not be stopped and started instantaneously and also its shutter speed is a function of its framing speed. This limited the time for which an entrapment could be photographed. With this camera it was about 25 secs., the maximum film capacity being about 150m. With the Nikon camera it was possible to run the camera continuously for the first part of the entrapment and then take pictures at any set interval. This had to be done by pressing the firing button of the camera continuously for the first part and then at discreet intervals which were timed with a stop-watch.

With the Nikon camera H.P.4 film was used, which required a shutter speed of about $\frac{1}{250}$ seconds. The Miliken running at 400 f.p.s. had a shutter speed of $\frac{1}{2500}$ seconds and so a much faster film was required. Eventually the most suitable film was found to be Kodak 2485 recording film, combined with maximum development. For any faster shutter speed it would have become necessary to increase the intensity of the fringes as this was the fastest film available. There were problems with loading the camera with this film as it was so sensitive that the normal procedure of loading the camera in subdued light could not be used. It was found necessary to open the spool in complete darkness and then seal the spool again leaving a few feet of the film trailing. The camera could then be loaded in the normal way until the last stage when the spool had to be mounted in darkness.

The magnitude of θ_1 and θ_2 were found by measuring the angle through which the upper half of the apparatus had to be rotated for beams to be reflected normally by a mirror, which was put in place of the hemisphere. The upper half was mounted on a spectrometer table so that the angle it was rotated through could be accurately measured to within $\pm$ 10 seconds of arc.

The ambient temperature was measured by a conventional mercury thermometer.

The deeper the entrapment was, the smaller the percentage errors in measuring it were. For this reason the conditions were varied to try and optimise the entrapment size for each fluid tested. It was found that increasing the load from a low value would increase the size up to some critical weight. Above this the entrapment would seem to get smaller and sometimes damage to the glass surface would result. It was found eventually that this was due to the ball bouncing away from the surface (see section 6.6). This bouncing could be reduced by damping the motion of the ball using the dashpots. By varying the damping with different dashpots, larger entrapments were formed, although no quantitative relationship could be found between the various parameters and entrapment size.

The load, damping and also the height the ball was dropped from, were all varied until a reasonable sized entrapment was obtained. It was found that only for relatively viscous oils was it possible to obtain large entrapments. The thinner oils formed entrapments of such shallow depth that only one or two fringes would be visible, and no useful measurements could be made.

Analysis of the Photographs

The following analysis assumes that the entrapments are

symmetrical around an axis passing through the centre of the ball. This was found to be valid, as long as the ball dropped perpendicularly to the surface and there were no particles of dirt or scratches on the glass. The apparent a-symmetry in the photographs is, of course, due to the cosine term introduced from the oblique view of the fringes.

A photograph of an entrapment is shown in Fig. 12. This was taken with a high viscosity cylinder stock (BP 1065) designated as fluid 1, at 23°C and a load of 2 kilograms. The picture was taken 2 seconds after the entrapment formation. The left hand side shows the fringes photographed at 8° and the right hand side shows the same entrapment at 47°. The fringe diameters along AB and CD were measured with a travelling microscope from the prints. For some of the results a densitometer, which plots the density of the negatives as a function of distance, was used. This was found to be unnecessary as the microscope gave sufficient accuracy. When the Miliken was used, the fringes were measured directly from the negatives with an analyzer. This projects the image onto a screen which has an X, Y measuring grid and with this the fringes can be measured to very high accuracy. The fringe diameters were then plotted against fringe orders. A typical plot is shown in Fig. 11.

From this graph the fractional fringe orders at θ_1 and θ_2 were read off at given values of the diameter D. Due to the symmetry of the entrapment this gives the fringe order corresponding to the same position and therefore film thickness at both angles. The diameters of the fringes were converted from arbitrary to absolute units by multiplying by the magnification. This was found by comparing the separation of the two scale lines on the photograph and their absolute separation which was measured very accurately before the

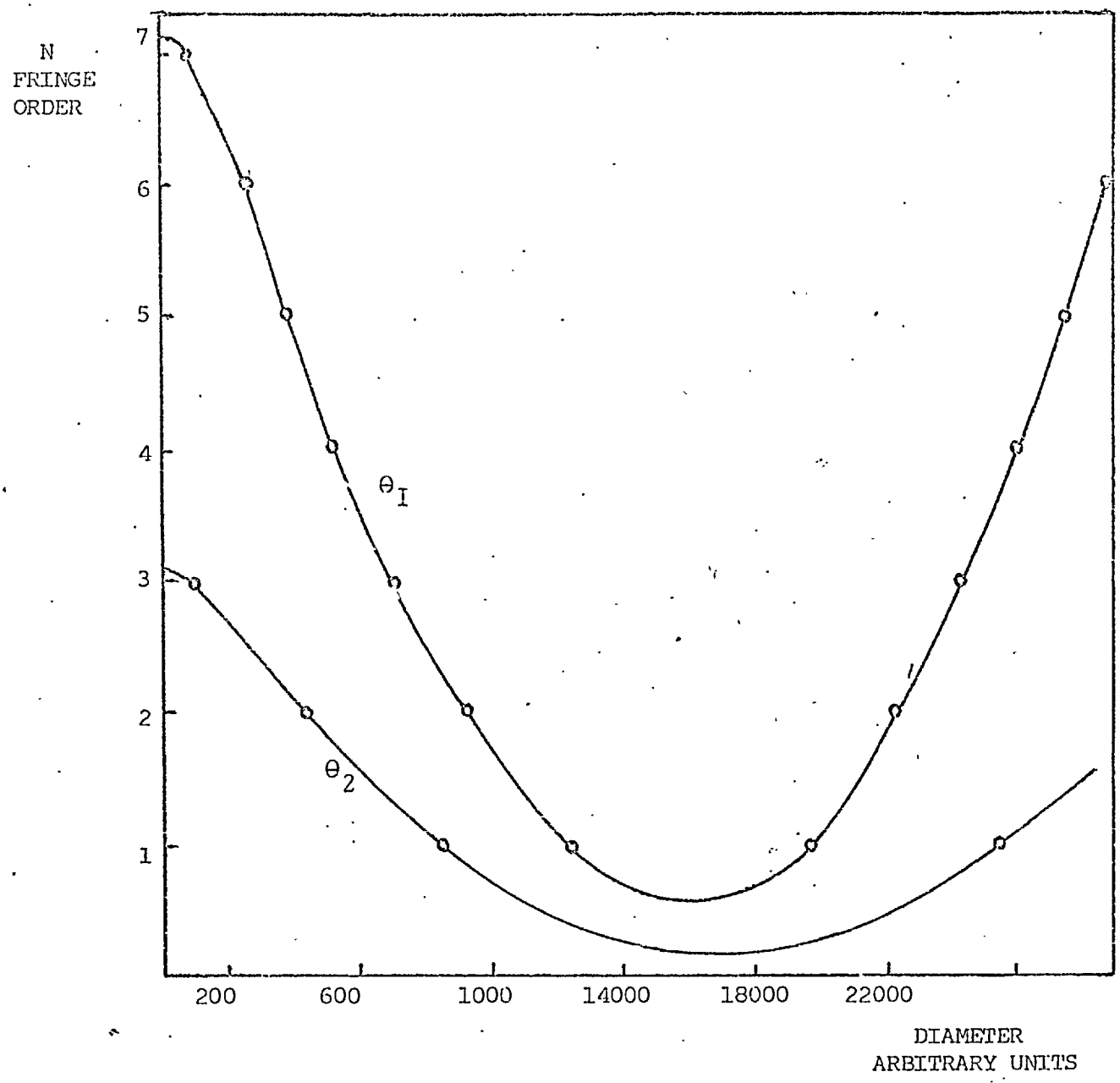

TYPICAL GRAPH OF FRINGE ORDER

AGAINST DIAMETER AT θ_1 AND θ_2

FIG. 11

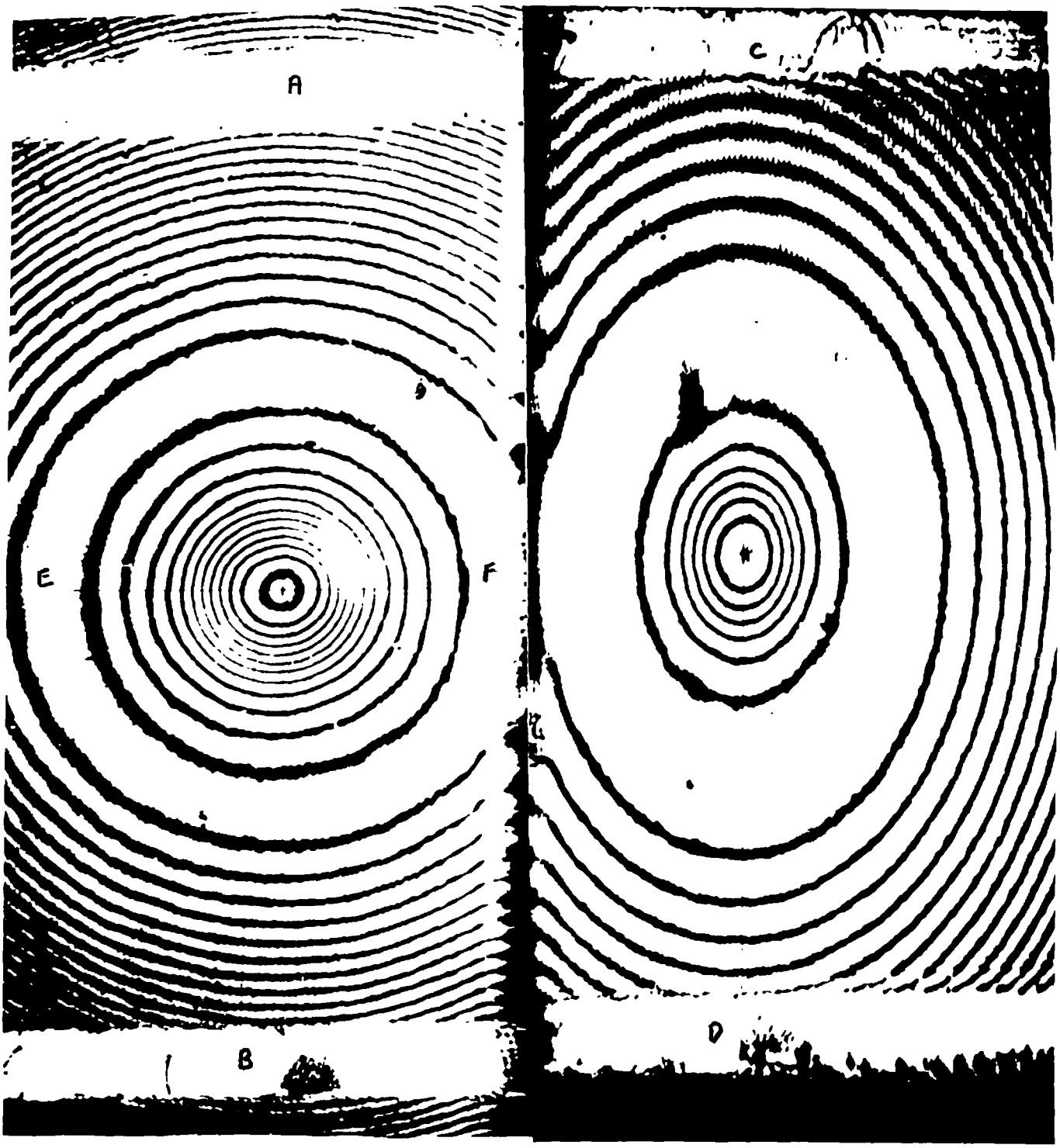

PHOTOGRAPH OF INTERFERENCE PATTERN
FOR AN ENTRAPMENT WITH FLUID 1

MAGNIFICATION x 237

FIG. 1?

experiment with a travelling microscope.

Equation (21) is the governing equation from which the refractive index is derived. It is:

$$n_3^2 = n_2^2 \left(\frac{N_1^2 \sin^2 \theta_2 - N_2^2 \sin^2 \theta_1}{N_1^2 - N_2^2}\right) \quad \ldots\ldots\ldots(21)$$

By substituting in for these measured quantities the refractive index inside the entrapment was found and hence the absolute film thickness from equations (29) and (30):

$$2\, n_3 h \cos \varphi_1 = N_1 \lambda \quad \ldots\ldots\ldots(29)$$

and

$$\frac{n_3}{n_2} = \frac{\sin \theta_1}{\sin \varphi_1} \quad \ldots\ldots\ldots(30)$$

therefore

$$h = N_1 \lambda \frac{1}{2\left(n_3^2 - n_2^2 \sin^2 \theta_1\right)^{\frac{1}{2}}} \quad \ldots\ldots\ldots(33)$$

A computer programme was written to calculate the refractive index and absolute thickness by substituting in the measured fringe orders and angles. The wavelength of the laser beam was 6328A°.

4.4 Conclusion on Experimental Techniques of Measurement

The new interferometric technique described in Chapter 3 had now been developed so that the film thickness of the fluid entrapped inside a normally approaching point contact could be accurately measured as the ball approached the flat surface. For the first time the variation of the refractive index inside an E.H.L. contact could be accurately measured. The variation of both these parameters at intervals of time as small as $\frac{1}{400}$ seconds had been found.

CHAPTER 5

METHOD OF ANALYSIS

5.1 Introduction

Using the techniques described in Chapter 4 it was now possible to measure very accurately the distortion and refractive index inside an entrapment. The variation of these functions with time had also been measured. At this stage a computer programme was written, with the assistance of A. Ranger (37). This calculated the pressures inside the entrapment due to the elastic deformation of the two surfaces.

5.2 Pressure Determination

The distortion can be assumed to be elastic, because no indentation could be found in either material. If plastic flow had occurred there would have been clear evidence of it.

The program calculates the pressure field over an entrapment. A pressure field is suggested and the resulting deformation calculated. This is compared with the experimental shape, and the pressure is adjusted in proportion to the fit. This is then used to calculate a new deformation, and this procedure is continued until the computed shape converges to the experimental.

A polar grid is used having 18 sectors and 51 rings, the pressure being defined over the inner 21 rings, the first ring being the centre point.

A normalised pressure field is used for the deformation calculation and then a value for the maximum pressure is obtained by constraining the computed deformation to give the correct

difference between the centre and edge of the entrapment.

The input is the experimental values derived from the photographs, together with the numerical value of Young's modulus (E) and Poisson's ratio (σ) for the ball and plane surface.

The deformation is calculated from the formula:

$$w = \frac{1 - \sigma^2}{\pi E} \iint P \, dr \, d\theta \qquad \text{.....(34)}$$

$$= A \times P_{max} \iint p^* dr \, d\theta \qquad \text{.....(35)}$$

p^* the normalised pressure.

At each point of the grid, a minor grid, over which the integration is approximated, is set up; this consists of lines at angles of $\pi/24$. For each of these lines, the intersections with the sectors and rings of the main grid are found, and the values of pressure at each point are calculated by interpolating for the values of pressure on the adjacent mesh points of the main grid. The summation $\Sigma_1 p_i dr_i$ is then made for each line, and then the summation of these over θ, giving the approximation $\Sigma\Sigma$ p dr dθ for the integral required.

The original shape of the ball is approximated locally by a parabola. The value for A x P_{max} is then calculated as the multiple of the deformation due to the normalised pressure required to give a final shape with zero on the 21st ring. 'A' can be calculated from the values for σ and E feed in, to give a value for P_{max}.

The shape computed is compared with the experimental shape at each point and the pressure is then modified as previously explained. Due to the constraint that the centre point and boundary of the experimental shape and computed shape were already equal, the new pressure was also normalised. A new value for P_{max} is

found with the new calculation of the deformation due to this distribution. After 5 iterations a close fit is usually obtained.

The programme then prints out the normalised pressures at 19 values of the diameter of the entrapment. The values of the Young's modulus and Poisson's ratio were specially measured by Messrs Pilkington (40). The glass used for fluids 1, 3 and 4 (see section 6.1 for description) was an Extra Dense Flint. Its properties are given below:

Refractive Index = 1.742

Young's Modulus = 7.9×10^6 p.s.i.

Poisson's Ratio = 0.2

Fluid 2 had a refractive index of 1.623. This meant that the reflectivity when used in conjunction with the above glass was too low. For this reason a low refractive index Crown glass was used. Its properties are listed below:

Refractive Index = 1.513

Young's Modulus = 10×10^7 p.s.i.

Poisson's Ratio = 0.2

The Young's modulus of a substance is a function of pressure. Bondi (41) shows that the change in Young's modulus is of the order of the ratio of the applied pressure to the Young's modulus. This gives a maximum change of:

$$\frac{P_{max}}{\text{Young's modulus}} \approx \frac{100{,}000}{10{,}000{,}000} = 1\%$$

This is the same order as the accuracy to which the modulus can be measured and is less than the accuracy to which the pressure can be calculated. For this reason the change in the modulus can be ignored.

5.3 Method of Finding Density Variation

From sections 4.4 and 5.2 the variation of refractive index and pressure against the entrapment diameter have been measured. The change in density that corresponds to this change in refractive index can be easily calculated from the Lorentz-Lorenz formula:

$$\frac{n^2 - 1}{n^2 + 2}\rho = K \qquad \text{.....(22)}$$

(see section 2.10).

From these results, it was a simple matter to work out the change in density with pressure by reading off the pressure and density changes at set values of the radius.

5.4 Method of Calculating the Viscosity

The viscosity of the oil inside the entrapment was calculated in the following way:

Using Reynold's Equation in Polar coordinates:

$$\frac{1}{r}\frac{\partial}{\partial r}\left(\frac{rh^3}{\eta}\rho\frac{\partial p}{\partial r}\right) + \frac{1}{r^2}\frac{\partial}{\partial \varphi}\left(\frac{h^3}{\eta}\rho\frac{\partial p}{\partial \varphi}\right) = \frac{6}{r}\left[\frac{\partial}{\partial r}(hrZ\rho) + \frac{\partial}{\partial \varphi}(hT\rho) + 2\left(\frac{\partial}{\partial t}(\rho h)r\right)\right] \qquad \text{.....(36)}$$

Where Z is the relative velocity of the two surfaces in the radial direction and the other symbols have their usual meanings.

This equation is derived in Principles of Lubrication (14) Ch. 3. The following assumptions have been made in the derivation:

1) External forces such as gravitational have been ignored.
2) The pressure is assumed to be constant along the Z axis.
3) There is no slip at the boundaries.
4) The lubricant is Newtonian.
5) The flow is laminar.

6) The fluid inertia can be neglected.

7) The viscosity is taken as constant in the Z axis (through the thickness of the film).

The entrapment is symmetrical about its centre so taking the Z axis through the centre of the ball and the contact area reduces the equation to:

$$\frac{\partial}{\partial r}\left(\frac{rh^3}{\eta}\rho\frac{\partial p}{\partial r}\right) = 12\frac{\partial}{\partial t}(\rho h)\,r \qquad \text{.....(37)}$$

Integrating this equation with respect to r, and rearranging gives:

$$\eta = rh^3\rho\frac{\partial p}{\partial r} \Big/ 12\int_0^r \left(\frac{\partial}{\partial t}\rho h\right) r\,dr \qquad \text{.....(38)}$$

To find the viscosity it is necessary to solve the above equation. From the interferometric measurements made, the variations of film thickness (h) with entrapment radius (r) and time (t) were found.

The method is described in Chapter 4. Sections 5.2 and 5.3 describe the method used to determine the variation of pressure and density with the radius (r) and time. Equation (38) was solved at given values of the radius on a computer. This was programmed to calculate the magnitude of each term in the equation at a given radius, and hence the viscosity by substituting for the terms in the equation. The full listing for the programme is given in appendix I, but a short description is given here.

Nineteen values of the radius at which the viscosity was to be calculated were chosen. From the data of h against r the programme finds the value of h at these 19 set values of r. It does this by curve fitting a quadratic equation to the three nearest data points and then solving the equation for h at each given radius. The values of the pressure and density at the given r are found with a similar method. The values of the differential

of P with respect to r was found by differentiating the quadratic equation fitted to the three nearest data points and substituting in the given radii. This procedure was carried out for each picture taken of the entrapment, using of course, the same 19 values of the radii. The derivative $\frac{\partial(\rho h)}{\partial t}$ was found in a similar way by curve fitting a quadratic to the values of ρh in each picture at a given radius and differentiating. This was repeated for each of the 19 radii and for each picture. The integral $\int_o^r r \frac{\partial(\rho h)}{\partial t} dr$ was found by curve fitting a quadratic equation to the value of this function at three adjacent radii, and integrating the equation between r_1 and r_2. The total integral can be found by summing these integrals from r = 0 to r = r. This can be seen by reference to Fig. 13.

The programme then calculates the viscosity at each of the 19 chosen radii and on each picture, and prints out this viscosity along with the pressure at that point. An estimate of the shear rate was also made at each point. The rate of shear is defined by $\frac{du}{dz}$ (see Equation 5). From Cameron (14) we have the formula:

$$\frac{du}{dz} = \frac{1}{\eta} \frac{\partial p}{\partial r} (z - \frac{h}{2})$$

This was derived ignoring the squeeze film term. It will give the rate of shear to a good approximation, in the case under consideration. Hence the value of $\frac{du}{dz}$ was calculated in the programme from this equation and so an estimate of the rate of shear was obtained.

5.5 Method of Obtaining the Velocity of Approach

The absolute velocity of the ball was found by measuring the induced voltage produced in a coil by a magnet moving with the same velocity as the ball. (see section 4.3). This was measured on

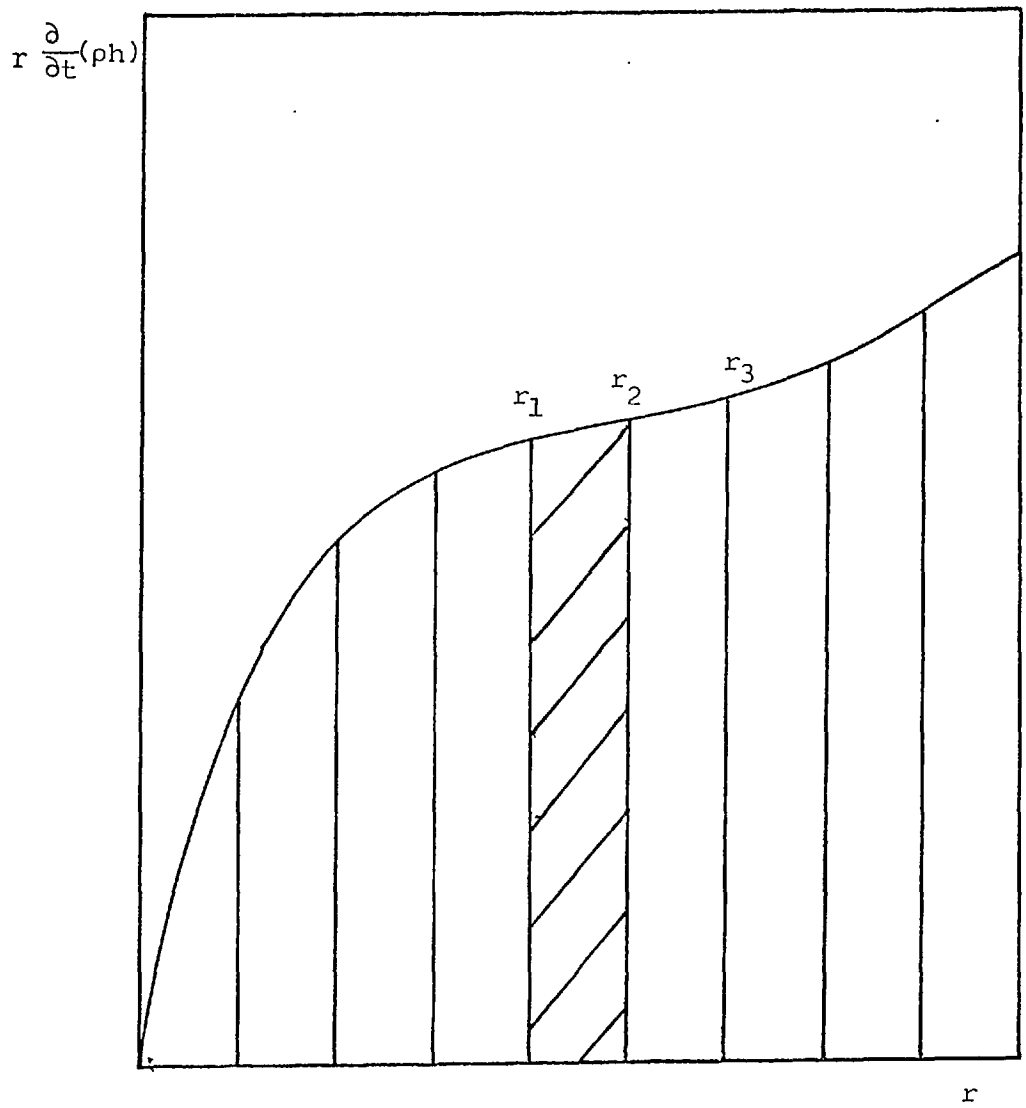

TO DETERMINE INTEGRAL FROM r_1 TO r_2

A QUADRATIC IS FITTED TO r_1, r_2 AND r_3 AND THE

INTEGRAL BETWEEN r_1 AND r_2 FOUND

FIG. 13

a U.V. recorder and it was hoped to correlate this absolute velocity with the entrapment size.

The relative approach of the two surfaces at the centre of the contact was found by measuring the slope of a graph of maximum entrapment thickness against time. These parameters were found by measuring the maximum depth in each picture, and using the framing rate of the camera to find the time elapsed between each picture.

CHAPTER 6

RESULTS

6.1 Introduction

The results for each fluid take a considerable time to calculate and also high speed camera work is expensive. For these reasons only 4 fluids were tested and only two were studied with the high speed camera.

These four fluids are listed below. Appendix II gives all the obtainable data on them. Fluids 1 and 2 were both tested by Westlake and Cameron (5) in their study of entrapments.

Fluid 1 a BP1065, high viscosity cylinder stock

Fluid 2 a 5P4E fluid

Fluid 3 a polychlorotrifluoro-ethylene

Fluid 4 a Krytox 143 A.C.

6.2 Entrapment Formation Results

Figs. (14-17) show plots of the distortion of the surfaces with time for the four fluids tested. The minimum film thickness was difficult to measure accurately because of the lack of detail in monochromatic fringes. Previous work by Westlake and Cameron (5) using a white light source, showed that for 5P4E the minimum film thickness was less than 100°A after the ball had come to rest.

Fluids 1, 3 and 4 all show a similar entrapment formation. As the ball falls there is considerable leakage of fluid, so that the distortion of the surfaces does not vary very much until the minimum thickness becomes less than 1000°A.

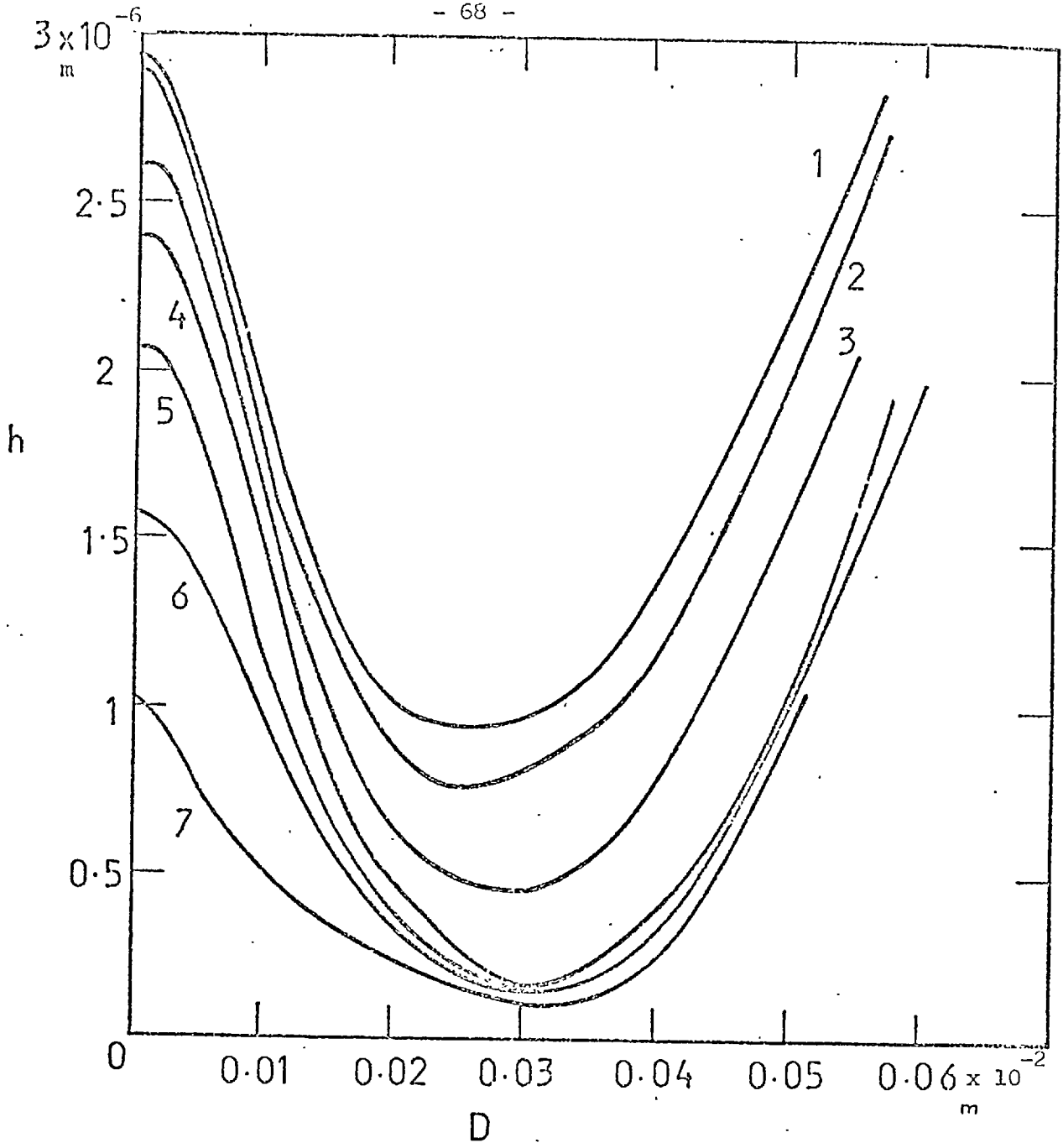

FOR 1 t = 0.0025 sec.
FOR 2 t = 0.005 sec.
FOR 3 t = 0.025 sec.
FOR 4 t = 1.33 sec.
FOR 5 t = 1.66 sec.
FOR 6 t = 4.33 sec.
FOR 7 t =20.00 sec.

GRAPH OF ENTRAPMENT DEPTH AGAINST DIAMETER

FLUID 1 TEMPERATURE 23°C

FIG. 14

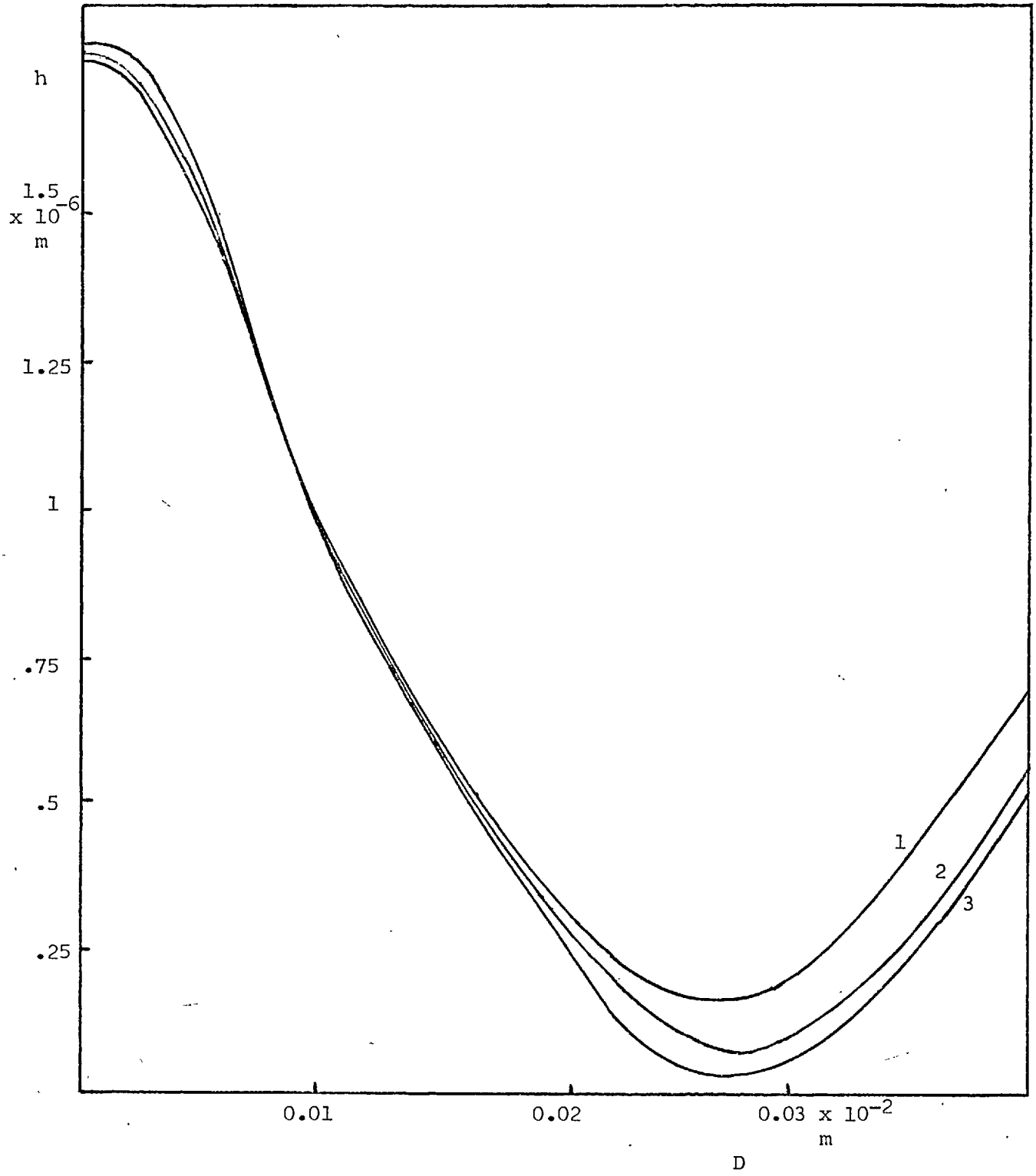

FOR I t = 0.33
FOR 2 t = 1.66
FOR 3 t = 2.66

GRAPH OF ENTRAPMENT DEPTH AGAINST DIAMETER

FLUID 2 TEMPERATURE 22.5°C

FIG. 15

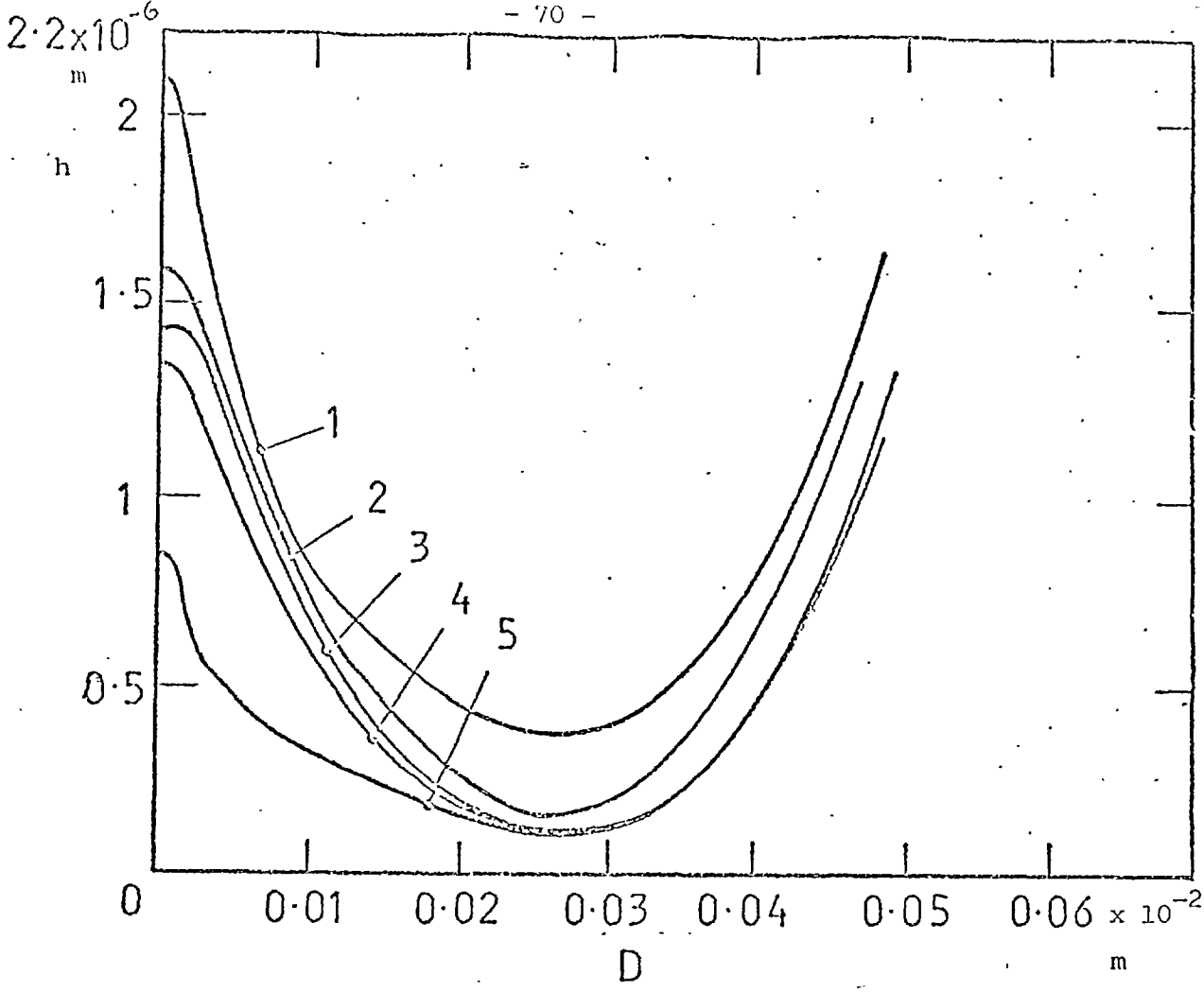

FOR 1 t = 0.0075 sec.
FOR 2 t = 0.0225 sec.
FOR 3 t = 1.625 sec.
FOR 4 t = 4.00 sec.
FOR 5 t = 9.00 sec.

GRAPH OF ENTRAPMENT DEPTH AGAINST DIAMETER

FLUID 3 TEMPERATURE 26°C

FIG. 16

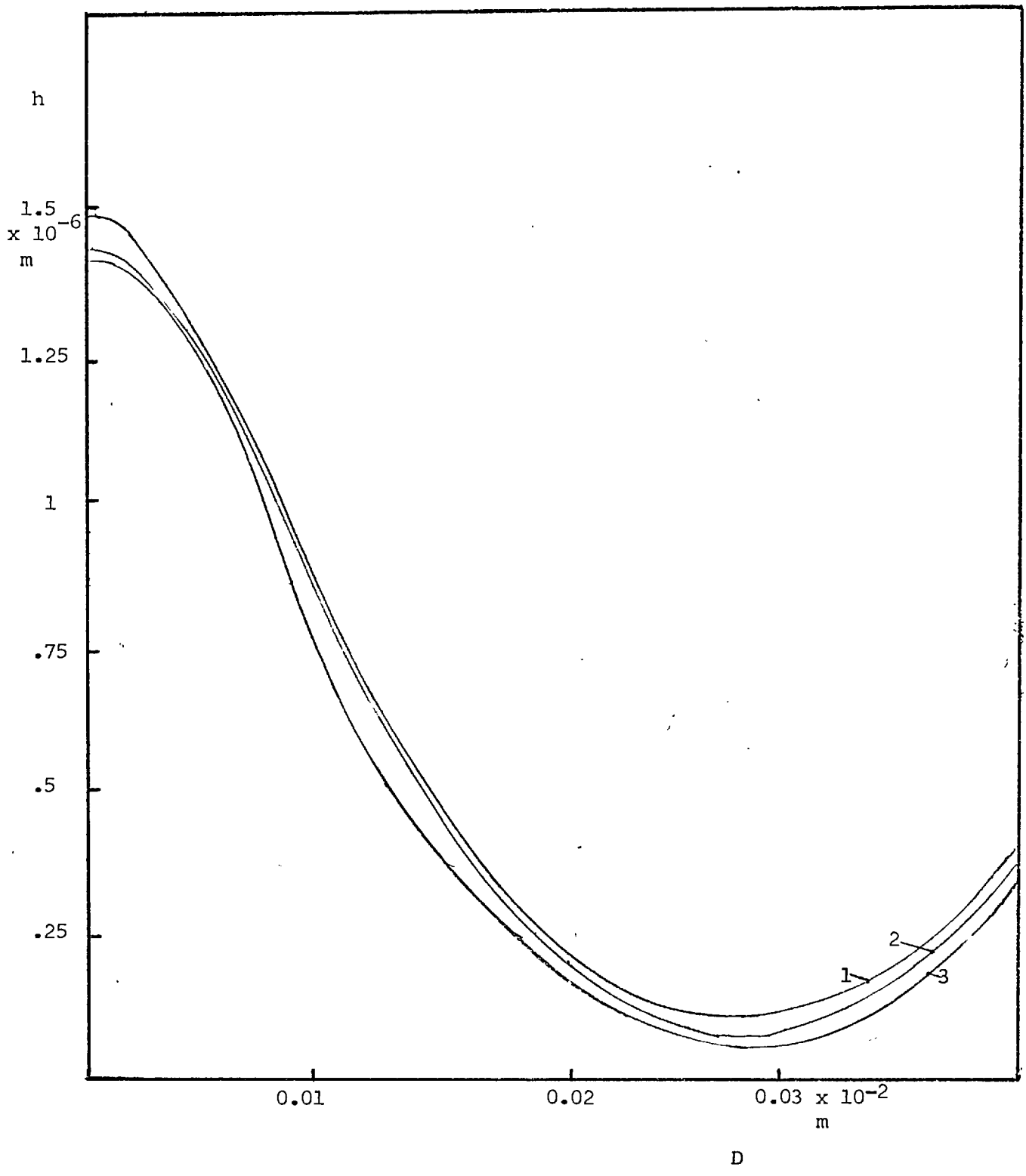

FOR 1 t = 0.33 sec.

FOR 2 t = 0.66 sec.

FOR,3 t = 1.00 sec.

GRAPH OF ENTRAPMENT DEPTH AGAINST DIAMETER

FLUID 4

FIG. 17

At this stage the reduction of the minimum thickness slows down considerably and fluid flows from the contact, decreasing the distortion until all the fluid has flowed out. The time scale of this varies; with fluid 3, the ball came to rest very much quicker than for the other two. Fluid 2, however, shows a totally different entrapment formation. There appears to be almost no leakage and the ball deforms (around the entrapped fluid) until the minimum film thickness becomes less than $100^{o}A$. There is then very little fluid flow. These observations on fluid 2 were also mentioned by Westlake and Cameron.

Refractive Index Results

Figs. 18-21 show typical refractive index plots for the four fluids tested. The refractive index increases steadily from the edge of the entrapment to the centre. The increase of the refractive index in the centre of the entrapment is not as large as was expected. This was because the bulk modulus of all the fluids fell with increasing pressure and this results in the refractive index becoming less sensitive to pressure changes.

Pressure Variation Results

Figs. 22-25 show plots of the pressures computed inside the contact. These are considerably in excess of the equivalent Hertz pressure, which would be about 30×10^{3} p.s.i. (2×10^{8} N/M^{2}). This shows that there is a large error in the common assumption that the maximum pressure in normally approaching bodies, such as gear teeth, can be taken as the equivalent Hertz maximum. This could lead to an underestimation of the pressure by a factor of 5 or 6 times.

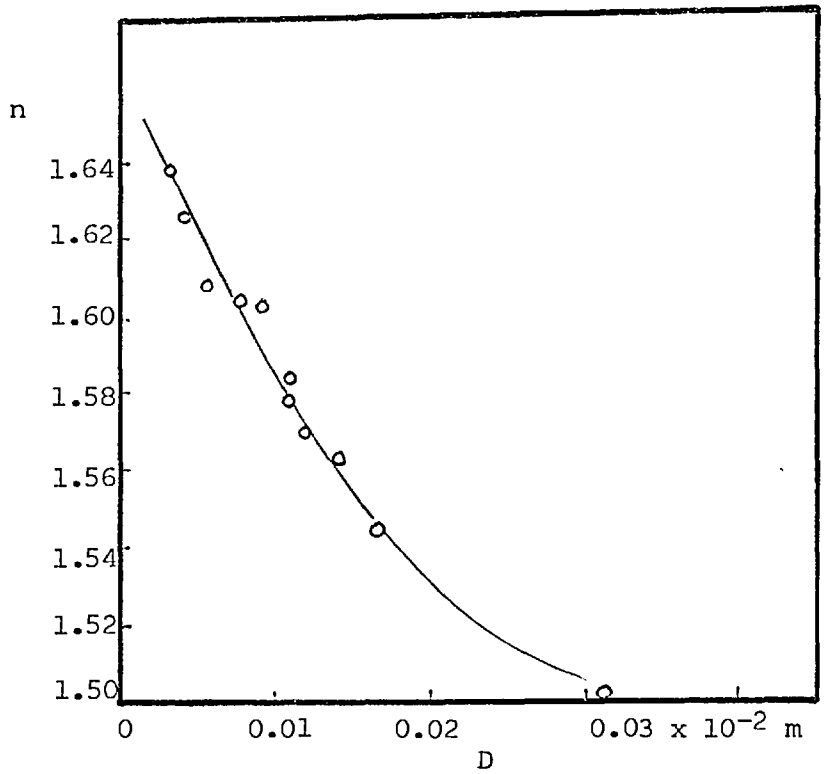

REFRACTIVE INDEX AGAINST ENTRAPMENT DIAMETER

FLUID 1

FIG. 18

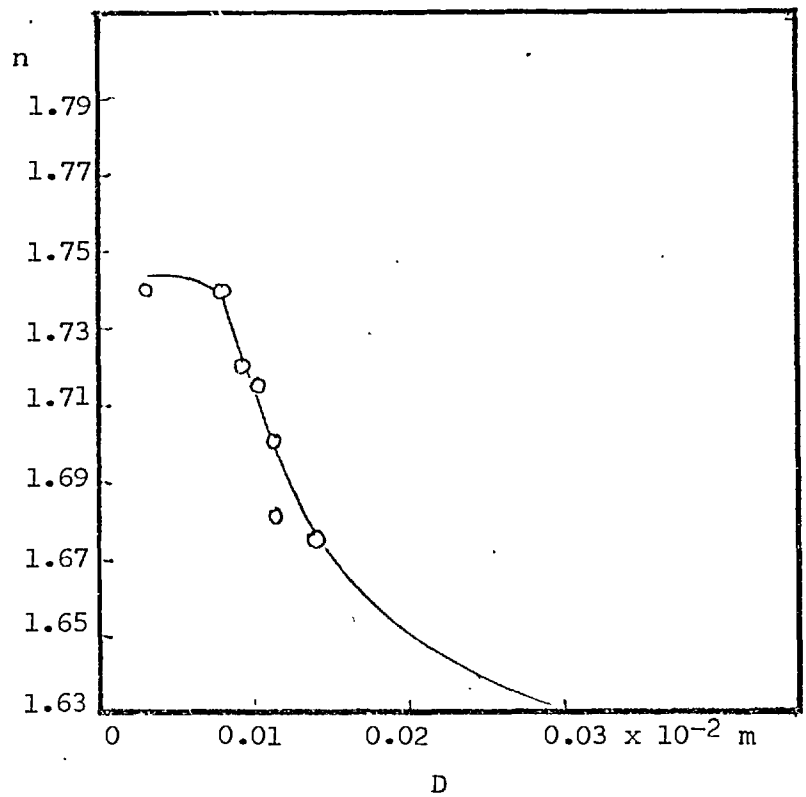

REFRACTIVE INDEX AGAINST ENTRAPMENT DIAMETER

FLUID 2

FIG. 19

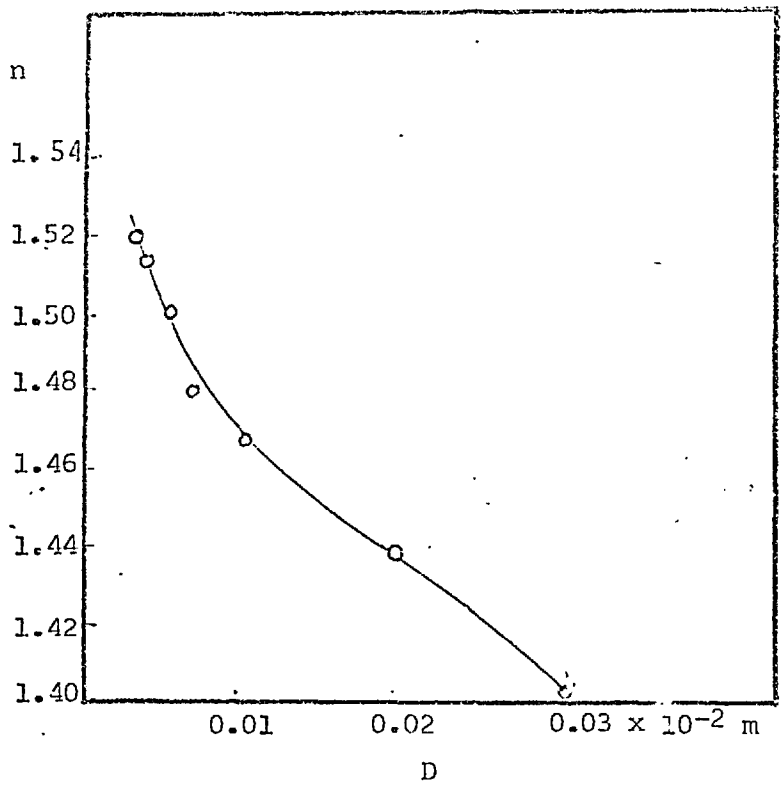

REFRACTIVE INDEX AGAINST ENTRAPMENT DIAMETER

FLUID 3

FIG. 20

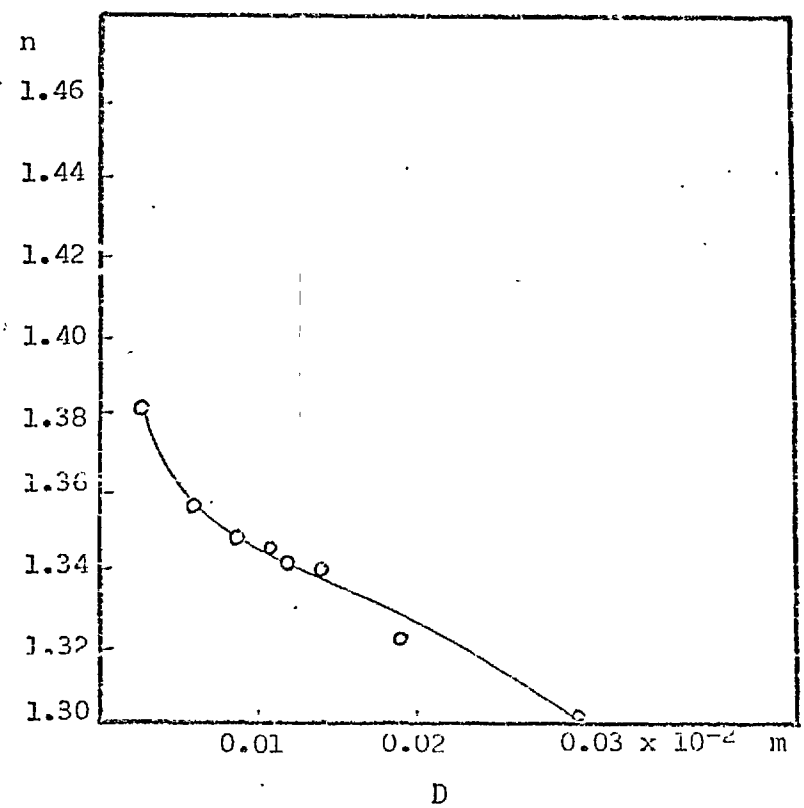

REFRACTIVE INDEX AGAINST ENTRAPMENT DIAMETER

FLUID 4

FIG. 21

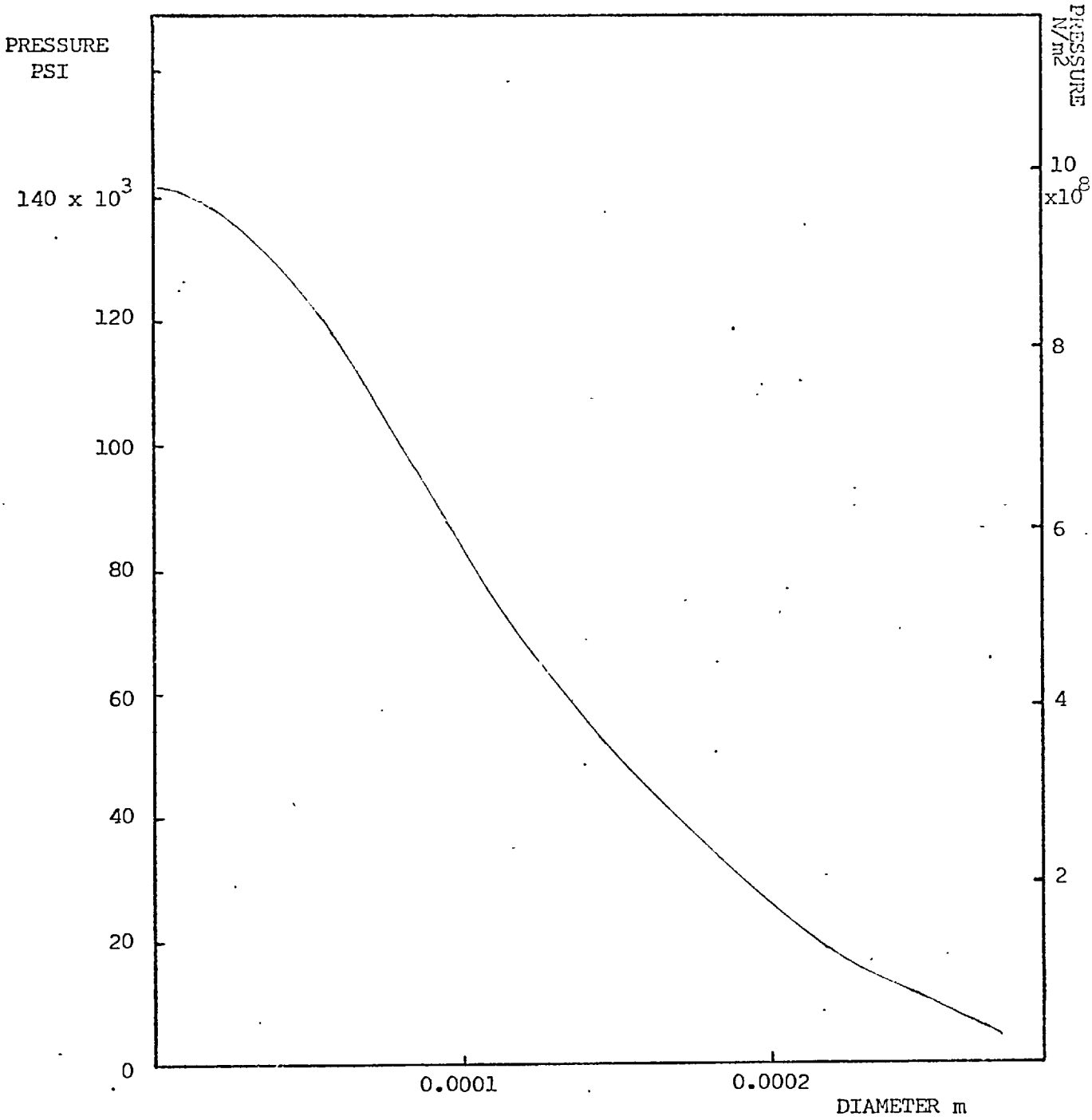

PRESSURE AGAINST DIAMETER FOR A TYPICAL ENTRAPMENT

FLUID 1
TEMPERATURE 23°C

FIG. 22

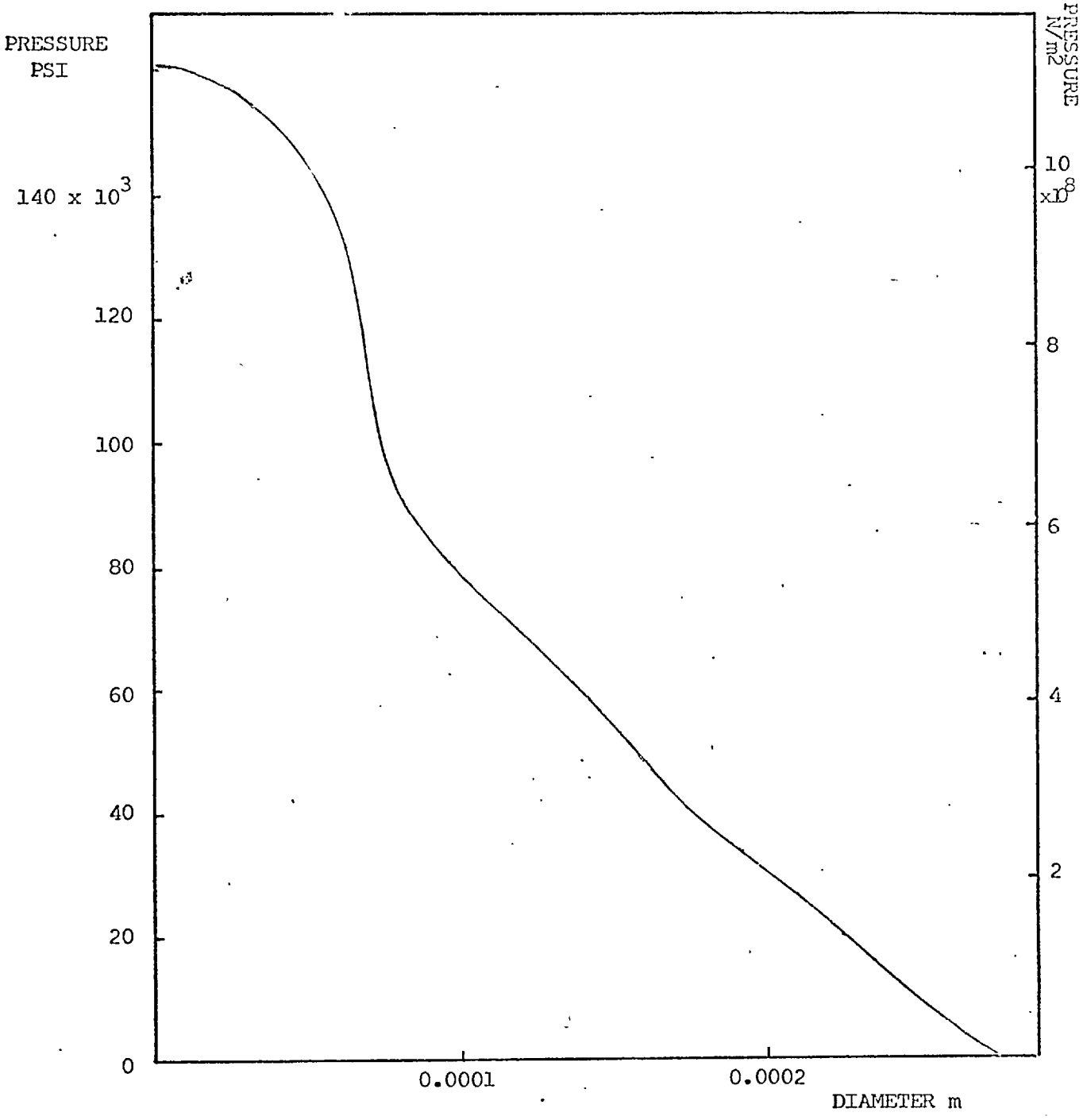

PRESSURE AGAINST DIAMETER FOR A TYPICAL ENTRAPMENT

FLUID 2
TEMPERATURE 22°C

FIG. 23

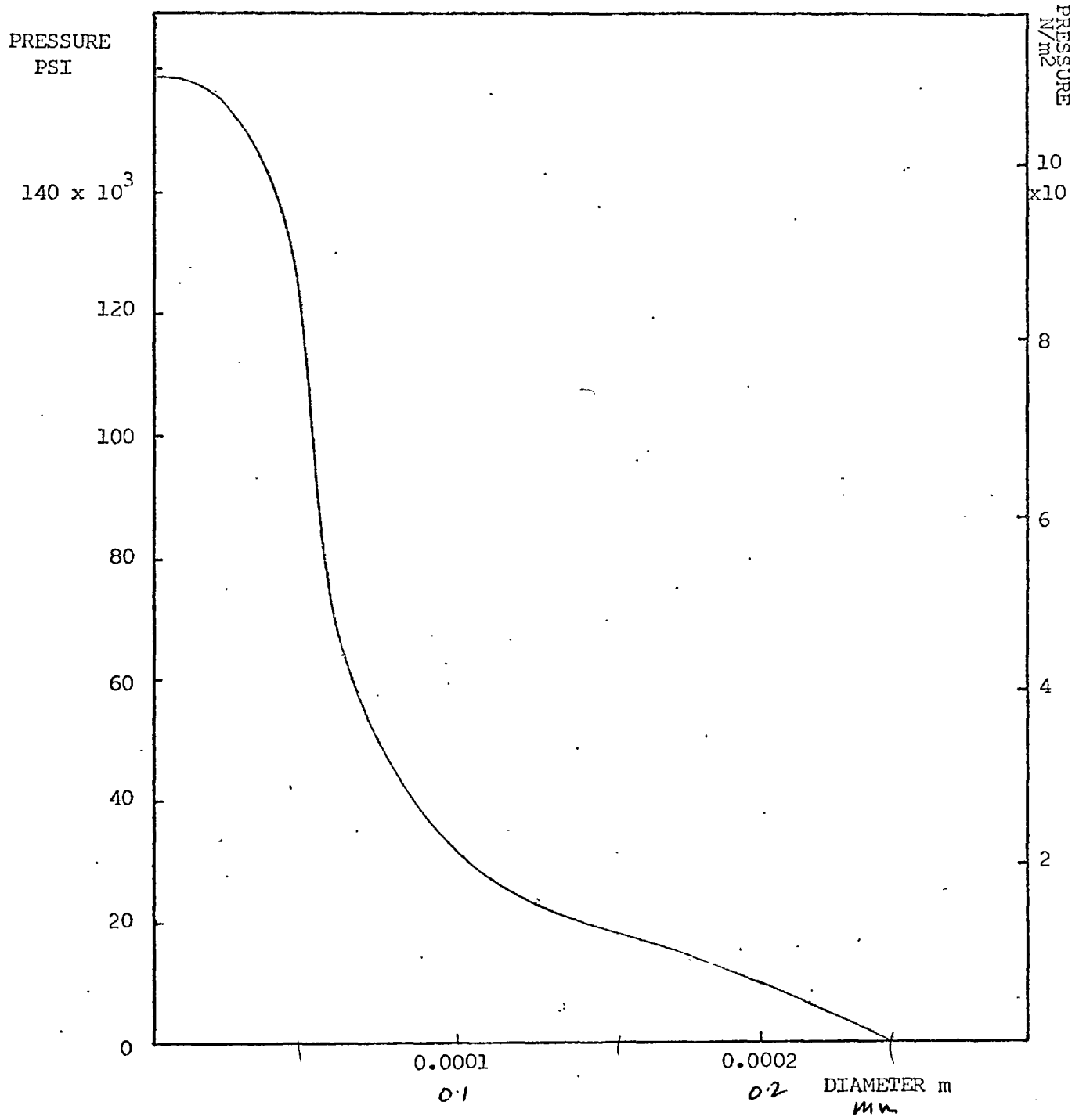

PRESSURE AGAINST DIAMETER FOR A TYPICAL ENTRAPMENT

FLUID 3
TEMPERATURE 26°C

FIG. 24

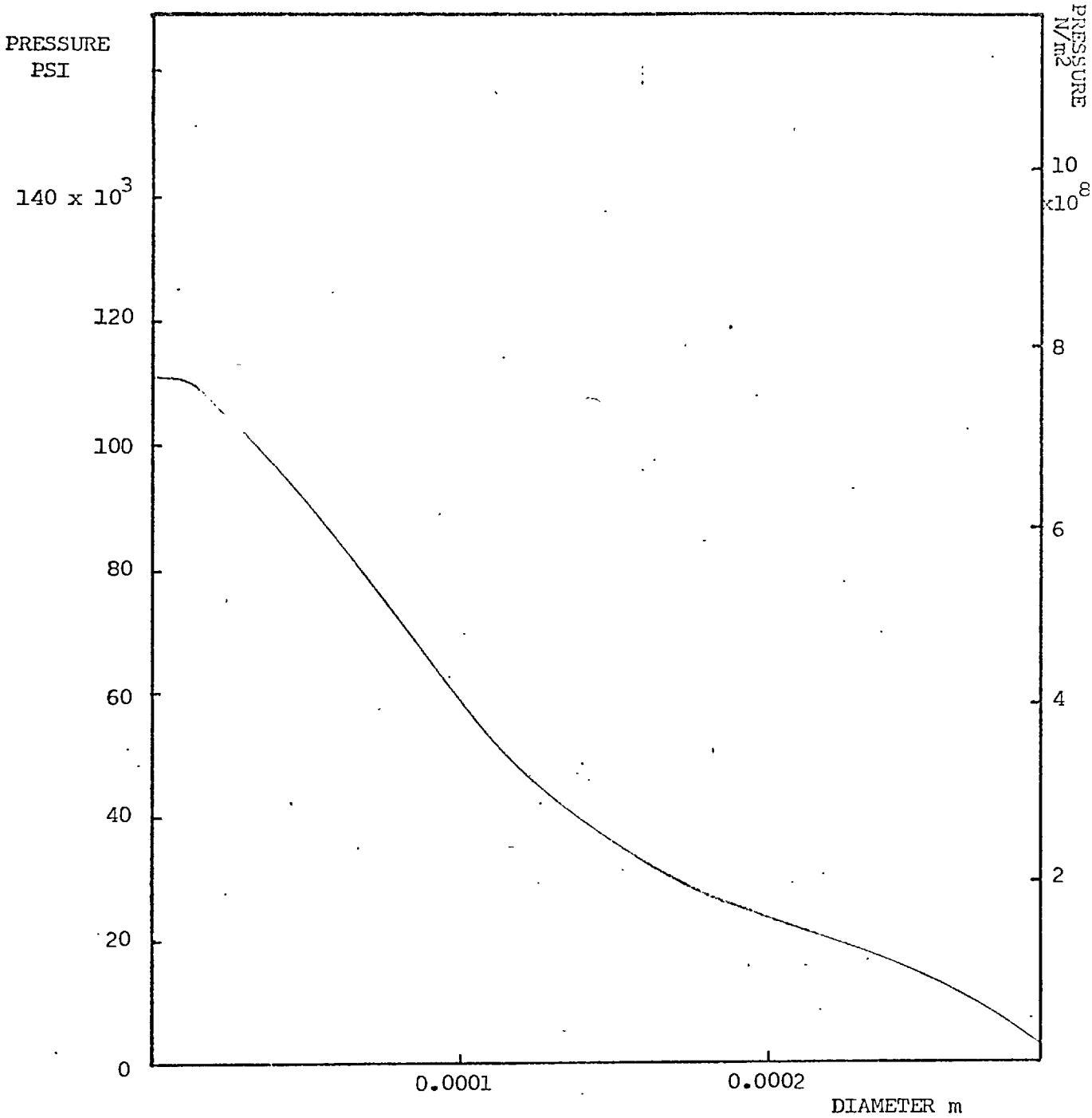

PRESSURE AGAINST DIAMETER FOR A TYPICAL ENTRAPMENT

FLUID 4
TEMPERATURE 23°C

FIG. 25

6.3 Density Measurements and Results

The results for these measurements are shown in Figs. (26-29). For three of the fluids bulk modulus data was available and it is possible to compare the value measured from the graphs.

Fluid	Bulk Modulus Quoted	Bulk Modulus Measured
2	3.15	$3.3 \times 10^9 N/m^2$
3	1.77	$1.5 \times 10^9 N/m^2$
4	1.00	$1.1 \times 10^9 N/m^2$

It would appear from these figures that there is a reasonable correlation. However, there appears to be a random error in the density measurements. A full treatment of the possible errors involved in these results is given in section 6.7.

6.4 Viscosity Determination Results

The results for this section are shown in Figs. (30-33). These results are the most exciting and important of the whole project. Previous capillary or falling weight measurements of viscosity against pressure have stopped at viscosities of about 10^4 poise (10^3 NS/m^2), whereas these measurements go up to 10^8 poise (10^7 NS/m^2), four orders of magnitude higher. This is an important advance in study of oils under the pressures developed in a typical bearing. The only comparable work done previous to this was from traction measurements such as those of K.L. Johnson and R. Cameron (20) (see section 1.3).

Data available on the fluids has been included on the graphs and shows a very good correlation with the measurements. Gentle (45) measured the apparent α value of the four fluids using the rolling ball technique, as pioneered by Westlake and Cameron (5).

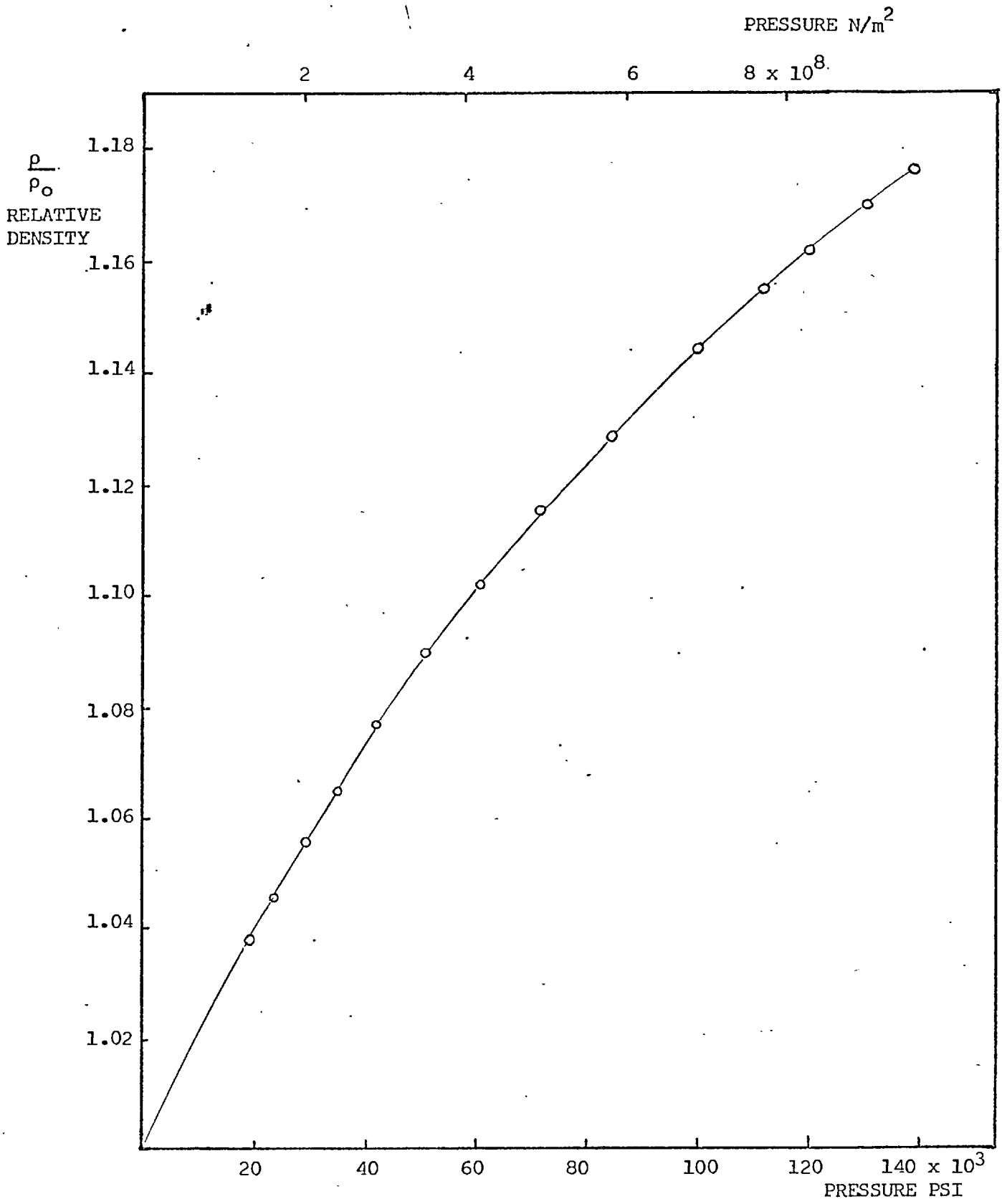

RELATIVE DENSITY AGAINST PRESSURE

FLUID 1
TEMPERATURE 23°C

FIG. 26

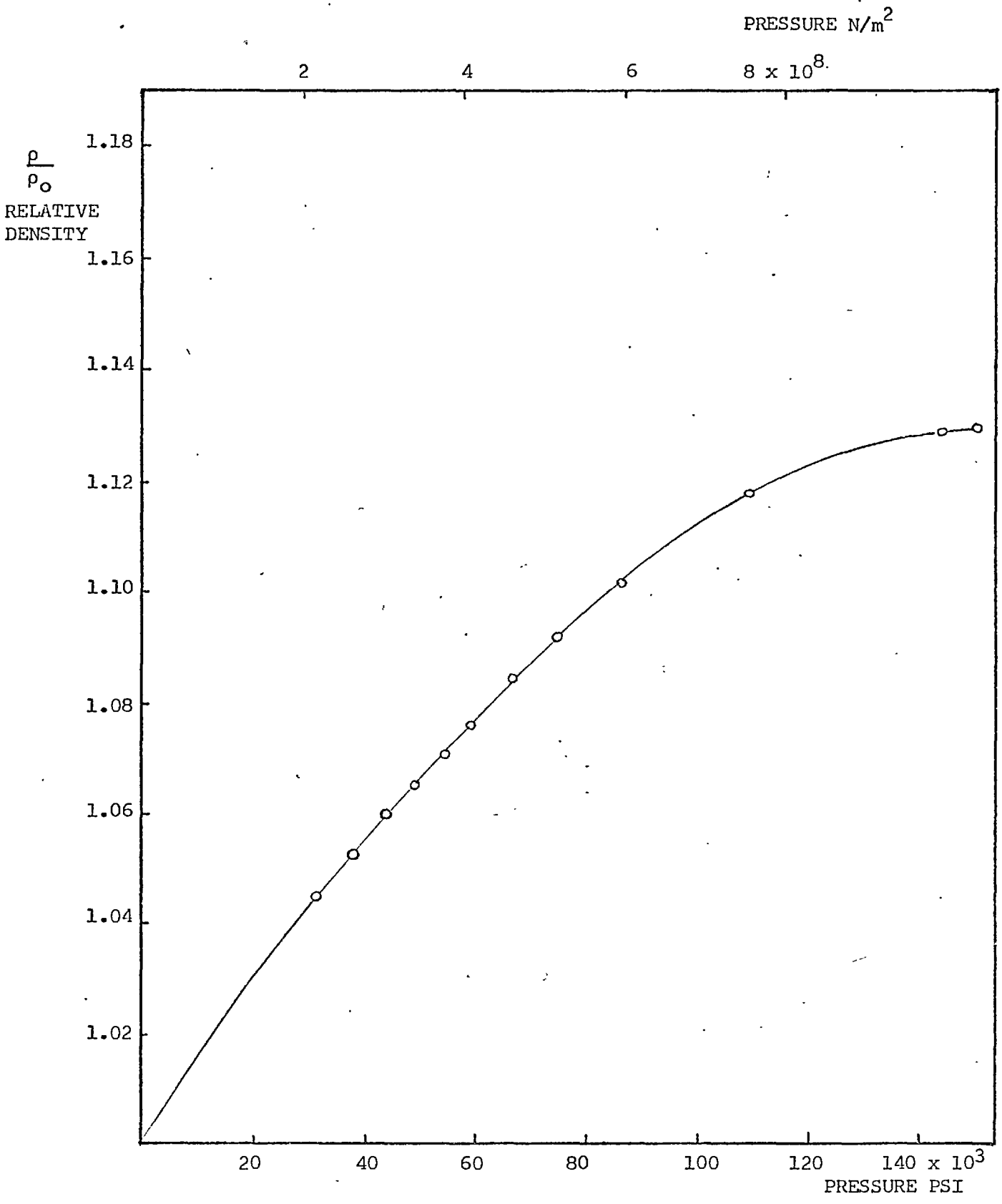

RELATIVE DENSITY AGAINST PRESSURE

FLUID 2
TEMPERATURE 22°C

FIG. 27

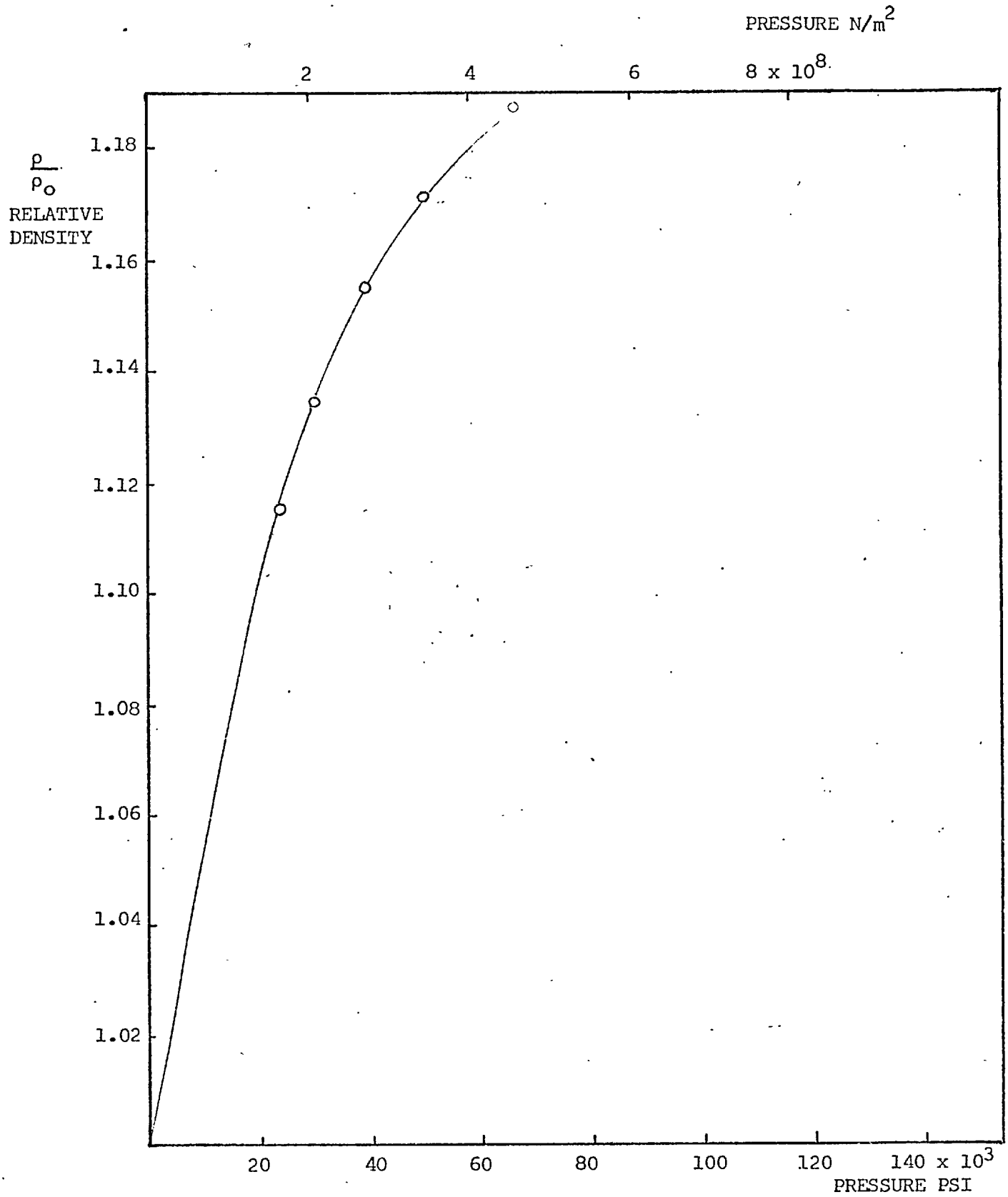

RELATIVE DENSITY AGAINST PRESSURE

FLUID 3
TEMPERATURE 26°C

FIG. 28

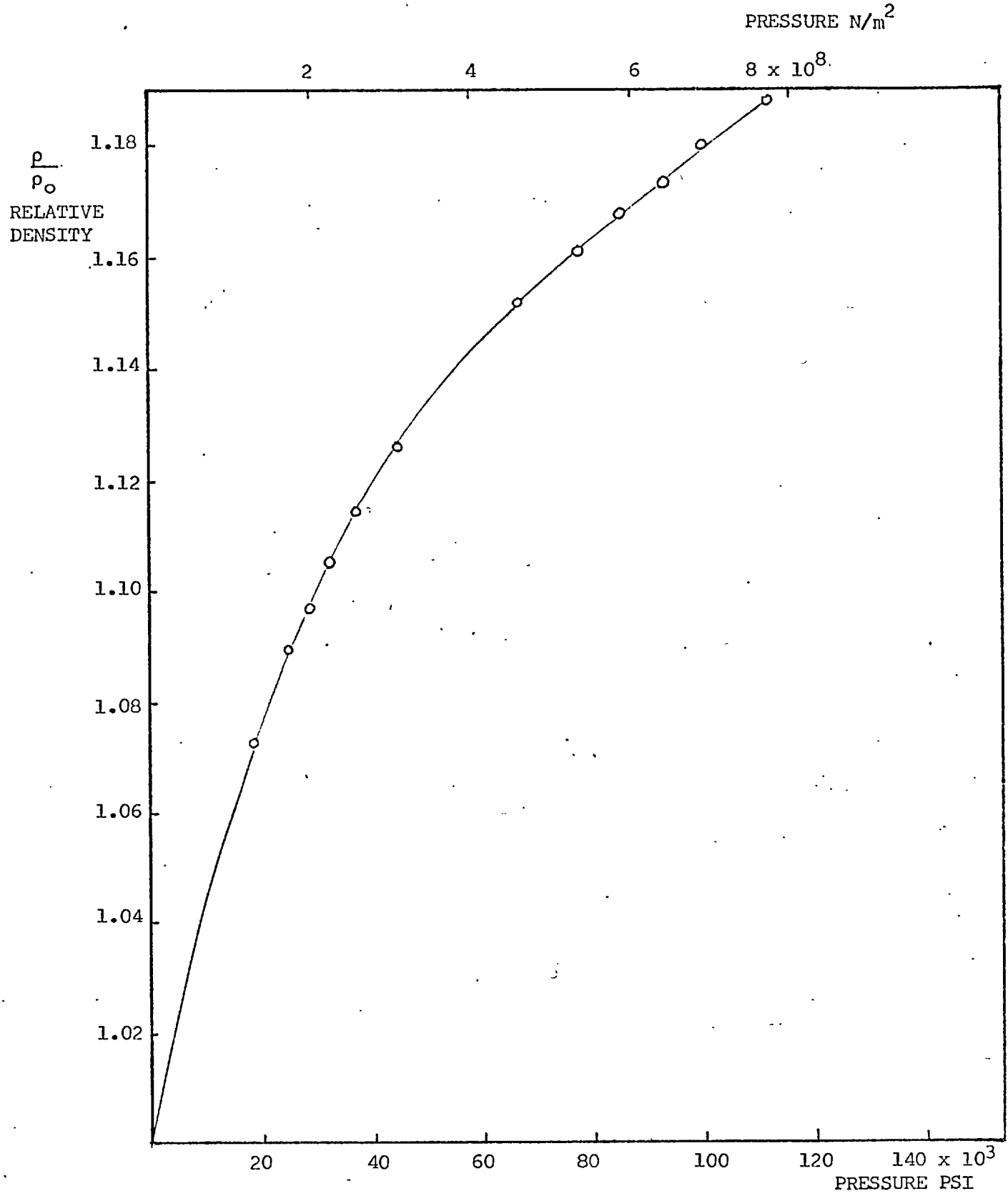

RELATIVE DENSITY AGAINST PRESSURE

FLUID 4
TEMPERATURE 20.2°C

FIG. 29

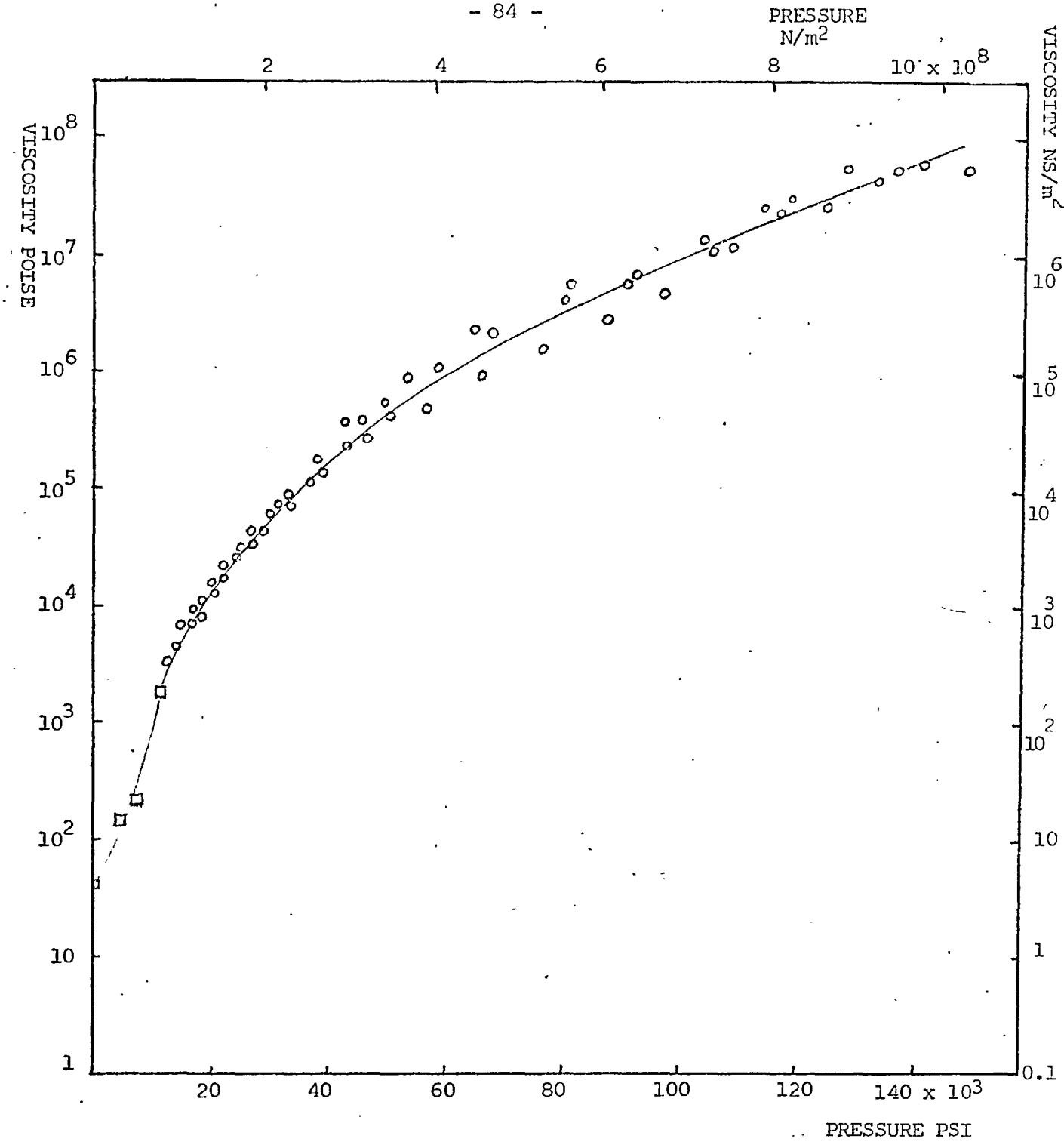

VISCOSITY AGAINST PRESSURE

FLUID 1
TEMPERATURE 23°C

o DATA POINTS FROM ENTRAPMENT MEASUREMENTS

□ DATA POINTS QUOTED

FIG. 30

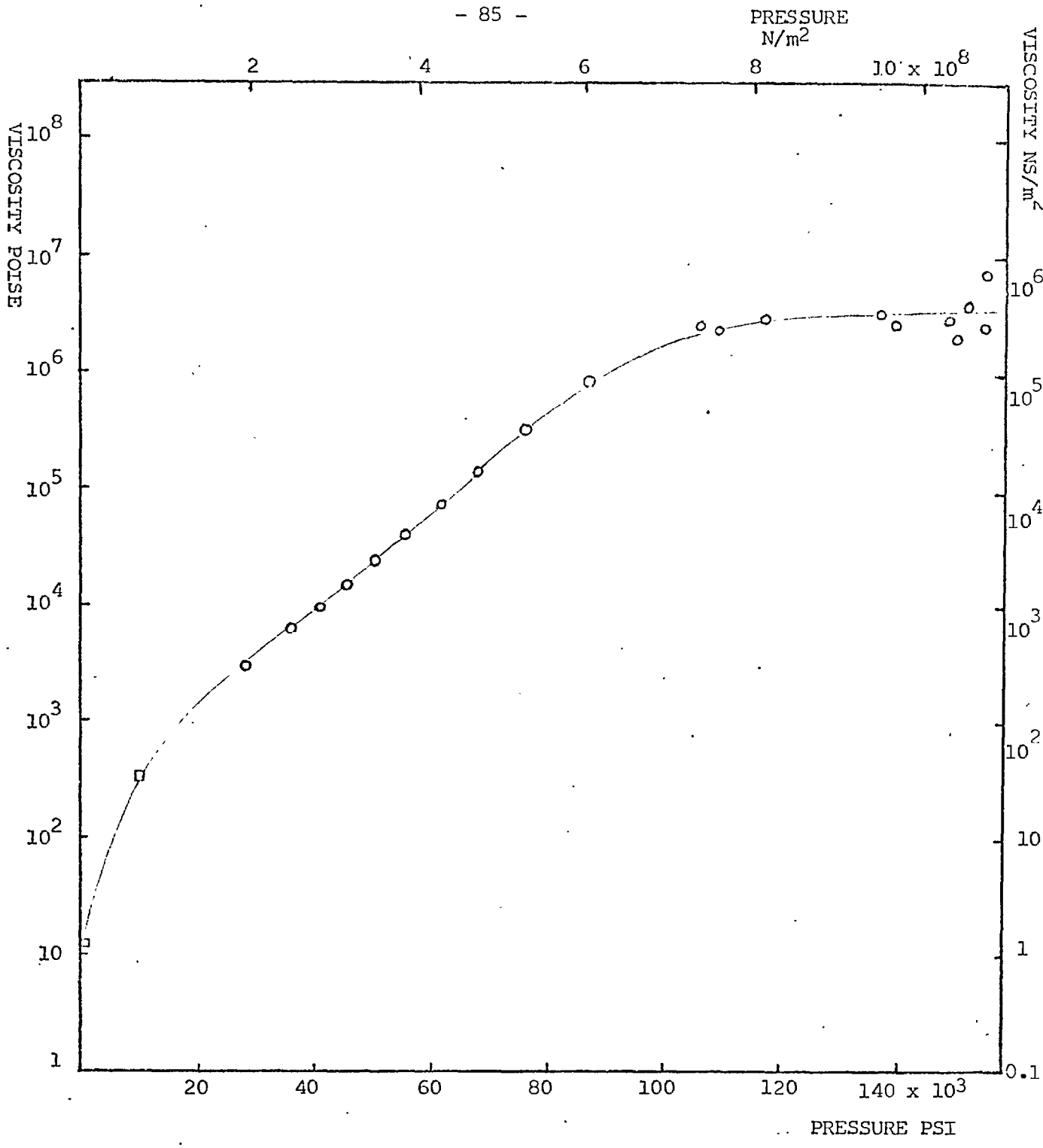

VISCOSITY AGAINST PRESSURE

FLUID 2
TEMPERATURE 22°C

o DATA POINTS FROM ENTRAPMENT MEASUREMENTS

□ DATA POINTS QUOTED

FIG. 31

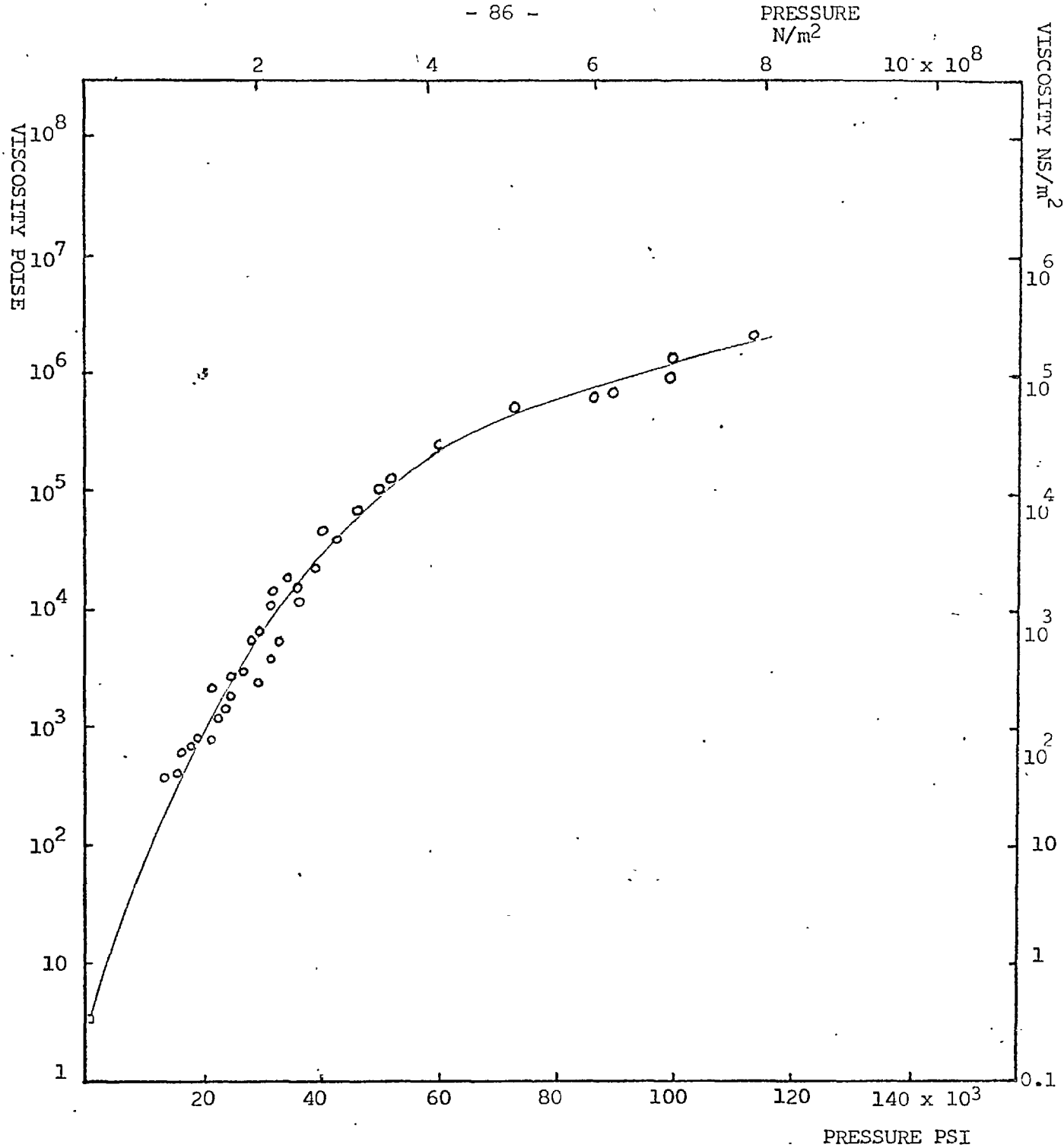

VISCOSITY AGAINST PRESSURE

FLUID 3
TEMPERATURE 26°C

o DATA POINTS FROM ENTRAPMENT MEASUREMENTS

□ DATA POINTS QUOTED

FIG. 32

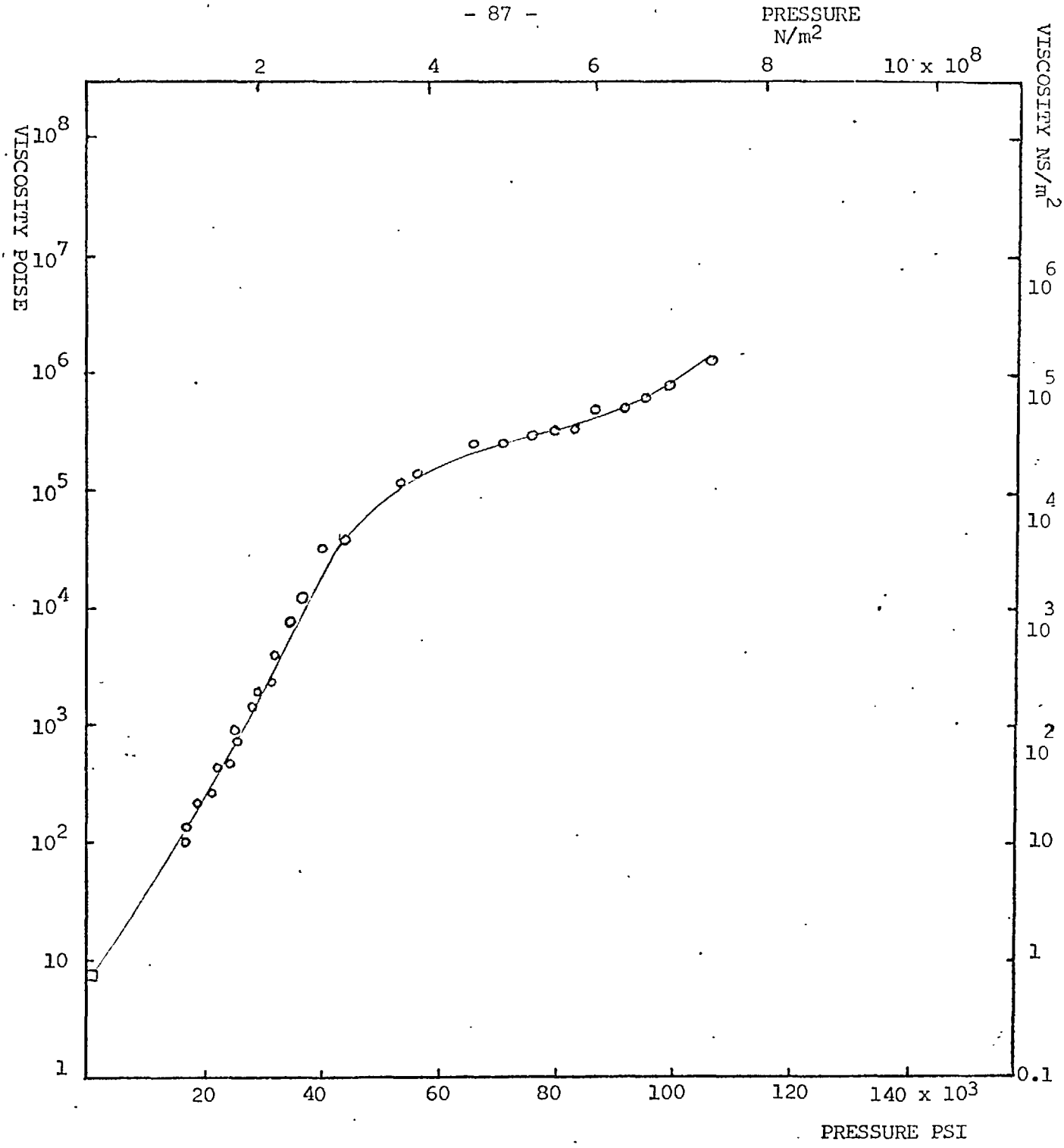

VISCOSITY AGAINST PRESSURE

FLUID 4
TEMPERATURE 20.2°C

o DATA POINTS FROM ENTRAPMENT MEASUREMENTS

□ DATA POINTS QUOTED

FIG. 33

Unfortunately it is not possible to calculate the pressure for which these measurements apply. The curves show that the α value of the four fluids, given by the slope of the lines, is a function of pressure. For this reason it was found impossible to correlate the two measurements. The overall trend of the 'α' value of the four fluids was confirmed, however, if a pressure of about 20,000 p.s.i (1.6×10^8 Newtons/m^2) is taken. Johnson and Cameron (20) found a change in the slope of the log viscosity, pressure curve at a viscosity of $10^4 - 10^5$ poise ($10^3 - 10^4$ NS/m^2). This is apparent for the four fluids tested here although for fluid 2 the change occurs at a lower viscosity and the other fluids show a rather more gradual alteration of the slope.

It appears that this is the first time that the full Reynolds Equation has been solved by substituting measured values of film thickness , density and pressure to obtain the viscosity variation.

Pressure Freezing

Fluid 2 has a limiting viscosity of 10^6 poise (10^5 NS/m^2), at a pressure 110,000 p.s.i. (6.8×10^8 NS/m^2). The viscosity of the other fluids continue to increase with increasing pressure beyond the knee in the curves but less rapidly than at low pressures. It would seem to be important to consider whether an explanation can be found for the different behaviour of fluid 2. The fluid was tested by Gentle and Cameron (46) in their rolling point contact rig. They were able to show that under the influence of pressure the pour point temperature rose. (In this context 'pour point' is used as a general term for solidification with no precise significance and it does not have the standard institute of petroleum meaning).

As the pressure was generated in a Hertzian contact the increase in temperature could not be referred to any one pressure, an unfortunate limitation of their technique. They were able only to quote the Hertzian maximum pressure. For fluid 2 the pressure required to raise the pour point to 22°C was 150 x 10^3 p.s.i. (10^9 N/m^2) Hertzian maximum pressure. When the pour point temperature is reached the fluid has vitrified and is in a glassy state. This is a continuous process and is not a phase change. It is difficult to decide how the viscosity pressure characteristics of the fluid should behave as the substance passes into a glassy stage. Bingham and Stevens (47) measured the viscosity pressure characteristics of colophonium which behaves as a glass (48) and found that the viscosity was independent of pressure in the range of 0 - 27 x 10^3 p.s.i. (1.8x 10^8 N/m^2). This would suggest that as the pressure increased on fluid 2 the rate of change of viscosity with pressure should gradually fall until it becomes independent of pressure. This is what is observed in the results. There are two possible reasons why none of the other fluids exhibit this behaviour. Either they do not form a glassy substance or the pour point temperature is so far below ambient, that the pressure is not high enough to raise the pour point up to room temperature. In connection with this, it can be seen from Appendix II that fluid 2 has an exceptionally high pour point(5°C) and so this was the most likely fluid to show this effect.

Shear Rate

The shear rate was found to vary from 10^{-5} s^{-1} near the centre of the entrapment to about 10^{-1} s^{-1} near the edge. These are extremely low values.

6.5 Approach Velocity Results

Christensen's theoretical treatment of a dropping ball, which is described in more detail in section 1.2, states that a graph of the square root of the approach velocity of the centre of the entrapment against the film thickness should be a straight line passing through the origin. The slope of the straight line is proportional to $\alpha^{-\frac{1}{2}}$. Figs. 34 and 35 show a plot of the square root of the approach velocity against film thickness. For fluids 1 and 3 it can be seen that the theory does not predict this velocity very accurately. The slope is not constant as the curve appears to be a series of straight lines. For fluid 1 it is possible to extrapolate part B back to the origin. The situation would be much worse for fluid 2 which has an almost zero approach velocity with a film thickness of 1.5×10^{-6} m. The theory also predicts the fluid will drain from the contact until the normal Hertzian contact shape is obtained. The entrapment with fluid 2 lasted indefinitely as there was no apparent change after 80 hours. The closing of the entrapment centre apparent in Fig. 15 only occurred whilst there was a significant separation at the edge of the entrapment.

From the theory it is possible to calculate the 'α' value from the slope. It was decided to do this for fluids 1 and 3 to see if there was any correlation between the values predicted by the theory and the range of values measured from the graphs of viscosity against pressure.

The theory states that:

$$v^{\frac{1}{2}} = s^{\frac{1}{2}}h \qquad \text{.....(39)}$$

where h is the film thickness at the centre, and v is the approach velocity of the centres.

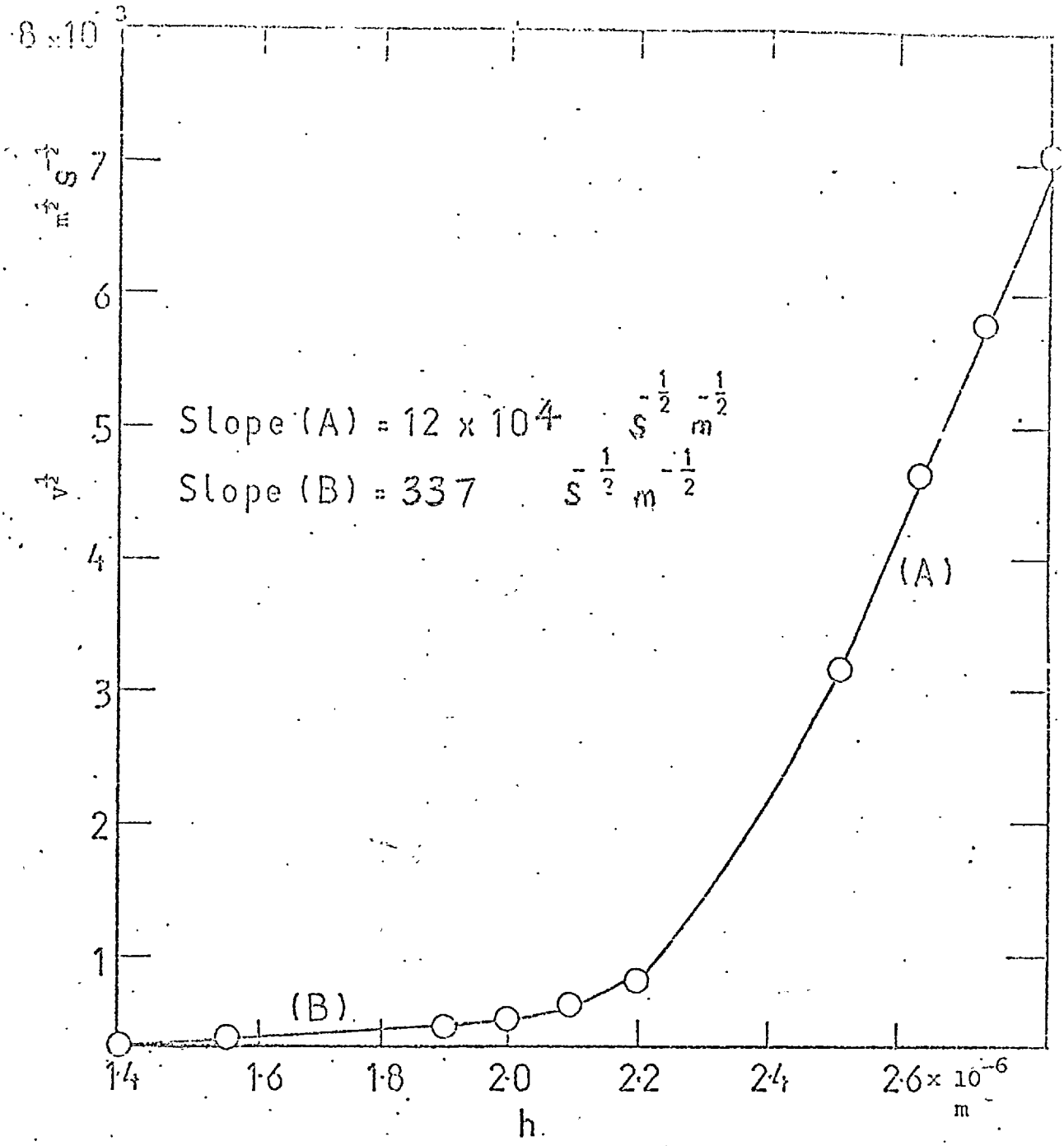

GRAPH OF SQUARE ROOT APPROACH VELOCITY OF THE BALL CENTRE AGAINST FILM THICKNESS

FLUID 1

FIG. 34

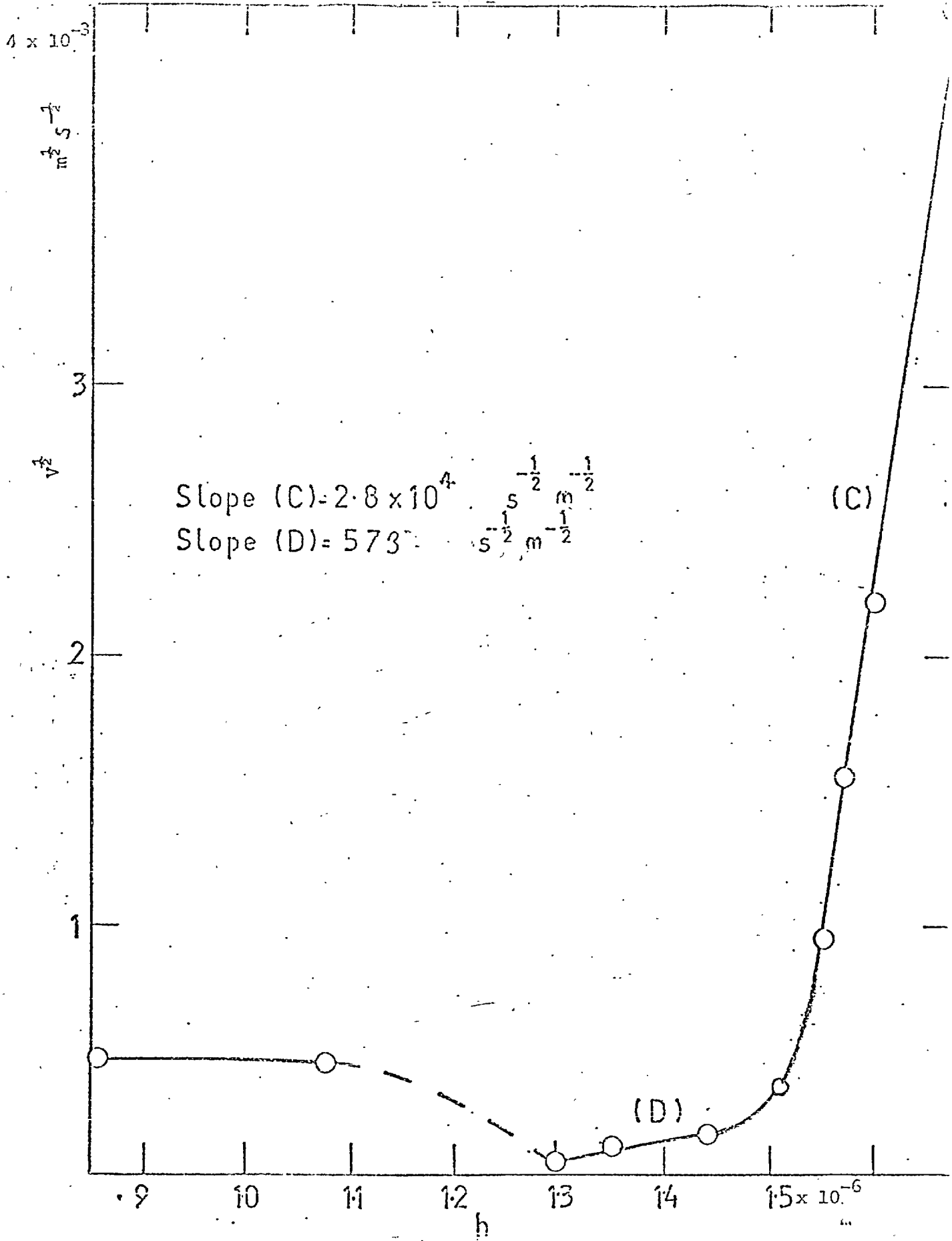

GRAPH OF SQUARE ROOT OF APPROACH VELOCITY OF

CONTACT CENTRE AGAINST TIME

FLUID 3

$$s = \frac{5.1}{12\eta_o R\alpha} \qquad \text{.....(40)}$$

where η_o is the viscosity of the fluid at atmospheric pressure and α is pressure viscosity coefficient of the fluid (assumed constant) and R is the radius of the ball.

The above equation should hold for central pressures greater than 7×10^3 p.s.i. (5×10^7 N/m^2). From (39) and (40):

$$\alpha = \frac{5.1}{12\eta_o R} \times \frac{1}{(\text{slope of curve})^2} \qquad \text{.....(41)}$$

By measuring the slope of the graph, and substituting this into equation (41) the apparent α value can be found.

For <u>fluid 1</u> we have:

$\eta_o = 4.4$ NS/m^2

slope A = 12×10^4 $s^{-\frac{1}{2}}$ $m^{-\frac{1}{2}}$

slope B = 3.37×10^2 $s^{-\frac{1}{2}} m^{-\frac{1}{2}}$

Hence:

$\alpha_A = 5.27 \times 10^{-10}$ m^2/N (3.6×10^{-6} p.s.i.$^{-1}$)

$\alpha_B = 6.67 \times 10^{-5}$ m^2/N (4.6×10^{-1} p.s.i.$^{-1}$)

For <u>fluid 3</u> we have:

$\eta_o = 0.7$ NS/m^2

slope C = 2.8×10^4 $s^{-\frac{1}{2}}$ $m^{-\frac{1}{2}}$

slope D = 5.73×10^2 $s^{-\frac{1}{2}} m^{-\frac{1}{2}}$

Hence:

$\alpha_C = 6.1 \times 10^{-8}$ m^2/N (4.2×10^{-4} p.s.i.$^{-1}$)

$\alpha_D = 1.45 \times 10^{-4}$ m^2/N (1 p.s.i.$^{-1}$)

It can be seen from these results, that only for slope C, which is for fluid 3, is the computed 'α' value within an order of magnitude of the normally accepted value

It is possible that the damping of the dashpots and the inertia of the ball which Christensen does not consider, lead to an inaccuracy in the magnitude of the velocity, but neither of these factors should affect the overall trend of the results.

The reason for this discrepancy is almost certainly due to Christensen's assumption that the 'α' value of the fluid remains constant with pressure. It was shown in section 5.4 that the 'α' value falls with pressure. Chu and Cameron (19) have also pointed out the inaccuracy of this law when taken over a wide pressure range. This must have a considerable effect on the results. It can be seen from the plots of viscosity against pressure that taking α as constant would result in errors of the order of 10^8 poise (10^8 NS/m^2) in a pressure range of 0 - 140 x 10^3 p.s.i. (0 - 10^9 N/m^2).

The problem appears to be how to explain the way in which a fall of the 'α' value can cause the relative approach velocity of the centre of the entrapment to be much less than expected. In the extreme case this velocity falls to zero. A qualitative explanation is as follows:

Christensen shows that the pressure inside an entrapment is proportional to αE. A fall in α towards the centre will reduce the pressure gradient there . This reduction will reduce the force driving the oil from the middle, so that the rate of flow of the oil will greatly decrease. The surfaces around the edge of the entrapment are normally prevented from touching by this oil flow, in the extreme case, where there is no flow, these two surfaces will touch completely.

Christensen's theory was of course developed for a fluid with a constant α value, and so no exact prediction can be made for the fluids tested. It does seem likely however, that the assumption

that a fall in the α value towards the centre will have this result of reducing the pressure gradient inside the contact. The resultant reduction in flow will allow the edges to come together quicker and will slow down the descent of the centre. The pressure gradient will be large at the edge of the entrapment, but as the film thickness is very small this will not result in very much fluid flow.

This explanation shows why some fluids are bad lubricants despite initially high 'α' values. If the increase of viscosity with pressure ceases, the surfaces will come into actual contact during normal approach of the two elements. Surface damage would then be caused during subsequent rolling or sliding. It is widely accepted that polyphenyl ethers (fluid 2 is a 5P4E) are bad lubricants, a fact which has been commented on by several workers, Westlake and Cameron (5) and Gentle (46). This is the first theory which explains the lack of lubricating quality. It is one based on bulk properties and does not need to involve any theory of boundary lubricity. In summary then it would appear that Christensen's results can only be taken qualitatively. The most important prediction, that the pressure inside the contact zone is much greater than the equivalent Hertz maximum pressure has been amply verified. The maximum pressure measured was found to be almost six times the equivalent Hertz pressure.

6.6 High Speed Photography Results

A rather troublesome effect was ball bounce. It was found that under certain conditions the ball bounced away from the surface and then returned leaving a much smaller entrapment. This was first noticed when the velocity transducer was used. There appeared to be no correlation between the velocity of the ball and

the size of the entrapment produced. It was then decided to investigate the initial impact using a high speed camera.

Several runs were made using the Miliken camera at 400 frames/sec. The following results were obtained:

When the fluid 1 was used the ball dropped steadily and about .1 sec. elapsed between the time the fringes first became visible and the appearance of the first order fringe (minimum film thickness less than about 3×10^{-7} m). Pictures of the ball falling steadily are shown in Fig. 36. With fluid 3 a rather different result was found. Figs. 37-39 show pictures of various entrapments taken under a range of conditions. It can be seen quite clearly that the ball sometimes bounces away from the surface after the initial impact and there are pictures of cavitation occurring. A number of observations can be made from these photographs:

a) The maximum amount of cavitation, largest entrapment before bounce and smallest after, occurred in Fig. 37, at a temperature of 26°C and load of 2.16 Kg.

b) Figs. 37 and 38 show that at a temperature of 26°C a much deeper entrapment is formed after bouncing with a load of 1.69 Kg than with a load of 2.16 Kg. The reverse is true before the ball bounces.

c) Fig. 39 shows that at a load of 1.03 Kg and a temperature of 26°C there is very little bouncing effect.

From these observations the following was deduced:

Before the ball bounces the maximum depth entrapment is formed by the largest load. This produces the greatest amount of cavitation. After the ball has bounced, there is a critical load which produces the maximum depth of entrapment. A higher load produces more cavitation and allows more fluid to escape. A lower

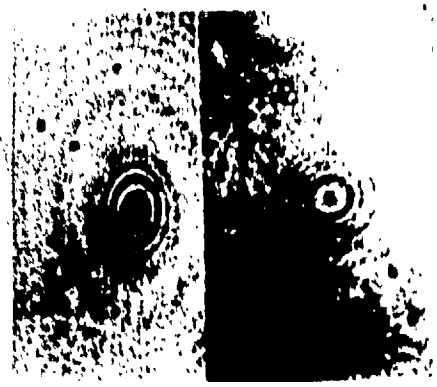

t = 0.0025 secs

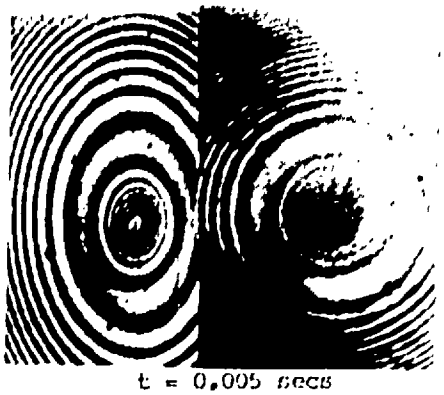

t = 0.005 secs

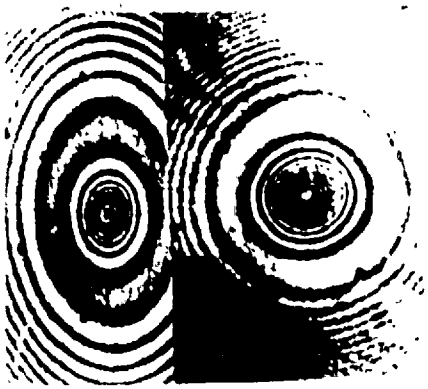

t = 0.0075 secs

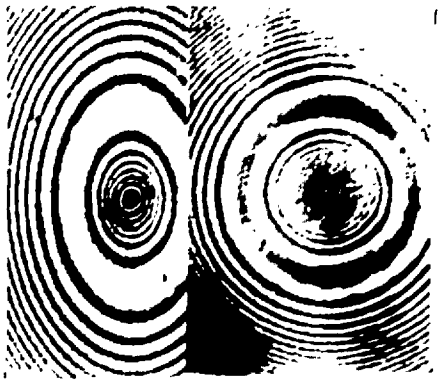

t = 0.02 secs

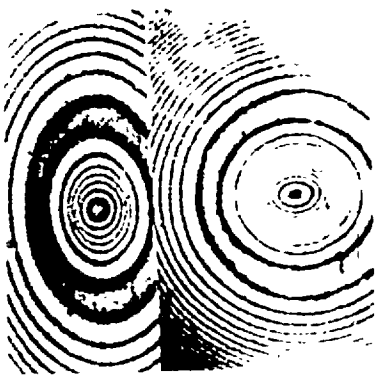

t = 0.04 secs

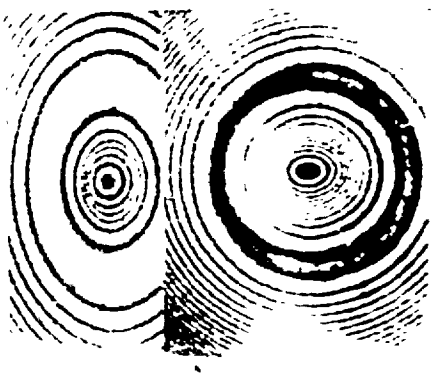

t = 0.01 secs

HIGH SPEED PHOTOGRAPHY RESULTS

FLUID 1

TEMPERATURE 23°C LOAD 0.1 gms

FIG. 5

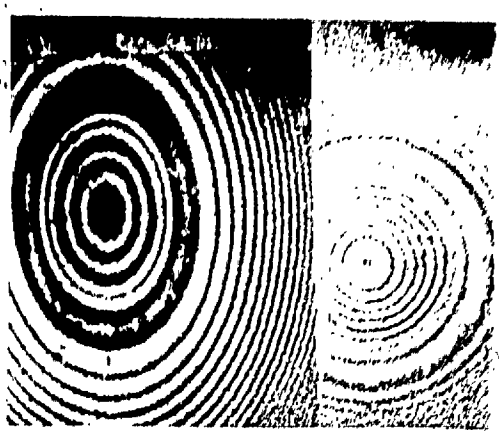

t = 0.0025 secs

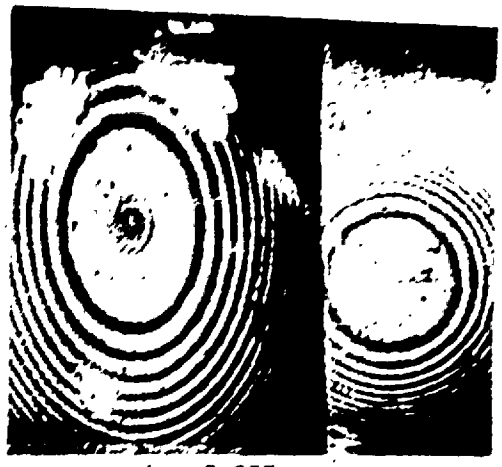

t = 0.005 secs

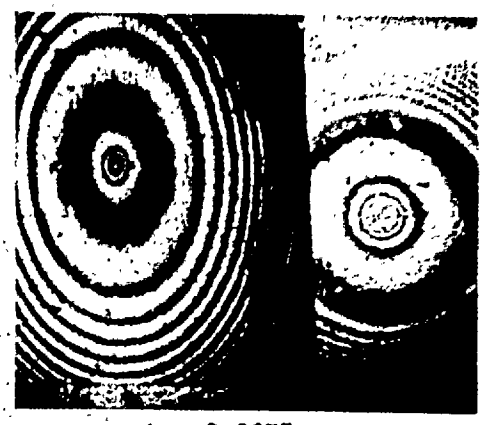

t = 0.0075 secs

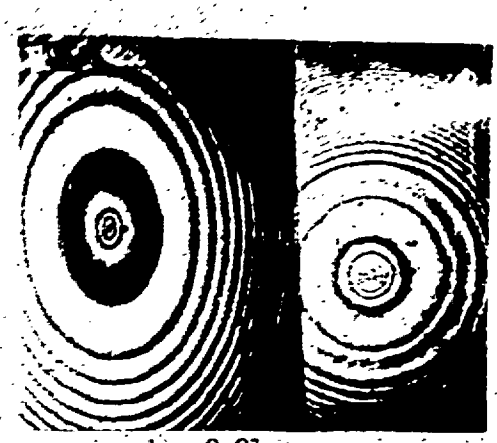

t = 0.01 secs

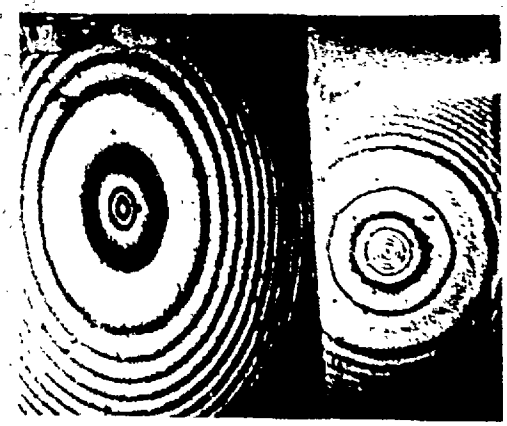

t = 0.0125 secs

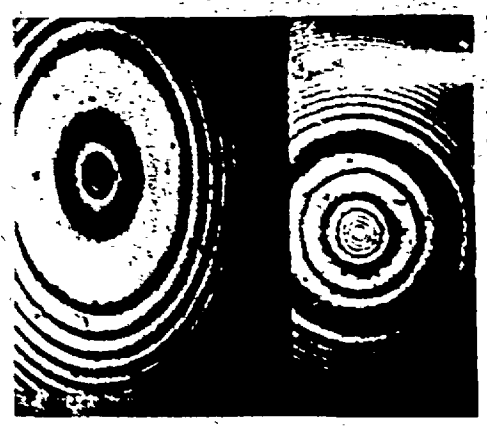

t = 0.0150 secs

HIGH SPEED PHOTOGRAPHY RESULTS

FLUID 3

TEMPERATURE 26°C LOAD 2.16Kg

FIG. 37

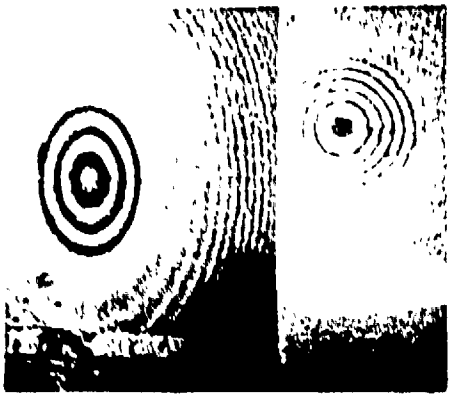

t = 0.0025 secs

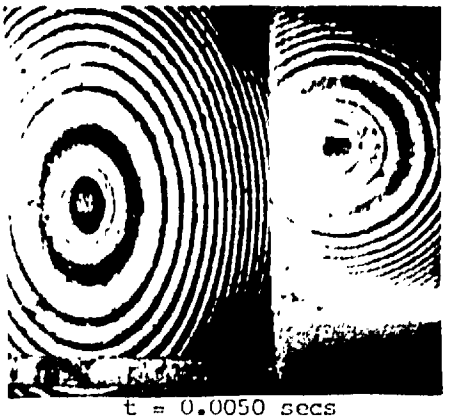

t = 0.0050 secs

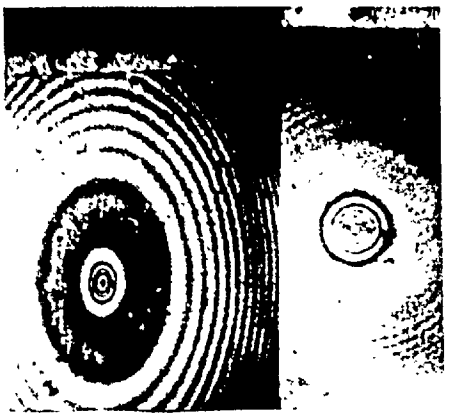

t = 0.0075 sec

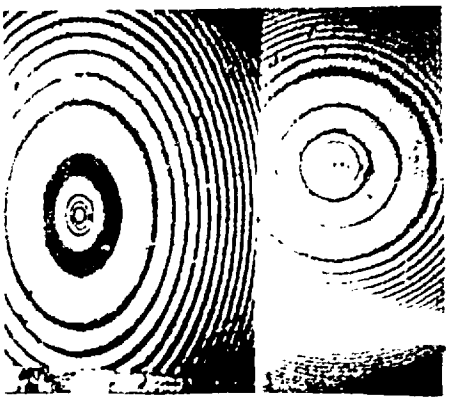

t = 0.01 sec

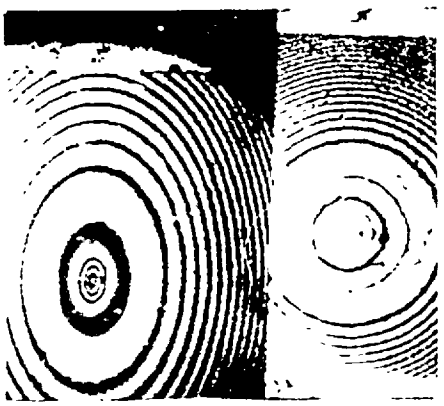

t = 0.0125 sec

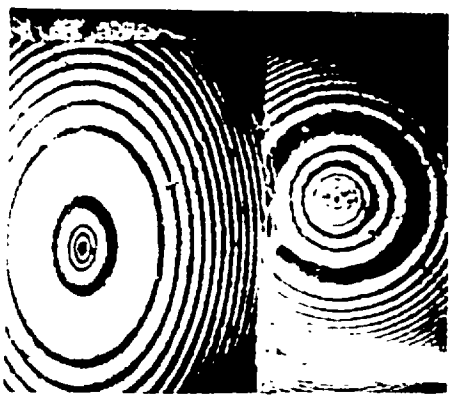

t = 0.0150 sec.

HIGH SPEED PHOTOGRAPHY RESULTS

FLUID

TEMPERATURE 26°C - LOAD 1.69Kg

FIG. 3H

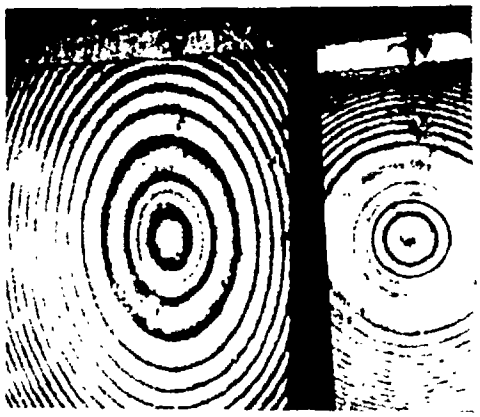

t = 0.0000 secs

t = 0.005 secs

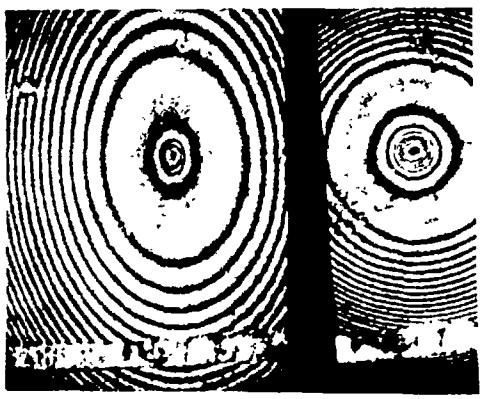

t = 0.0075 secs

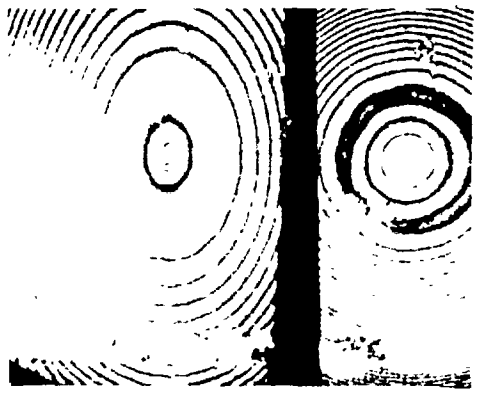

t = 0.01 secs

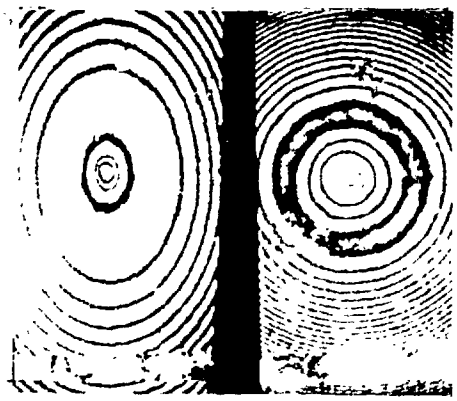

t = 0.0125 secs

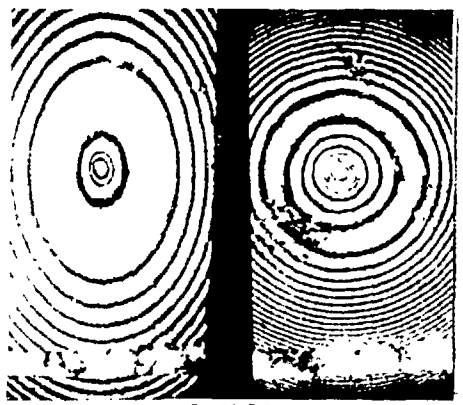

t = 0.0150 secs

HIGH SPEED PHOTOGRAPHY RESULTS

FLUID 3

TEMPERATURE 26°C LOAD 1.03Kg

FIG. 39

load produces hardly any cavitation and consequently little fluid loss, but since the original entrapment before the bouncing is much smaller, the resultant entrapment is also smaller. The critical load for maximum entrapment size is around 1.6 Kg at 26°C although this is almost certainly dependant on the amount of damping in the system. It was also found that the lower the temperature and consequently the higher the viscosity, the less the ball bounced away and so by having a lower temperature a higher load could be used.

The reason that the ball did not bounce away when fluid 1 was used was because it had a higher viscosity. This damped down the ball sufficiently to prevent the ball coming away from the surface, under all the loads tried with the high speed camera. Evidence was obtained of bouncing with fluid 1 when the damping due to the dashpots (see Fig. 10) was reduced.

6.7 Experimental Accuracy

Some consideration must be given to the accuracy of the quantities measured in the previous sections.

The temperature of the oil was taken as room temperature. This was measured with a mercury thermometer accurate to better than .5°C. There was some consideration as to whether the compression of the oil would lead to a significant temperature rise. The dissipation of heat during the time the ball falls is clearly a problem of some complexity and must be taken into account if calculations during this phase of the process are undertaken. The viscosities are computed from results after the ball has virtually come to rest and as conduction from such a thin film is virtually instantaneous, the assumption of isothermal conditions is justified.

The rate of flow from the entrapment is of course very small. This assumption is confirmed by the fact that viscosity measurements do not show any variation with time. If there was a significant temperature rise, the measured viscosity would increase with time, as the oil cooled. No such effect was observed.

The accuracy of all the measurements depends on the accuracy with which the refractive index and elastic distortion can be measured . Over most of the area of the entrapment this was very high as the refractive index and the distortion were measured to better than 1%. At the centre and edge of the entrapment, however, where the two surfaces are approximately parallel, the accuracy falls considerably. This is due to the lack of detail in monochromatic fringes. For the rest of the entrapment it is quite a simple matter to interpolate between the fringes; this is much more difficult to do beyond the first and last fringes in the entrapment. The absolute error might be as high as 4×10^{-7} m which would lead to errors of about 2% in the maximum film thickness and as much as 50% in the minimum . There was a scatter of the individual pressure calculations, but these were eliminated by drawing a smooth curve through the points. The pressure results were therefore thought to be as accurate as the maximum film thickness measurement, which was within 2%.

This limit on the accuracy of the pressure curve sets the limit on the accuracy to which the density can be measured, providing that the refractive index is accurately known and assuming that the Lorentz-Lorenz relationship is valid, see section 2.10.

The greater the fringe order, the greater the accuracy of the refractive index measurement, because the separation between the fringe orders at the two angles becomes greater. For this reason

the index is known far more accurately towards the centre of the contact (about .1%) than near the edge (5% accuracy). This gives an error in the density measurement varying from .3% to 12%. This error is greater than the error in the pressure determination towards the edge of the contact, but near the centre the error in the pressure determination error will predominate. Hence the accuracy of the density measurement will vary from 12% at low pressures to 2% at high pressures.

For the viscosity measurements the accuracy for the pressure calculations give a systematic error of up to 2% in the results. The random errors were reduced by drawing a smooth curve through the points. The error in the distortion measurements were only really significant above the highest order fringe and below the first order fringe. For this reason these results were not plotted. Hence the overall accuracy of the viscosity results given should be better than 2%.

An interesting way of examining the errors is by considering the correlation with measurements made by other methods. Although it was not possible to make measurements at a low enough pressure to compare directly with the available data on the fluids, the general continuity of the pressure viscosity measurements does give confidence in the results. Bulk modulus measurement gives a slightly less satisfactory correlation, but even still the results are not significantly different from the separate data obtainable on the fluids, and just fall within the predicted accuracy.

6.8 Conclusions and Suggestions for Future Work

A novel approach to the measurement of absolute film thickness has lead to a new technique for measuring the distortion

and refractive index for fluids in a point contact with normal approach. Using this absolute distortion the pressure distribution has been calculated inside the contact - the first time this has been done.

The most interesting part of the whole project is the measurement of viscosity. Using the pressure, density and film thickness measurements taken at various intervals of time, a complete solution of Reynold's equation has been found and the variation of viscosity with pressure calculated. The range of viscosity measurements made have extended from 10^2 - 10^8 poise ($10 - 10^7$ NS/m^2), an extremely wide range. The only other technique capable of reaching these values of viscosity are rolling discs which measure apparent viscosities. The method described here is absolute. It could make an important contribution to basic rheological research in the future. Evidence has been found that fluid 2 goes into a glassy state which has a viscosity independent of pressure. This is related to the pour point temperature.

Christensen's theoretical approach to a dropping ball has been tested experimentally and does not appear to make very good predictions with the four fluids tested under the comparatively high load used. This deviation is almost certainly due to the failure of the assumption that the viscosity - pressure coefficient is not a function of pressure. Some high speed films show that the ball will bounce away from the surface under certain conditions.

From a somewhat nebulous starting point which was merely to attempt to find a method for measuring the refractive index in an E.H.L. contact, this project has produced useful data on fluid properties at high pressures. From small acorns, great oaks grow.

New techniques have been developed in this project which

could play an important part in rheological research. The work should now be extended to higher pressures and a greater range of fluids. This can be done by using sapphire instead of glass for the ball and hemisphere and finding an effective damping system to prevent the ball from bouncing away from the surface. The large Young's modulus (50×10^6 p.s.i. or 3.8×10^{11} N/m^2) of the sapphire would mean that the pressures would be greatly increased for the same load. Preventing the ball from bouncing would enable less viscous fluids to be tested.

Another necessary development is to vary the ambient temperature of the fluid.

APPENDIX I

In this section a flow chart and listing for the programme to calculate the viscosity of the oil is given. The programme was written in Fortran IV and was run on an I.B.M. 70.94. The programme was designed to be flexible as to the number of pictures it works from and for the number of data points taken from each picture.

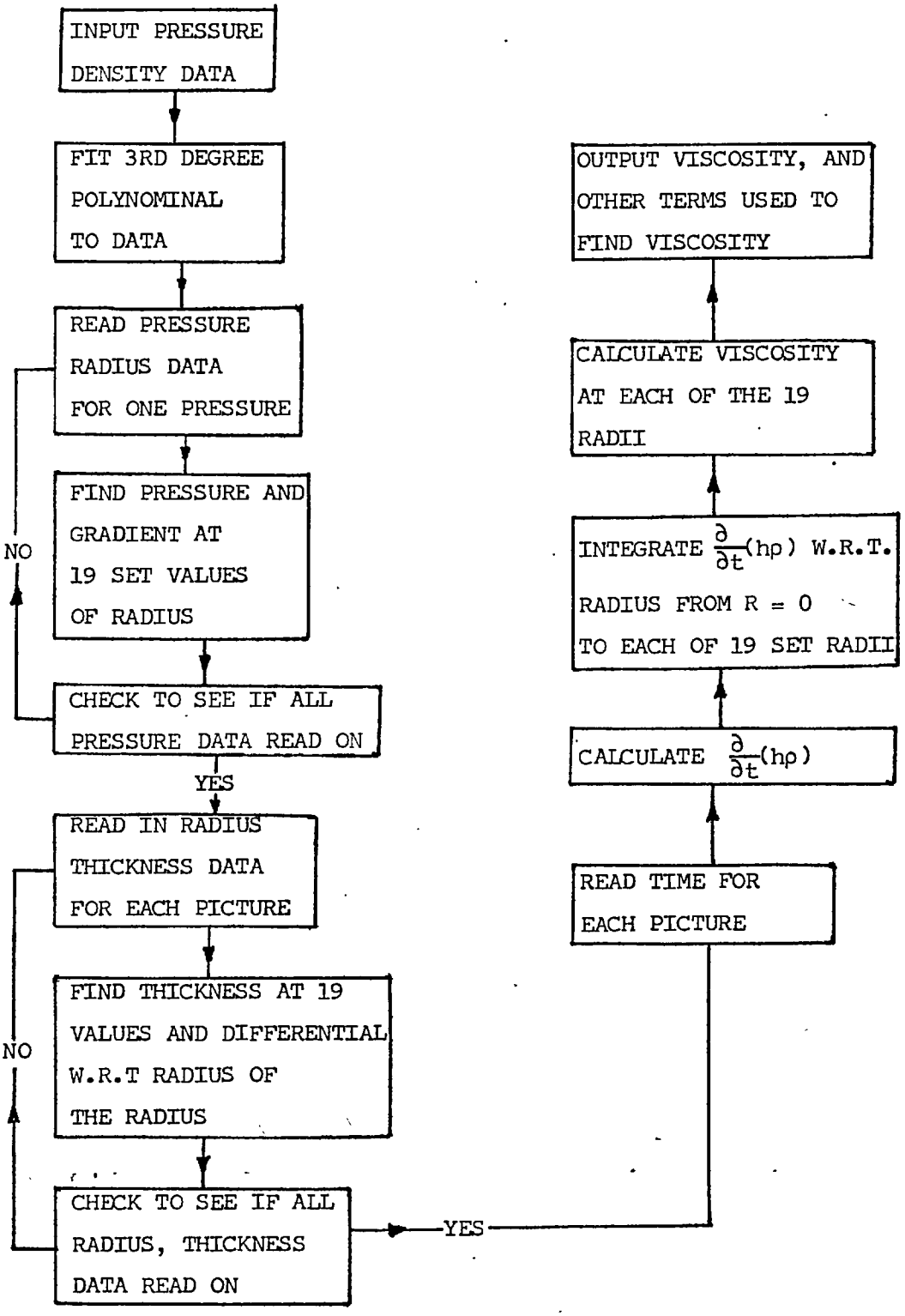

FLOW CHART FOR VISCOSITY CALCULATION PROGRAMME

```
      NB=19
C     NB= NOS OF POINTS AT WHICH VISCOSITY IS CALCULATED
      NC= 0
      ND=8
C      NA= NOS OF DATA POINTS FOR PRESSURE AND DIAMETER
C      ND=  NOS OF SETS OF DATA
       ND=7
      ND=3
      ND=6
      ND=5
      ND=3
      NA= 10
      NA=21
C     READS ON PRESSURE DENSITY DATA
      READ(5,555)(PREN(N),N= 1,12)
      READ(5,555)(DEN(N) ,N=1,12)
  555 FORMAT(8F8.2)
  556 FORMAT(8F8.7)
      DO 9999 N=1,12
      PREN(N)=PREN(N)*11.0/7.9*33.0/32.0*10.0/7.9*33.0/32.
 9999 CONTINUE
C     POLYFT IS ROUTINE TO FIT A POLYNOMINAL TO POINTS
      CALL POLYFT(PREN,DEN,12,3,C,CO,A,6)
C     ARRAY AR STORES PRESSURE DENSITY COEFFICENTS
      AR(1)=C(1)
      AR(2)=C(2)
      AR(3)=C(3)
      AR(4)=CO
C     DIL IS NUMBE / BY 19 TO GIVE RADII TO FIND VISCOSITY
      READ(5,111)DIL
```

```
      DO 1 N=1,NB
      D(N)= DIL /20.0*(FLOAT(N))/2.0
    1 CONTINUE
   41 FORMAT(40H  RADIUS  AT WHICH VISCOSITES CALCULATED)
      WRITE(6,41)
      WRITE(6,60)(D(N),N=1,NB)
   60 FORMAT(8F8.5)
  201 CONTINUE
C     APMAX IS FACTOR TO CONVERT NORMALISED PRESSURES TO P.S.I.
      READ(5,91)(APMAX)
C     PRE IS ARRAY TO STORE PRESSURES
      READ(5,10)(  PRE(N),N=1,NA)
   91 FORMAT(F8.7)
C     DIT IS RADIUS AT WHICH PRESSURE IS PUT TO 0
      READ(5,111)DIT
      WRITE(6,750)DIT
  750 FORMAT(20H RADIUS AT MIN FILM=1PE13.5)
  111 FORMAT(F8.7)
      WRITE(6,751) APMAX
  751 FORMAT(10H APMAX    =1PE13.4)
      PIT=APMAX*1000000.00
      PIT=APMAX*1000000.00 /7.9*10.0/32.0*33.0
      WRITE(6,24)PIT
    10 FORMAT(8F8.6)
      DO 90 N=1, NA
C     DIA IS ARRAY TO STORE DIAMETER DATA
      DIA(N)= DIT    /20.0*(FLOAT(N)-1.0)/2.0
       PRE(N)= PRE(N)*PIT
      BOAD=PRE(N)*DIA(N)*2.0*3.142/2.54/2.54*DIT/20.0    +BOAD
   90 CONTINUE
```

```
  902 FORMAT( 25H  PRESSURE  DIAMETER DATA)
      WRITE(6,902)
  901 FORMAT(1X,F10.0,1X,F10.7)
   11 FORMAT(8F8.7)
      NC=NA*NA
      NX=2*NA
C     FIT 6TH DEGREE CURVE TO PRESSURE/DIAMETER DATA
      C(6)= 0.0
      C(5)= 0.0
      NR=NA-2
C     WORKS OUT PRESSURE + GRADIENT AT VALUES OF D
      DO 802NY=1,NR
      DO 801 N=1,3
      NN=N+NY-1
      DIK(N)=DIA(NN)
      PIK(N)=PRE(NN)
  801 CONTINUE
      CALL POLYFT(DIK,PIK,3,2,C,CO,A,6)
      NX=NY
      NP=NX+NC
      PRESDI(1,NP)= C(1)+ 2.0*C(2)*D(NX)
      PRESDI(2,NP)=D(NX)*C(1)+C(2)*(D(NX))**2+CO
  802 CONTINUE
      NZ=NZ+1
C     PRESDI(2,--- IS PRESSURE (1---- IS GRADIENT
C     PRESDIF(2,----- = PRESSURE
      WRITE(6,24) BOAD
      BOAD=0.0
      NC= NC+NB
      NE=ND*NB
```

```
      IF(NP.LT.NE) GO TO 201
 2779 FORMAT(1X,1PE13.4,1PE13.4)
      WRITE(6,2779)(PRESDI(1,N),PRESDI(2,N),N=1,NE)
C     CHECKS TO SEE IF ALL DATA HAS BEEN READ ON
C     NF= NOS OF DATA PTS FOR DIAM THICKNESS
      NE= 0
      NZ=1
   13 CONTINUE
      NE= NE+ 1
      NF=11
C     BMIN IS MINIMUM FILM THICKNESS ADDED TO DATA
      READ(5,815)BMIN
C     DI IS  THE MAXIMUM DIAMETER
      READ(5,111)DI
C     THIK IS ARRAY TO STORE THICKNESS DATA
      READ( 5,11)(THIK(N),N=1,NF)
      B=270000.0
      WRITE(6,723) BMIN
  723 FORMAT( 24H MINIMUM FILM THICKNESS=  1PE13.4)
      WRITE(6,24) DI
      DO 817 N=1,NF
      DIAM(N)= DI/10.0*(FLOAT(N)-1.0)/2.
C     CONVERTS DATA TO CENTIMETRES
      THIK(N)=THIK(N)/10000.0
  817 CONTINUE
  815 FORMAT(F10.9)
      NR= NF-2
C     WORKS OUT VALUES OF THICKNESS AT 'D
      DO 803 NY=1,NR
      DO 804 N=1,3
```

```
      NN= N+NY-1
      DIK(N)=DIAM(NN)
      PIK(N)=THIK(NN)
  804 CONTINUE
      CALL POLYFT (DIK,PIK,3,2,C,CO,A,6)
      DO 822NQ=1,2
      NP=NY
      NP= NY*2+NQ-2
  831 CONTINUE
C     ARRAY H STORES VALUES OF THICKNESS
      DIFR(NE,NP)=C(1)+2.0*C(2)*D(NP)
      H(NE,NP)=C(1)*D(NP)+C(2)*D(NP)**2+CO
C     CHECK TO ENSURE THAT ROUTINE WORKING D-DIK MUST BE SMALL
      NV=NB-1
      IF(NP.EQ.NV) GO TO 830
      GO TO 832
  830 NP= 19
      NP=NB
      GO TO 831
  832 CONTINUE
  822 CONTINUE
  803 CONTINUE
  820 FORMAT(1PE13.4,1PE13.4)
      WRITE(6,1002)
C     INTEGRATES TO GIVE VOLUME INSIDE RADIUS D
      DO 805 NY=1,NR
      DO 806 N=1,3
      NN= N+NY-1
      DIK(N)=DIAM(NN)
      NUT=NN
```

```
      NUT=NN+NS*(NE-1)
      PIK(N)=THIK(NN)                                    *DIAM(NN)*3.142*2.
  806 CONTINUE
      CALL POLYFT (DIK,PIK,3,2,C,CO,A,6)
      DO 821 NQ=1,2
      NP=NY
      NP= NY*2+NO-2
  842 CONTINUE
      NU=NP-1
       IF(NU.EQ.0) GO TO 850
      GO TO 851
  850 CONTINUE
      NU= 25
      D(25)=0.0
  851 CONTINUE
      NUT= NP+NB*(NE-1)
      NUP=NUT-1
      IF (NP.EC.1) GO TO 402
      GO TO 401
  402 NUP=200
      AJ(200)= 1.0
  401 CONTINUE
      PI=PRESDI(2,NUT)
      AJ(NUT)= PI*AR(1)+AR(2)*(PI**2)+AR(3)*(PI**3)+AR(4)
C     BNTEGIS THE INTEGRAL FROM D(X)TO D(X+1)
      BNTEG(NP)=(C(1)/2.0*(D(NP)**2-D(NU)**2)+C(2)/3.0*(D(NP)**3-D(N
     1 **3)+(D(NP)-D(NU))*CC)*(AJ(NUT)+AJ(NUP))/2.0
C     AJ MULTIPLIES BY THE AVERAGE DENSITY FROM D(X) TO D(X+1)
      IF(NP.EC.NV) GO TO 840
      GO TO 841
```

```
  840 NP= 19
      NP=NB
      GO TO 842
  841 CONTINUE
  821 CONTINUE
  805 CONTINUE
      DO 808 N=1,NB
      NOT=N+NB*(NE-1)
C     WORKS OUT H*DENSITY
      VOL(NE,N)=H(NE,N)*AJ(NOT)
  808 CONTINUE
  403 FORMAT(15H DENSITY     =  1PE13.5)
  810 FORMAT(1X, F8.6,F8.6)
   92 FORMAT(I4)
C      FINDS THICKNESS AT VALUES OF D'
      NZ=NZ+1
C     INTEGRATES CURVE FROM D=C TO D= D
   15 CONTINUE
 1001 FORMAT(1X,F10.9,1X,F10.9)
 1002 FORMAT(22H   THIK       DIAM      )
 1004 FORMAT(30H   DENS= DIAM*THIK*2*3.142     )
      IF( NE.LT.ND) GO TO 13
      READ(5,16)(TIME(N),N=1,ND)
      WRITE(6,24) (TIME(N),N=1,ND)
   16 FORMAT(F7.0)
      DO 113 N=1,ND
      TIME(N)= TIME(N)/400.0
      TIME(N)=TIME(N)*400.0/3.0
C     READS ON TIME BETWEEN PICTURES AND COVERTS TO SECONDS
  113 CONTINUE
```

```
    6 CONTINUE
      DO 17 NJ= 1,NB
C     WORKS OUT D/DT(H*DENSITY TERM)
      DO 18 N=1,ND
      V(N)= VOL(N,NJ)
      HA(N)= H(N,NJ)
   18 CONTINUE
      NU= ND-2
      DO 2NNN=1,NU
      DO 3 N=1,3
      NN= N+NNN-1
      TIM(N)= TIME(NN)
      VIM(N)=V(NN)
      DIK(N)=TIME(NN)
      PIK(N)=HA(NN)
    3 CONTINUE
      CALL POLYFT( TIM,VIM,3,2,C,CO,A,6)
      C(3)= 0.0
      C(4)= 0.0
      C(6)= 0.0
      C(5)= 0.0
      NS= NNN+1
      VOLDIF(NS,NJ)=   C(1)+C(2)*2.0*TIME(NS)
C     VOLDIF IS D/DT(H*DENSITY TERM)
      CALL POLYFT(DIK,PIK,3,2,C,CO,A,6)
       DIFH(NS,NJ)=C(1)+C(2)*2.0*TIME(NS)
      IF(NS.EQ.2) GO TO 361
      GO TO 362
  361 CONTINUE
      DIFH(1,NJ)=C(1)+C(2)*2.0*TIME(1)
```

```
      VOLDIF(1,NJ)=C(1)+C(2)*2.0*TIME(I)
  362 CONTINUE
      NZ=ND-1
      IF(NS.EQ.NZ) GO TO 363
      GO TO 364
  363 CONTINUE
      DIFH(ND,NJ)=C(1)+C(2)*2.0*TIME(ND)
      VOLDIF(ND,NJ)=C(1)+C(2)*2.0*TIME(ND)
  364 CONTINUE
    2 CONTINUE
C     VOLDIF STORES THE RATE OF FLOW CALCULATIONS
C      RATE OF FLOW FOR THE FIRST AND LAST PICTURES  IS PUT = TO NEX
      NUT=ND-1
      VOLDIF(ND,NJ)=VOLDIF(NUT,NJ    )
      DIFH(ND,NJ)=DIFH(NUT,NJ)
  924 FORMAT(40H DIFFERENTIAL,RATE FILM SQEEZED          )
      WRITE(6,924)
      WRITE(6,244)(DIFH(NT,NJ),VOLDIF(NT,NJ),NT=1,ND)
  244 FORMAT(1X,  1PE13.4,4X,1PE13.4)
   17 CONTINUE
      DO 950 NK=1,ND
      DO 951 NL=1,NB
      N=NL+(NK-1)*NB
      XX(NK,NL)=(H(NK,NL)**3)*D(NL)*PRESDI(1,N)
      YY(NK,NL)=H(NK,NL)*DIFH(NK,NL)/DIFR(NK,NL)*D(NL)
     1 *AJ(N)
  951 CONTINUE
  950 CONTINUE
      NZ=NB-2
      DO 903 NK=1,ND
```

```
      DO 991 NY=1,NZ
      DO 992 N=1,3
      NL=N+NY-1
      PIK(N)=XX(NK,NL)
      DIK(N)=D(NL)
  992 CONTINUE
      CALL POLYFT(DIK,PIK,3,2,C,CO,A,6)
      NO=NL-1
      DIFXX(NK,NO)=C(1)+2.0*C(2)*D(NO)
  991 CONTINUE
      DIFXX(NK,1)=DIFXX(NK,2)
      NO=NB-1
      DIFXX(NK,NB)=DIFXX(NK,NO)
  993 CONTINUE
C     PRINTS OUT SOME OF THE TERMS IN REYNOLDS EQATION
      WRITE(6,398)
  398 FORMAT(40H   H**3*RAD*DP/DR                              )
      WRITE(6,309)(XX(1,N),XX(2,N),XX(3,N),XX(4,N),XX(5,N),N=1,NB)
      WRITE(6,309)(XX(6,N),XX(7,N),XX(8,N),XX(9,N),XX(10,N),N=1,NB)
  237 FORMAT(40H    H*RAD*DH/DT*DR/DH                          )
      WRITE(6,237)
      WRITE(6,309)(YY(6,N),YY(7,N),YY(8,N),YY(9,N),YY(10,N),N=1,NB)
      WRITE(6,309)(YY(1,N),YY(2,N),YY(3,N),YY(4,N),YY(5,N),N=1,NB)
      WRITE(6,397)
  397 FORMAT(40H DIFFERENTIAL OF H AGAINST RADIUS               )
      WRITE(6,309)(DIFR(1,N),DIFR(2,N),DIFR(3,N),DIFR(4,N),DIFR(5,N),
     11,NB)
      WRITE(6,309)(DIFR(6,N),DIFR(7,N),DIFR(8,N),DIFR(9,N),DIFR(10,N)
     3N=1,NB)
      DO 913 NK=1,ND
```

```
      DO 911 NY=1,NZ
      DO 912 N=1,3
      NL=N+NY-1
      PIK(N)=YY(NK,NL)
      DIK(N)=D(NL)
  912 CONTINUE
      CALL POLYFT(DIK,PIK,3,2,C,CO,A,6)
      NO=NL-1
      DIFYY(NK,NO)=C(1)+2.0*C(2)*D(NO)
  911 CONTINUE
      DIFYY(NK,1)=DIFYY(NK,2)
      NQ=NB-1
      DIFYY(NK,NB)=DIFYY(NK,NQ)
  913 CONTINUE
      WRITE(6,914)
  914 FORMAT(40H  DIF OF  H *RAD*DR/DH*DH/DT                    )
      WRITE(6,309)(DIFYY(1,N),DIFYY(2,N),DIFYY(3,N),DIFYY(4,N),DIFYY(
     2 N),N=1,NB)
      WRITE(6,309)(DIFYY(6,N),DIFYY(7,N),DIFYY(8,N),DIFYY(9,N),DIFYY
     6 ,N),N=1,NB)
C     INTEGRATES THR RADIUS*D/DT(DENSITY*H)
      DO 270 NL=1,ND
      NV=NB-2
      DO 271 NK=1,NV
      DO 272 N=1,3
      NN= N+NK-1
      DIK(N)=D(NN)
      PIK(N)=D(NN)*VOLDIF(NL,NN)*2.0  +DIFYY(NL,NN)
      PIK(N)=D(NN)*VOLDIF(NL,NN)*2.0
  272 CONTINUE
```

```
      CALL POLYFT(DIK,PIK,3,2,C,CO,A,6)
      DIF=D(2)-D(1)
      IF(NK.EQ.1) GO TO 273
      GO TO 274
  273 CONTINUE
      BNTEG(1)=C(1)/2.0*((D(1))**2.0)+C(2)/3.0*(D(1)**3.0)+DIF*CO
  274 CONTINUE
      NZ=NK+1
      BNTEG(NZ)=C(1)/2.0*((D(NZ))**2.0-(D(NZ)-DIF)**2.0)+C(2)/3.0
     1*((D(NZ))**3.0-(D(NZ)-DIF)**3.0)+DIF*CO
      IF (NK.EQ.NV) GO TO 275
      GO TO 276
  275 CONTINUE
      BNTEG(NB)=C(1)/2.0*((D(NB))**2.0-(D(NB)-DIF)**2.0)+C(2)/3.0*(
     1 **3.0 -(D(NB)-DIF)**3.0)+DIF*CO
  276 CONTINUE
      BNTE(1) =BNTEG(1)
      BNTE(NZ)=BNTEG(NZ)+BNTE(NK)
  271 CONTINUE
      BNTE(NB)=BNTE(NZ)+BNTEG(NB)
      DO 278 N=1,NB
      VOL(NL,N)=BNTE(N)
  278 CONTINUE
  270 CONTINUE
   46 FORMAT(40H    INTEGRAL OF DH/DT*RAD*2.0                          )
      WRITE(6,46)
      WRITE(6,309)(VOL(1,NL),VOL(2,NL),VOL(3,NL),VOL(4,NL),VOL(5,N
     2 ,NL=1,NB)
      WRITE(6,309)(VOL(6,NL),VOL(7,NL),VOL(8,NL),VOL(9,NL),VOL(10 ,
     2 ,NL=1,NB)
```

```
      DO 20 NK=1,ND-
      DO 21 NL=1,NB
      N=NL+(NK-1)*NB
C     WORKS OUT THE VISCOSITY IN POISE
      VISC(N)=H(NK,NL)**3.0*D(NL)*PRESDI(1,N)/(VOL(NK,NL)
     1 6.0*68965.0*AJ(N)
C     REST OF THE PROGRAMME IS DIFFERENT WAYS OF PRESENTING THE DAT
      ASTRES(N)=PRESDI(1,N)*H(NK,NL)/2.0
      ASHER(N)=ASTRES(N)/VISC(N)
C      REYNES TO POISE DIAMETER CMS TO INCHES-1
C     USES EQATION FOR FLOW IN X DIRECTION
   21 CONTINUE
   20 CONTINUE
      NM= NB *ND
   44 FORMAT(28H VISCOSITY          PRESSURE)
      WRITE(6,44)
      WRITE(6,23)(VISC(N),PRESDI (2,N),ASHER(N),ASTRES(N),N=1,NM
   23 FORMAT(1X,F20.5 ,3X,F10.0,1X,E13.5, 1X,E13.5)
      DO 100 N=1,NM
      VIS(N)= ALOG10(ABS(VISC(N)))
      P(2,N)= ALOG(ABS(VISC(N)))
      P(1,N)= PRESDI(2,N)
  100 CONTINUE
      WRITE(6,1003)
      NX=NB*ND
      WRITE(6,309)(AJ(N),N=1,NX)
      WRITE(6,51)(P(1,N),P(2,N),VIS(N),N=1,NM)
      DO 102 NT=1,ND
      DO 101 NP=1,NB
      N= (NT-1)*NB+NP
```

```
      PA(2,NP)= ALOG(ABS(VISC(N)))
      PA(1,NP)= PRESDI(2,N)
  101 CONTINUE
  102 CONTINUE
 1003 FORMAT(36H  PRESSURE  LOGE VISCOSITY VISCOSITY)
   51 FORMAT(1X,F20.5,3X,F10.5,3X,F10.5)
      NM=NB*ND
      NE=ND*NB
      WRITE(6,45)
      NH=ND*NB
   45 FORMAT(6H DP/DD)
      WRITE(6,48)
      WRITE(6,309)(H(1,NL),H(2,NL),H(3,NL),H(4,NL),H(5,NL),NL=1,NB
      WRITE(6,309)(H(6,NL),H(7,NL),H(8,NL),H(9,NL),H(10,NL),NL=1,N
   48 FORMAT(18H THICKNESS OF FILM)
      WRITE(6,47)
   47 FORMAT(23H VOLUME FROM D=0,TO D=D)
   24 FORMAT(1X, 1PE16.7)
  309 FORMAT(1PE13.4,1PE13.4,1PE13.4,1PE13.4,1PE13.4)
      WRITE(6,24)((H      (NK,NL),NL=1,NB),NK=1,ND)
      WRITE(6,92)(NB)
      END
```

APPENDIX II

Fluid 1

This fluid was supplied by B.P. (42) and was described as a paraffinic cylinder stock.

The following data was supplied with it:

At atmospheric pressure:

Temperature	Viscosity	Density
210°F	0.4482 poise	0.863 gm/cc
100°F	10.79 poise	0.8985 gm/cc
68°F	45.00 poise	0.91 gm/cc

Also at 70°F:

Pressure	Viscosity
4000 p.s.i	158.5 poise
6000 p.s.i.	224.0 poise
11000 p.s.i.	2000.0 poise

Fluid 2

This fluid was supplied by Monsanto Corp.(44) and is a 5-phenyl 4-ether (5P4E).

The following data was supplied with it:

Viscosity	Pressure	Temperature
419.0 cps	14.7 p.s.i.	100°F
5536.0 cps	10,000.0 p.s.i.	100°F
17.98 cps	14.7 p.s.i.	210°F
28.0 cps	5,000.0 p.s.i.	210°F
46.5 cps	10,000.0 p.s.i.	210°F

Pour point: 40°F

Bulk modulus 4.6×10^5 p.s.i.

For general properties see Gunderstone and Hart (49)

Fluid 3

This is a polychlorotrifluoro-ethylene oil.

The following data was supplied with it:

At $77^{\circ}F$ the viscosity was 2.66 stokes and its density 1.95 gm/cm^2.

The bulk modulus was quoted as 2.87×10^5 p.s.i.

Fluid 4

This was a Krytox 143 AC fluid. Its properties were as follows:

Viscosity	Temperature
33,000 cs	$0^{\circ}F$
270 cs	$100^{\circ}F$
26 cs	$210^{\circ}F$

Density = 1.9 gm/m at $100^{\circ}F$.

Specific heat = .226 Btv/lb/$^{\circ}F$

Isothermal bulk modulus = 1.5×10^5 p.s.i.

REFERENCES

Ref. (1) Dowson, D. and Jones, D.A. "An Optical Method of Measurement of Time Dependent Elastohydrodynamic Film Profiles" PROC. INST. MECH. ENG. 1967-68 182. Pt. 3b 49-52

Ref. (2) Foord, C., Hamman, W. and Cameron, A. Ph.D. Thesis London 1968

Ref. (3) Christensen, H. "Elastohydrodynamic Theory of Spherical Bodies in Normal Approach" A.S.M.E. Paper No. 69 LUBS.

Ref. (4) Rabinowicz, E. "Metal Transfer During Static Loading and Impacting" PROC. PHYS. SOC. 1952 B65 pp. 630-40

Ref. (5) Westlake, F. and Cameron, A.C. Ph.D. Thesis London 1970

Ref. (6) Klemz, B., Gohar, R. and Cameron, A. Ph.D. Thesis London 1970

Ref. (7) Roberts, A. and Tabor, R. "Fluid Film Lubrication of Rubber" Wear 1968 II pp. 163-66

Ref. (8) Kannel, J.W. Discussion on "Elastohydrodynamic Theory of Spherical Bodies in Normal Approach" A.S.M.E. Paper No. 69 LUBS.

Ref. (9) Christensen, H. "The Oil Film in a Closing Gap" PROC. ROY. SOC. Series A Vol. 266 1962 P31

Ref. (10) Brenner, A. "Chemical Engineering Science" VOL. 16 (1961) P242

Ref. (11) Maxwell, J.C. "On Viscosity and Internal Friction of Air and Other Gases" Bakerian Lecture (1860) Collected Works ed. W.D. Niven, Cambridge University Press 1890

Ref. (12) Maxwell, J.C. "Illustrations of the Dynamical Theory of Gases" British Association (1859) Aberdeen Collected Works 1 prop. XI. 377-409

Ref. (13) Newton, I. "Principia" Book 2 Section 9 (Hypothesis) Florians Cajons revision of Motles translation, University of California Press (1947), 385

Ref. (14) Cameron, A. "Principles of Lubrication" Chapter. 1 Longmans 1961

Ref. (15) Ostwald, W. "Lehrluch de Allgerdin" Chemie 2nd edition Engelmann Leipzig (1891) Part 1 Chapter 1,2,3, 550, Fig. 35

Ref. (16) Bridgemann, P .W. "The Effect of Pressure on the Viscosity of 43 Pure Liquids" Proc. AM. Acad. Arts Sci. 61:57, 1926

Ref. (17) Tichy, J.A. and Winer, W.D. Trans. A.S.L.E. VOL. II p. 338 1968

Ref. (18) Hersey, M.D. and Hopkins, R.F. "Viscosity of Lubricants under Pressure" Report to A.S.M.E. Research Committee A.S.M.E. New York (1954)

Ref. (19) Chu, P.S.Y. and Cameron, A. "Pressure Viscosity Characteristics of Lubricating Oils" Jour. Inst. Petrol 1962 48, (47-55)

Ref. (20) Johnson, K.L. and Cameron, R. "Shear Behaviour of Elasto-hydrodynamic Oil Films at High Rolling Contact Pressures" PRO. INS. MECH. ENGRS. 1967-68 VOL. 182 Pt. 1 No. 14

Ref. (21) Dowson, D. and Higginson, G.R. "A New Roller Bearing Lubrication Formula" Engineering, London 1961 192 158

Ref. (22) Hardy, W.B. "Collected Scientific Works of Sir William Bate Hardy" Cambridge University Press London 1936 609-632

Ref. (23) Kirk, M.T. Paper No. 69 Lubs - 11

Ref. (24) Archard, J.F. and Kirk, M.T. "Influence of Elastic Constant on the Lubrication of Point Contacts" INST OF MECH. ENGS. 1963 LUBRICATION AND WEAR Convention Paper 15 pp. 181-189

Ref. (25) Blok, H. and Koens, H.J. "The Breathing Film Between Flexible Seal and Reciprocating Rod" PROC. INST. MECH. ENGS. 1965-66 Pt. 3b pp. 221-223

Ref. (26) Gohar, R. and Cameron, A. Ph.D. Thesis London 1966

Ref. (27) Tolansky, S . "An Introduction to Interferometry" Longmans London 1966

Ref. (28) Francon, M. "Optical Interferometry" Academic Press New York 1966

Ref. (29) Michelson, A.A. "Light Waves and Their Uses" The Decennial Publications, University of Chicago Press, Chicago, 2nd series, VOL. III, 1907

Ref. (30) Jenkins, E. and White, H. "Fundamentals of Optics" McGraw Hill Book Co.

Ref. (31) Martin, L.C. and Welford, W.T. "Technical Optics" Pitman London 1966 p. 233

Ref. (32) Dekker, A.J. "Solid State Physics" p.146 Macmillian 1958

Ref. (33) Poulter, T.C., Richey, C. and Berz, C.A. "The Effect of Pressure on the Index of Paraffin Oil and Glycerin" Physical Review Aug. 1932 41 pp. 366-7

Ref. (34) Kingslake, W. "Applied Optics and Optical Engineering" Academic Press New York VOL. IV p.31

Ref. (35) Longhurst, R. "Geometrical Optics" LONGMANS 1957

Ref. (36) Israelarchrili, J. "Simultaneous Measurement of Refractive Index and Thickness in Thin Films" Nature Physical Science VOL. 229 No. 3

Ref. (37) Ranger, A. Ph.D. Student, Department of Mechanical Engineering, Imperial College of Science and Technology, London S.W.7. Private Communication

Ref. (38) Higginson, G.R. and Read, G. "Experimental Methods in Tribology" MECH. ENG. Report 5 1968 p.336

Ref. (39) Wedeven, V. Ph.D. Thesis London 1970

Ref. (40) Pilkington Company Ltd., Cheshire. Private Communication

Ref. (41) Bondi, A. "Physical Properties of Molecular Crystals, Glasses and Liquids" John Wiley and Sons Ltd. Inc. N.Y. 1968 p.404

Ref. (42) Pike, British Petroleum Ltd., Private Communication

Ref. (43) Allen, C.W., Townsend, D.P. and Zcretsky, E.V. "Elastohydrodynamic Lubrication of a Spinning Ball in a Non-Conforming Groove" Paper No. 69 LUBS II

Ref. (44) Monsanto Corporation Ltd., U.S.A. Private Communication

Ref. (45) Gentle, R. Mechanical Engineering Department, Imperial College of Science and Technology, London S.W.7. Private Communication

Ref. (46) Gentle, R. and Cameron, A. Ph.D. Thesis London 1971
To be published

Ref. (47) Bingham, E.C. and Stevens, R.A. Physics 5 217 1956

Ref. (48) Houwink, R. "Elasticity Plasticity and Structure of Matter" Cambridge University Press 1937 p.143

Ref. (49) Gunderson and Hart "Synthetic Lubricants" Rheinhold 1962